The magnetostriction of nikel and gadolinium

F. Hutchinson

THE MAGNETOSTRICTION OF NICKEL AND GADOLINIUM

by

F.HUTCHINSON B.Sc.

Presented in candidature for the degree

of Doctor of Philosophy.

December, 1958.

Abstract.

Nickel. An optical grid method has been used to check the anomaly in the λ_{100}, T curve (Corner and Hunt 1955) in a nickel crystal. The results appeared to confirm the anomaly but as the method could not be calibrated independently there was considerable doubt about their accuracy.

A solenoid capable of giving fields of 10,500 oersteds has been constructed, and magnetostriction measurements carried out using the capacitance bridge method of Corner and Hunt, on the [100] specimen in the temperature range 20 °K to 630 °K, and on the [111] specimen in the temperature range 78 °K to 630 °K. The results show that the $\lambda_{100,T}$ anomaly does not exist. Reasons are given for the error in the optical grid method, and the results obtained by the capacitance bridge method are discussed in relation to those of Corner and Hunt, and to the theoretical equation of Vonsovsky (1940). Extrapolation of the λ,T curves to 0 °K gives $\lambda_{111} = -28 \times 10^{-6}$, $\lambda_{100} = -57 \times 10^{-6}$.

Gadolinium. A zone melting apparatus has been constructed for the purpose of segregating the impurities in a piece of polycrystalline gadolinium in order to grow a single crystal. The grain size has been increased but no single crystal has been produced.

Magnetostriction and intensity of magnetization measurements have been made on an ellipsoid of polycrystalline gadolinium in the temperature range 78 °K to 350 °K. The results show that gadolinium has a large volume effect, and the volume magnetostriction is proportional to the square of the paramagnetic magnetization above the Curie point.

The saturation magnetization shows an anomaly at 150 $^{\circ}$ K, and becomes zero at 233 $^{\circ}$ K.

The contribution of the volume magnetostriction to the thermal expansion of gadolinium is shown to be too small to account for the thermal expansion anomaly except in the immediate neighbourhood of the Curie point.

Nomenclature.

$\frac{\Delta L}{L}$ = linear magnetostriction.

= change in length, ΔL of a specimen of length L, when placed in a magnetic field.

λ = saturation magnetostriction.

$\omega = \frac{\Delta V}{V} = 3\left(\frac{\Delta L}{L}\right)_V$ = volume magnetostriction.

I = intensity of magnetization (N.B. all results are expressed in c.g.s. units).

I_s = spontaneous or intrinsic magnetization.

I_v = paramagnetic magnetization.

σ = magnetic moment per gram.

χ = susceptibility.

H_a = applied field.

H = internal field.

D = demagnetizing factor.

CONTENTS

Chapter 1

INTRODUCTION

CHAPTER ONE

INTRODUCTION

1.1 Ferromagnetism. The theory of ferromagnetism is based on the following two hypotheses put forward by Weiss in 1907. The first is that the parallel alignment of the atomic dipoles is due to the existence of a molecular field, proportional to the intensity of magnetization. The second is that a ferromagnetic contains a number of small regions, domains, which are spontaneously magnetized. The resultant magnetization of the specimen is determined by the vector sum of the magnetic moments of the individual domains.

These hypotheses allow two of the most important characteristics of ferromagnetics to be explained. A development of Langevin's(1905) theory of paramagnetism gives a linear relationship between the reciprocal of the susceptibility and the temperature above the Curie point, the point below which the magnetization is present without the application of a magnetic field. At temperatures just approaching the Curie point, the experimental curve deviates from linearity, giving a lower critical temperature than that obtained by extrapolation from the linear behaviour at higher temperatures. The other successful prediction of the Weiss theory is, that using reduced units, there is a unique relationship between saturation magnetization and temperature below the Curie point, known as the law of corresponding states.

The Weiss theory in itself, offers no explanation for the existence of the molecular field ($\sim 10^7$ oersteds). Its origin was first explained

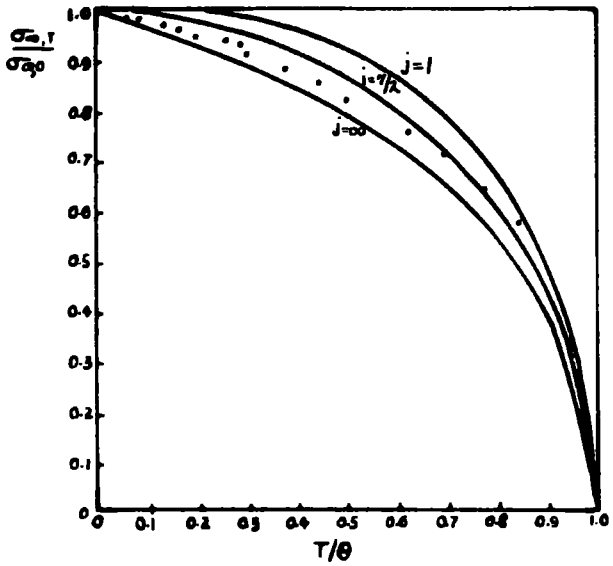

FIG. 1. Reduced magnetization curve for gadolinium (Spedding et al 1953), also the theoretical curves for $J = 1$, $J = 7/2$, and $J = \infty$.

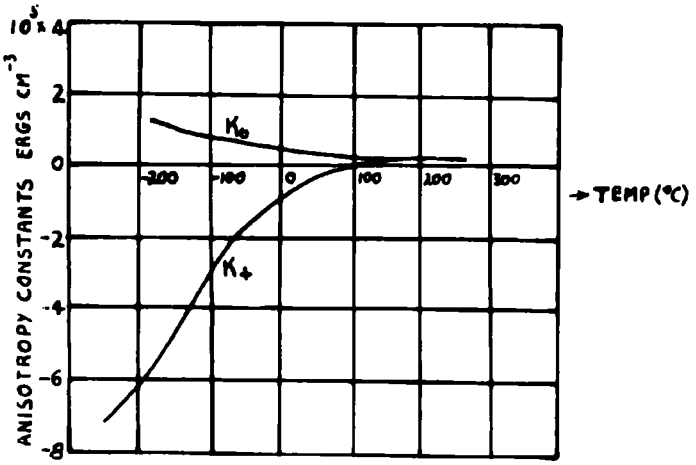

FIG. 2. Temperature dependence of the anisotropy constants of nickel (various workers).

by Heisenberg (1928) as due to electron exchange forces of a quantum mechanical nature. These forces, basically an electrostatic effect arising from the exclusion principle, arise from the overlapping of orbital wave functions. In effect, they appear as spin-spin coupling between atoms, though they have nothing to do with the magnetic moment of the electron.

Another important contribution to the theory of ferromagnetism from the quantum mechanics is that it gives a gyromagnetic ratio of 2, in close agreement with experiment. This shows that electron spins are mainly responsible for ferromagnetism, though the orbital contribution cannot be neglected, as seen from the fact that the measured gyromagnetic ratios of the common ferromagnetics are nearer 1.9 than 2.0.

The quantum mechanics modifies the molecular field theory by allowing for the discrete orientation of the carriers, effectively electron spins, rather than a continuous distribution. This gives better agreement with experiment in the law of corresponding states than the classical theory, but, as with the $\frac{1}{\chi}$, T curves, the modification still does not give an entirely satisfactory agreement. This is most evident in the case of gadolinium, in which there are seven electrons in the incomplete 4f band, where the experimental points (figure 1, Spedding et al 1953) for $\frac{\sigma_{\infty} T}{\sigma_0 T}$ lie well below the theoretical curve for $j = \frac{7}{2}$ up to $\frac{T}{\theta} = 0.75$, then lie well above the curve.

Heisenberg showed that the energy of interaction of atoms i,j, bearing spins S_i , S_j contains a term

$$E_{ex} = -2 J_{ij} S_i . S_j \qquad (1)$$

where J_{ij} is the exchange integral related to the overlap of the

electronic charge distributions i, j. Spontaneous magnetization necessitates that this exchange integral J_{ij} must be positive, though a positive J_{ij} does not necessarily cause ferromagnetism. This may be suppressed if electron migration causes a large spreading of energy levels. Slater (1930) has calculated that a substance may be ferromagnetic if the ratio of interatomic distance (r_{ab}) to the orbital radius (r_o) is larger than 3, but not much larger, e.g.

	Fe	Co	Ni	Cr	Mn	Gd
$\frac{r_{ab}}{r_o}$	3.26	3.64	3.94	2.6	2.94	3.1

The different types of lattice that can be ferromagnetic have been studied extensively (Weiss 1948). The necessary calculations are so complicated that it is necessary to approach the problem of the ferromagnetic lattice from two limiting cases. By a comparative deduction from the results of both of these cases it is possible to obtain fair agreement with the essential ferromagnetic characteristics. Heisenberg's model, where the electrons responsible for ferromagnetism always remain in the same atom, assumes that all states having the same resultant spin for the whole crystal, have the same energy. In the collective electron approach however, the electrons responsible for ferromagnetism are allowed to circulate freely throughout the lattice, and Stoner (1933) assumes a specific density of energy levels. These two approaches can be thought of as being complementary to each other, not opposed.

1.2 Anisotropy. Though numerous details still await a generally acceptable explanation, the general basis of the theoretical treatment is agreed with the exception of two important effects, magnetocrystalline

anisotropy and magnetostriction. The effects may be shown to be related (Kittel 1949), and any satisfactory explanation of one will automatically suffice for the other.

By magnetocrystalline anisotropy is meant the fact that it is considerably easier to saturate a ferromagnetic crystal in certain directions than in others. The "easy" directions are the [100] in iron, the [111] in nickel, and the hexagonal axis in cobalt. The origin of anisotropy is not really understood, but the following suggestions have been made. Classical dipole-dipole interaction contains only the second power of cosines so the resultant anisotropy energy can therefore exist only in crystals with a symmetry lower than cubic. Presumably, the dipole-dipole interaction contributes a small part of the observed anisotropy of cobalt at room temperature. There is a quantum mechanical dipolar contribution to the anisotropy in cubic crystals due to the fact that the spins are not completely parallel. The main part of the anisotropy is probably accounted for by spin-orbit interaction, effectively coupling the spins of adjacent atoms through the ordinary orbit coupling. Electrostatic fields and overlapping wave functions bind the orbits to the lattice directions, thus binding the spins to the crystal structure.

The magnitude of the anisotropy is best expressed as the difference between the energy required for magnetization in the easiest and most difficult directions. At room temperature the values for nickel, iron and cobalt are about

1.7×10^{4}, 1.4×10^{5} and 5.9×10^{6} ergs cm^{-3} respectively.

For cubic crystals, the anisotropy energy per unit volume may be expressed in terms of the direction cosines, $\alpha_1, \alpha_2, \alpha_3$ relative to the cube edges, and it may be shown by consideration of lattice symmetry that the fourth

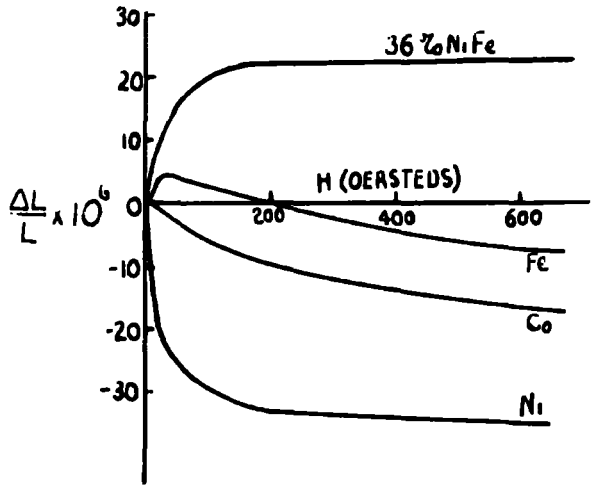

FIG. 3. Magnetostriction of polycrystalline materials as a function of magnetic field strength.

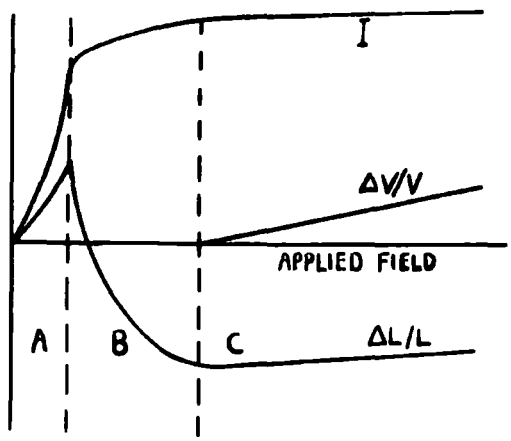

FIG. 4. Schematic representation of magnetization, linear and volume magnetostriction of iron as a function of magnetic field strength.

degree terms are the lowest possible. The energy can usually be expressed by

$$F = K_4 (\alpha_1^2\alpha_2^2+\alpha_2^2\alpha_3^2+\alpha_3^2\alpha_1^2) + K_6\alpha_1^2\alpha_2^2\alpha_3^2 \qquad (2)$$

Figure 2 shows how the anisotropy constants of nickel vary with temperature. The importance of the value of the anisotropy constants and their temperature variation cannot be over-emphasised, as such knowledge is a basic requirement for the quantitative treatment of magnetostriction and magnetization curves.

1.3 Magnetostriction. The magnetic energy of a ferromagnetic consists of the anisotropy, exchange, and magnetostatic energies. These vary with the state of strain of the substance, and so it will deform spontaneously if the deformation reduces the total energy (magnetic and elastic). The three magnetic energies respectively give rise to linear magnetostriction, volume magnetostriction, and the form effect. The linear magnetostriction (henceforth referred to as magnetostriction) is usually of the order of a few parts per million, while the volume magnetostriction, (ω) is much smaller. (e.g. Ni, $\frac{\partial\omega}{\partial H}\sim -10^{-10}/\text{oe}$). A comprehensive review of work on magnetostriction has been given by Lee (1955).

Though the variation of magnetostriction with applied field shows entirely different characteristics for the different ferromagnetics (fig.3), they can all be subjected to the same sort of general analysis. Consider figure 4, which shows a schematic representation of magnetization, linear and volume magnetostriction of polycrystalline iron as a function of field strength. The $\frac{\Delta L}{L}$, H and the I,H curves can be divided up into the same three sections. In A, an initial expansion occurs in the same field region as the domain boundary movement, and usually takes place in

a field of a few oersteds. In B, domain boundary movements are completed and the magnetization is increased by domain vector rotation. A contraction occurs until all the rotations are complete, both saturation magnetization and saturation magnetostriction being reached at the same field strength, usually $\sim$ 1,000 oe. Any further change in the magnetization can take place only by causing an increase in the intrinsic magnetization (C). The subsequent magnetostriction is then primarily a volume effect, proportional to the field strength.

1.31. Linear Magnetostriction. 1.311 Phenomenological Theory. (Cubic crystals) By minimising the total energy of a crystal, i.e. the crystal anisotropy energy, the magnetostrictive energy, and the elastic energy, Becker and Doring (1939), following the work of Akulov (1928), obtained the following expression for the magnetostriction,

$$\begin{aligned}\frac{\Delta l}{l} = {} & h_1\left(\alpha_1^2\beta_1^2 + \alpha_2^2\beta_2^2 + \alpha_3^2\beta_3^2 - \tfrac{1}{3}\right) + 2h_2\left(\alpha_1\alpha_2\beta_1\beta_2 + \alpha_2\alpha_3\beta_2\beta_3 + \alpha_3\alpha_1\beta_3\beta_1\right) \\ & + h_4\left(\alpha_1^4\beta_1^2 + \alpha_2^4\beta_2^4 + \alpha_3^4\beta_3^4 + \tfrac{2}{3}S - \tfrac{1}{3}\right) \\ & + 2h_5\left(\alpha_1\alpha_2\alpha_3^2\beta_1\beta_2 + \alpha_2\alpha_3\alpha_1^2\beta_2\beta_3 + \alpha_3\alpha_1\alpha_2^2\beta_3\beta_1\right) \\ & + h_3 S \qquad \text{when } K_1 > 0, \text{ eg iron} \\ & + h_3\left(S - \tfrac{1}{3}\right) \qquad \text{when } K_1 < 0, \text{ eg nickel} \end{aligned} \tag{3}$$

where K_1 = anisotropy constant, h's are constants dependent on temperature, $S = \alpha_1^2\alpha_2^2 + \alpha_2^2\alpha_3^2 + \alpha_3^2\alpha_1^2$, α is the direction cosine of the magnetization, β the direction cosine of the strain, both with respect to the crystal axes. h_3 represents a volume change associated with domain vector rotation and is usually small. The value of these constants for nickel are (Bozorth and Hamming 1953)

	$h_1 \times 10^6$	$h_2 \times 10^6$	$h_3 \times 10^6$	$h_4 \times 10^6$	$h_5 \times 10^6$
Ni	-68.8 ± 3.8	-36.5 ± 1.9	-2.8 ± 3.8	-7.5 ± 5.2	$+7.7 \pm 3.1$

These show that normally h_3 , h_4 and h_5 can be taken to be equal to zero, and then equation 3 reduces to

$$\frac{dl}{l} = \frac{3}{2}\lambda_{100}\left(\alpha_1^2\beta_1^2 + \alpha_2^2\beta_2^2 + \alpha_3^2\beta_3^2 - \frac{1}{3}\right) + 3\lambda_{111}\left(\alpha_1\alpha_2\beta_1\beta_2 + \alpha_2\alpha_3\beta_2\beta_3 + \alpha_3\alpha_1\beta_3\beta_1\right) \quad (4)$$

By averaging over all directions, it follows for a polycrystalline substance

$$\lambda_{poly.} = \frac{2}{5}\lambda_{100} + \frac{3}{5}\lambda_{111} \quad (5)$$

The corresponding equation to (3) has been worked out for hexagonal crystals (Bitter 1937) and the constants for cobalt measured (Bozorth and Sherwood 1954). Bitter obtained the following expression, which is the same as that obtained for cylindrical symmetry

$$\frac{dl}{l} = k_1\left(\alpha_1^2 - 1\right)\beta_1^2 + k_2\left(\alpha_2^2\beta_2^2 + \alpha_3^2\beta_3^2\right) + k_3\left(\alpha_3\beta_2 + \alpha_2\beta_3\right) + \alpha\left(k_2 - k_3\right)\alpha_2\alpha_3\beta_2\beta_3 + \alpha k_4\alpha_1\beta_1\left(\alpha_3\beta_3 + \alpha_2\beta_2\right) \quad (6)$$

where αi and βi are with respect to orthogonal axes such that $0z$ corresponds to the c axis and $0x$ or $0y$ to one of the hexagonal axes. Cylindrical symmetry is an adequate approximation for cobalt. For hexagonal symmetry, eight constants are required if the saturation magnetization is parallel or perpendicular to the direction of measurement, and eleven if not.

The above treatment is purely formal. It enables the characteristics of the material to be represented in terms of constants which are experimentally determinable, but it makes no attempt to explain the origin of them.

1.312 The Origin of Magnetostriction. Akulov (1928) and Becker (1930) considered the problem as one of purely magnetic interaction of dipoles at lattice points. For a perfect cubic lattice, (Kittel 1949) this does not give rise to anisotropy, but if the lattice is allowed to deform spontaneously, there is a small contribution to the anisotropy. The minimisation of the total energy gives values of magnetostriction and anisotropy (table 1) which, when compared with experimental values, show that spin-spin interaction can account for only a small part of the magnetostriction and anisotropy.

Table 1

Dipolar Magnetostriction and Anisotropy of Iron and Nickel

	$\lambda_{100} \times 10^6$	$\lambda_{111} \times 10^6$ calculated	$K_1 (=\Delta K) \times 10^{-4}$	$\lambda_{100} \times 10^6$	$\lambda_{111} \times 10^6$ observed	$K \times 10^{-4}$
Fe	4.9	-1.5	+ 0.004	20.7	-21.2	+ 47
Ni	0.15	-0.05	+0.00004	-45.9	-24.3	-5.9

where $K_1 = K^\circ + \Delta K$ = measured anisotropy constant, K° refers to the unstrained crystal, ΔK that caused by magnetostriction. One interesting result from Becker's calculations is that $\lambda \propto I_s^2$. The results of Doring(1936) and Corner and Hunt (1955) on nickel show this to be true over the temperature range 270° K to 470° K, but not generally true.

The next suggestion (Bloch and Gentile 1931) was that the orbital moments are rendered inoperative by inhomogeneous crystalline fields. The energy of orbital momentum depends on the orientation of the orbital moments relative to each other, and on their orientation with respect to the crystal axes. The spin moments are coupled to the orbital moments, and hence to the lattice, by spin-orbit coupling. Van Vleck (1937) developed

this idea, and showed that this coupling was of the right order to give rise to magnetocrystalline anisotropy, and hence magnetostriction.

Vonsovsky (1940), using the Heisenberg model, took into account both spin-spin and spin-orbit coupling. He obtained expressions of the form

$$\lambda_{100} = X \frac{I_s^2}{I_\infty^2} \left[A + B f(T) \right]$$
$$\lambda_{111} = Y \frac{I_s^2}{I_\infty^2} \left[A' + B' f(T) \right] \qquad (7)$$

where A, B, A', B' are constants, X,Y are terms containing the elastic moduli, and f(T) is an exponential function of temperature. By using reasonable values for these constants, equation 7 gives values of λ_{100} and λ_{111} of the right order of magnitude. The first term in each case corresponds to that derived by Becker and Akulov on the basis of spin-spin coupling, and the remainder, the contribution due to spin-orbit coupling. A knowledge of the variation of λ with T will therefore be of value in estimating the contribution due to spin-orbit coupling.

Recently, Fletcher (1955) has attempted to calculate the magnetostriction on a collective electron basis, using a tight-binding wave function approximation with spin-orbit coupling as a perturbation. The results have only been calculated for nickel at absolute zero, giving $\lambda_{100} = -187 \times 10^{-6}$ and $\lambda_{111} = -44 \times 10^{-6}$.

1.313 Magnetostriction below saturation. 1.3131 Polycrystals. Lee (1958), using as a basis Brown's (1938) statistical treatment of domain boundary movements, obtained the distribution function for domain vector rotation for cubic and hexagonal crystals (only where the hexagonal axis is the easy axis). He was then able to construct curves for Fe, Ni and Co using

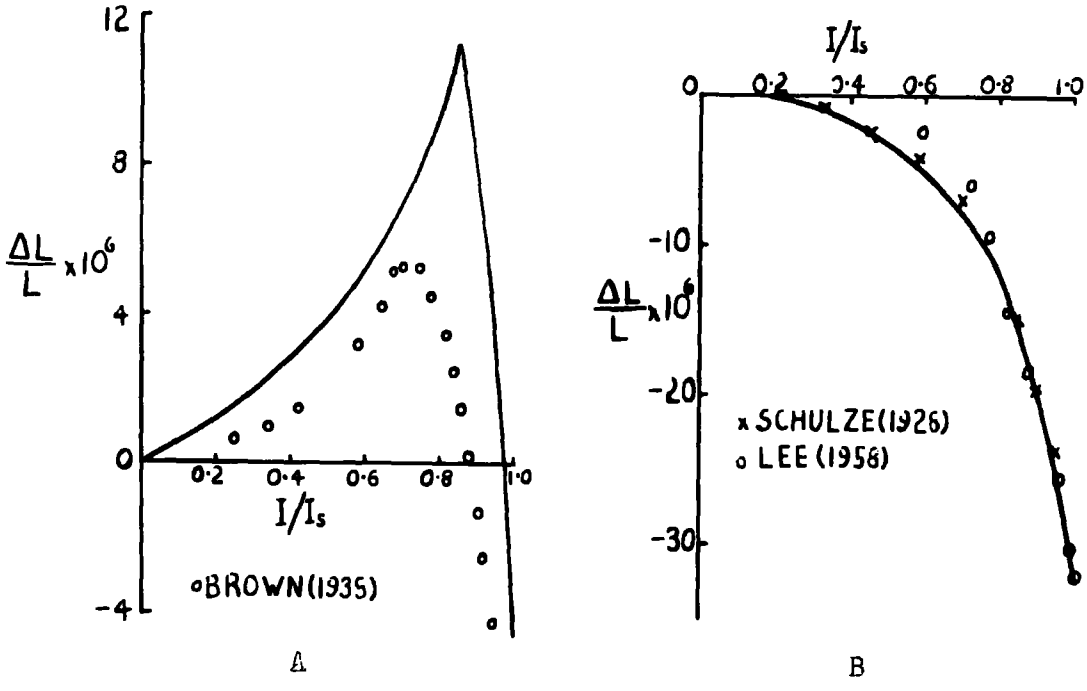

FIG. 5. Calculated magnetostriction curves of polycrystalline iron(A) and nickel (B) (Lee 1958) compared with experimental results.

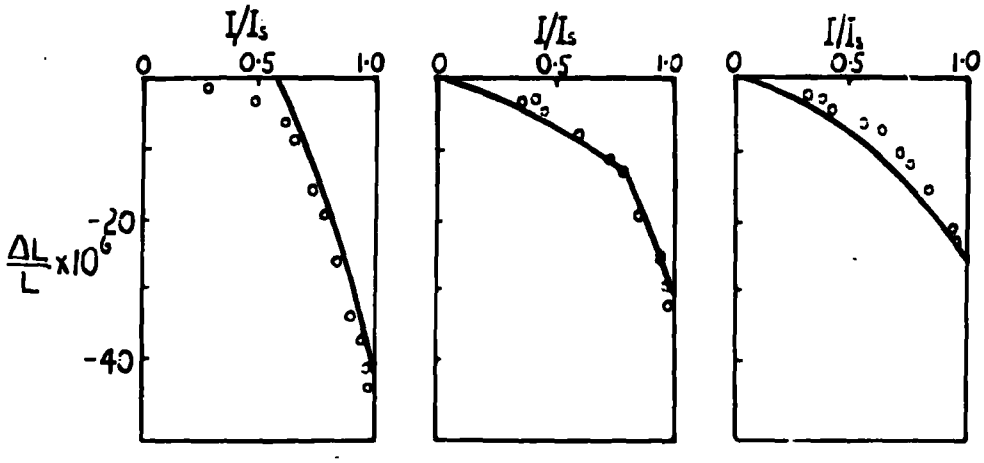

FIG. 6. Magnetostriction of nickel crystals calculated from the Heisenberg theory.

both sets of results. Figure 5 shows the curves compared with typical sets of experimental points. The Ni curve (using $\lambda 100 = -45.9 \times 10^{-6}$ and $\lambda 111 = -24.3 \times 10^{-6}$) fits the curve rather well, but the Fe curve shows a significant divergence. There are no figures for cobalt to allow a comparison to be made.

1.3132 Single Crystals. It is possible to calculate magnetostriction curves when the magnetization proceeds in a known manner, i.e. no overlapping of the different magnetization processes. The distortion of the whole crystal may be calculated by considering the number of domains of different orientations corresponding to particular values of the bulk magnetization.

For $K_1 < 0$ this gives for the following directions (Fowler 1936)

[111] I reaches saturation in very low fields, then

$$\frac{\Delta L}{L} = \lambda_{111} \frac{I^2}{I_s^2} \qquad (8)$$

[100] Before the knee of the curve, corresponding to $\frac{I}{I_s} = \frac{1}{\sqrt{3}}$, there is no magnetostriction. After the knee,

$$\frac{\Delta L}{L} = \lambda_{100}\left(\frac{3}{2}\frac{I^2}{I_s^2} - \frac{1}{2}\right) \qquad (9)$$

[110] There is domain rotation before and after the knee, corresponding to $\frac{I}{I_s} = \frac{\sqrt{2}}{\sqrt{3}}$

For $0 \leqslant \frac{I^2}{I_s^2} \leqslant \frac{2}{3}$ $\qquad \frac{\Delta L}{L} = \frac{3}{4}\lambda_{111}\frac{I^2}{I_s^2}$

and $\frac{2}{3} \leqslant \frac{I^2}{I_s^2} \leqslant 1$ $\qquad \frac{\Delta L}{L} = \lambda_{100}\left(\frac{3}{4}\frac{I^2}{I_s^2} - \frac{1}{2}\right) + \frac{3}{4}\lambda_{111}\frac{I^2}{I_s^2}$ (10)

Corresponding equations may be obtained for $K_1 > 0$

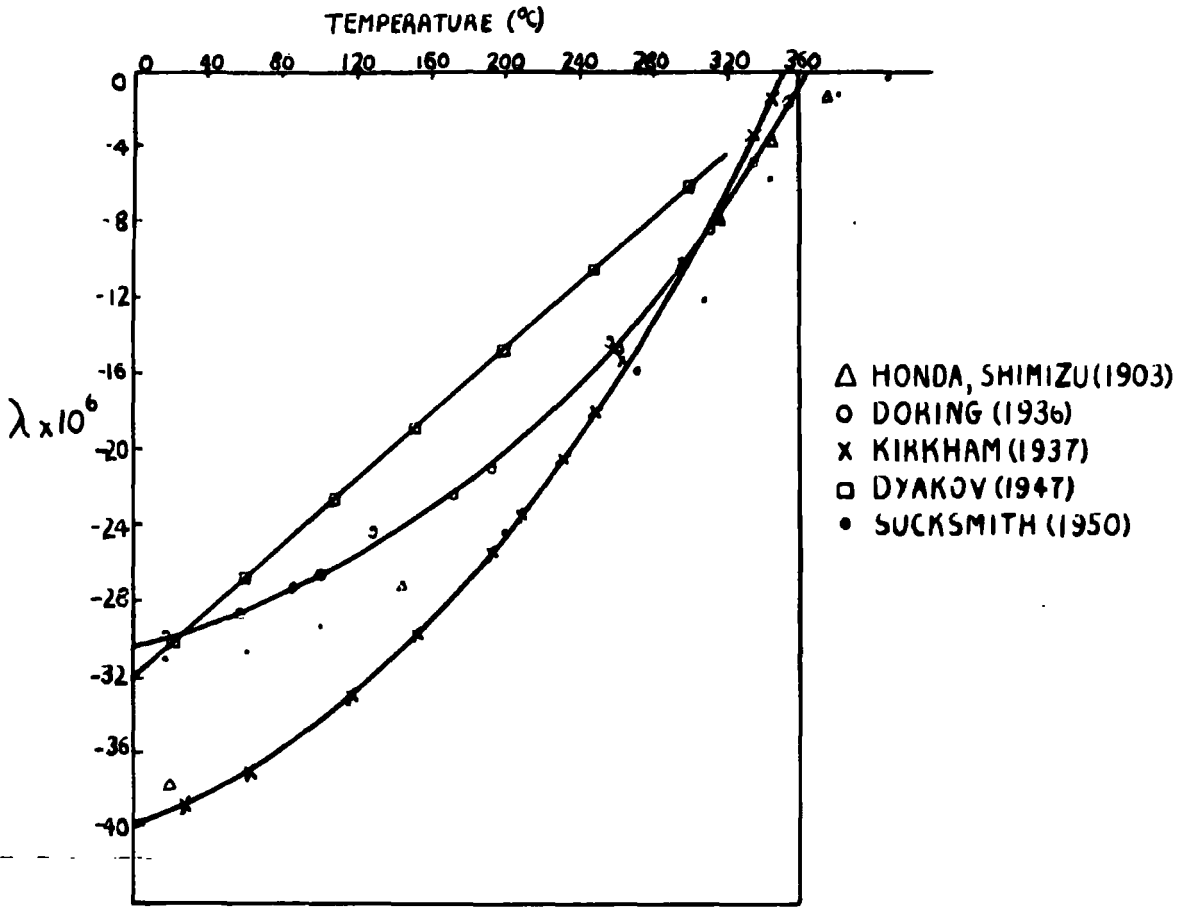

FIG.7. Temperature dependence of saturation magnetostriction of polycrystalline nickel.

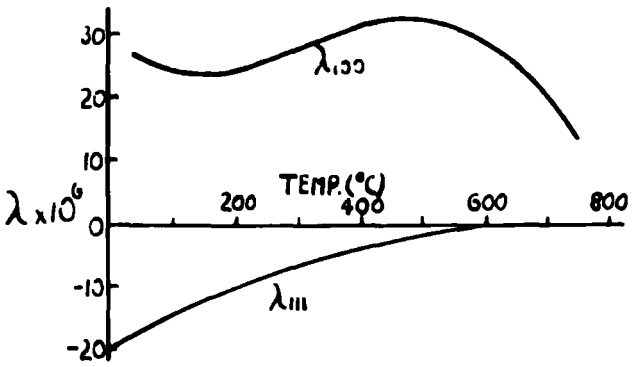

FIG. 8. Temperature dependence of the magnetostriction constants of iron (Takaki 1936).

Masiyama's results (1928) on nickel (fig.6), and Kaya and Takaki's (1935) results on iron give general agreement with this theory, though none of the predicted sharp bends are found. This is to be expected since some domain vector rotations will occur before all the domain boundary movements are complete.

1.314 Previous Results. 1.3141 Polycrystals. The divergence of the measured values of λ at room temperature for nickel can best be seen by considering the values obtained by Masumoto (1927), $\lambda = -47 \times 10^{-6}$, and Schulze (1931), $\lambda = -25 \times 10^{-6}$. Even a combination of experimental error, impurity, and difference in heat treatment cannot account for the difference. The main cause is probably a difference in the demagnetized state, caused by some preferred crystal grain orientation. The same reason probably accounts for the different curves and absolute values (fig.7) of the λ, T curves of Doring (1936), Kirkham (1937), Dyakov (1947) and Sucksmith (1950) The demagnetized state taken up by a specimen will depend on the method of preparation of the specimen, and its method of demagnetization, factors which should be standardized. Unfortunately, in the latter case, this is not possible unless all measurements are made on specimens of standard shape.

Both Doring and Kirkham also measured the intensity of magnetization of their specimens, and from their results it can be deduced that $\lambda \propto I_s^2$ from room temperature up to 473°K. Dyakov's curve differs considerably from those obtained by the other workers. His work was undertaken to provide experimental proof of a relationship obtained by Akulov (1939)

$$\lambda_{100,T} = \lambda_{100,0} \left(1 - \frac{T}{\theta}\right)$$

where θ is a constant.

1.3142 Single Crystals. Takaki (1937) measured the variation of λ 111 and λ 100 over the temperature range 273°K to 1,020°K for iron (fig.8) using remanence as the reference state. The λ, T curve is complicated and presumably shows considerable spin-orbit coupling.

The only measurement of the temperature variation of the magnetostriction of nickel single crystals has been made by Corner and Hunt (1955). Room temperature measurements have been made by various workers, however, and these will be discussed first.

Table 2.

Magnetostriction Constants of Nickel at Room Temperature. (all values x 10^{-6})

Constant	Masiyama (Direct)	Becker and Döring	Mason	Bozorth and Hamming	Corner and Hunt (Direct)
h_1		-27	-40	-68·8 ± 3·8	
h_2		-47	-46	-36·5 ± 1·9	
h_3		0(assumed)	0(assumed)	- 2·8 ± 3·8	
h_4		-51	-36	- 7·5 ± 5·2	
h_5		-52	+54	+ 7·7 ± 3·1	
λ_{100}	-53	-50	-51	-51	-52
λ_{110}	-36	-32	-37	-31	
λ_{111}	-27	-20	-19	-24	-19

Masiyama (1928) used an optical method to measure the magnetostriction, the specimens being in the shape of oblate spheroids, major axis 2 cms, minor axis 0·1 cms. He measured λ in the (100), (110) and (111) planes,

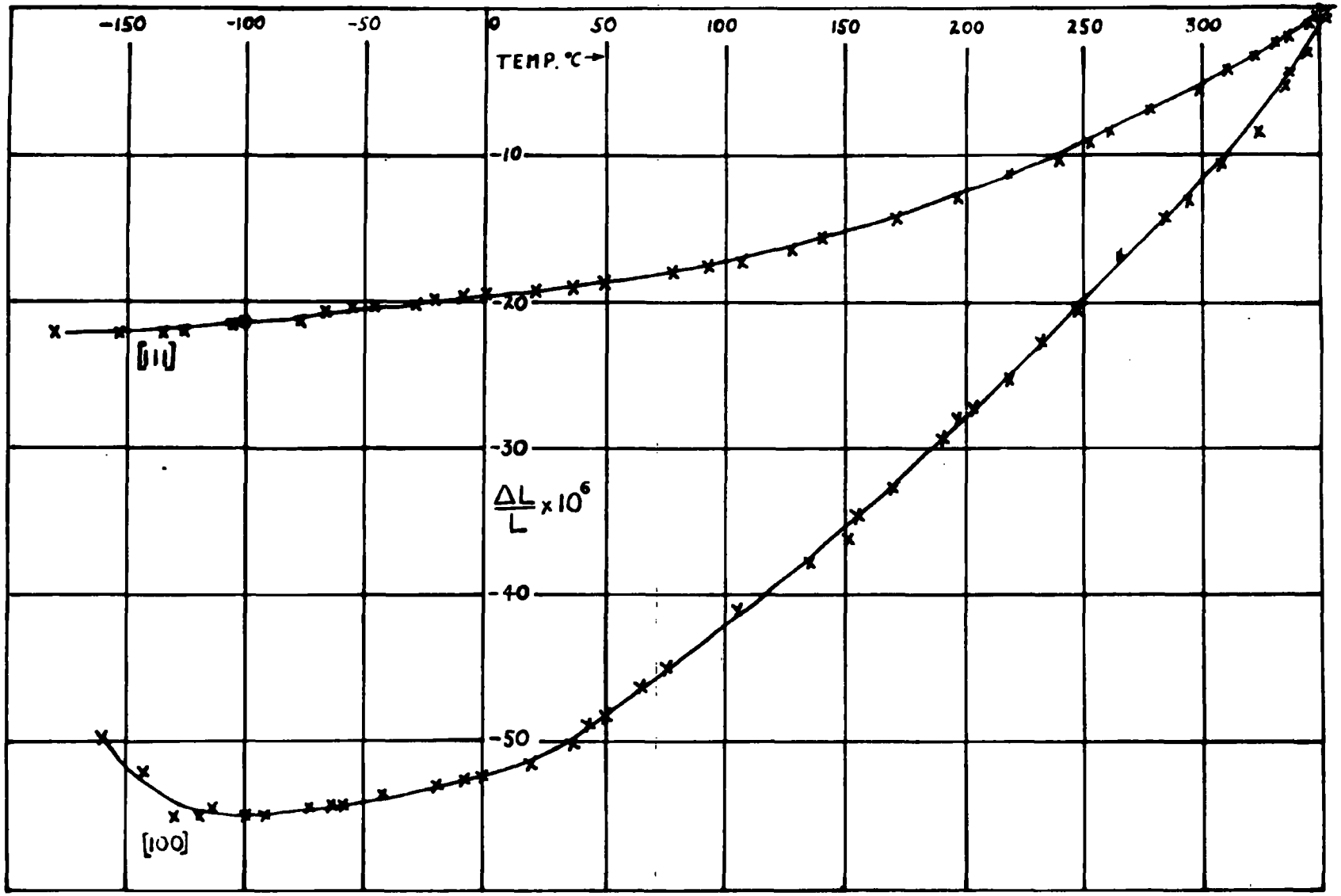

FIG.9. Temperature dependence of saturation magnetostriction of nickel crystals. (Corner and Hunt 1955)

and obtained results which could be expected from the lattice geometry. Some doubt must be cast on the absolute values however, as different values of λ were obtained from the same directions in different planes. This inaccuracy must be present in the values obtained by both Becker and Doring (1939) and Mason (1951), as they used Masiyama's figures to calculate the values of the constants $h_1 - h_5$ which best fit the results.

Bozorth and Hamming (1953) used strain gauges to measure the difference in the magnetostriction between different directions in the same plane on disc specimens. They then used a similar method as that used by Becker and Doring to calculate the values of $h_1 - h_5$ from their own results. Corner and Hunt's values were obtained directly by means of a capacitance bridge arrangement. They used specimens in the shape of prolate ellipsoids, major axis 1·8 cms, minor axis 0·27 cms. The only agreement in the values of h between the different workers is that $h_3 \rightarrow 0$. ie. there is very little change in volume associated with the rotation of the domain magnetization vector. Agreement between the other values can hardly be expected since the values on which Bozorth and Hamming's results are based are more accurate than those of Masiyama. A better method of comparison seems to be to use the values of λ, both observed and calculated. Good agreement is obtained with $\lambda 100$, but not with $\lambda 110$ and especially $\lambda 111$. The differences in $\lambda 111$ must be due to uncertainties in the reference state.

The temperature variation of $\lambda 111$ and $\lambda 100$ obtained by Corner and Hunt (fig 9) shows for the [100] direction, an anomalous maximum in the strain at about 125°K. As part of the present work undertaken has been to check this anomaly, a full discussion of the temperature variation

will be given later (2.210).

From the foregoing discussion, it is obvious that the main cause of difference between the values of λ obtained by different workers is an uncertainty in the reference state. The one most commonly used is the demagnetized state, which ideally is one in which the domain magnetization vectors are distributed uniformly over all possible directions. Kaya and Takaki's results on iron show that in the demagnetized state, the domain magnetization vectors need not necessarily be distributed equally along all the directions of magnetization. The demagnetized state is used as the reference state for all measurements in this thesis, and is obtained by successive reversing of the applied field from a value sufficient to saturate the specimen to zero.

An alternative reference state is that of remanence. Takaki, in his work on iron crystals (demagnetizing factor 0.003), which have only six directions of easy magnetization, assumed that at remanence, the resultant magnetization lies along the axis of his specimens. Thus the domains will align themselves in the three easy directions nearest to the field direction in proportion of their direction cosines with respect to the field direction. Such a distribution does not hold in the case of nickel, with eight directions of easy magnetization. The distribution of domain magnetization vectors is then not generally in any specifically defined proportion in the four easy directions nearest the field direction.

Bozorth and Hamming, in their measurements, used the difference between the magnetostriction measured in different directions in the same plane, and thus any error due to differential domain vector orientation

did not arise. This seems to be the best method, but unfortunately experimental conditions did not permit its use in the work described in this thesis.

1.4 The Form Effect and Magnetocaloric Effect. These two effects are factors which may influence the magnetostriction measurements, and so a brief description of them is given here. The demagnetizing factor (D) of a specimen depends on its shape, so a change in dimensions will cause a corresponding change in the energy associated with the demagnetizing field. This is known as the Form Effect. Becker (1934) has calculated the effect for a prolate ellipsoid and found the total volume strain (ω_f),

$$\omega_f = \frac{1}{2}\frac{DI^2}{K}$$

the longitudinal magnetostriction $\left(\frac{\Delta L}{L}\right)_f = \frac{1}{2} DI^2\left[\frac{1}{3K} + \frac{a}{2\eta}\right]$ (11)

the transverse magnetostriction $\left(\frac{\Delta L}{L}\right)_f$ trans. $= \frac{1}{2} DI^2\left[\frac{1}{3K} - \frac{a}{4\eta}\right]$

where K = bulk modulus, η = torsional modulus, a = a constant depending on the eccentricity (e) of the specimen given by

$$a = \frac{3-e^2}{e^2} - \frac{4\pi}{D}\left(\frac{1-e^2}{e^2}\right)$$

The magnetocaloric effect is the increase in temperature caused by an increase in the spontaneous magnetization when a field is applied. This increase in temperature then causes an increase in length of the specimen and so may effect the magnetostriction measurements. Fortunately, a large field is needed to produce any appreciable change in temperature, and the effect rapidly decreases at temperatures above and below the Curie point, where it has its maximum. Nickel (Weiss and Forrer 1926) gives an increase of 1.25 ^{o} K on the application of a field of 20,000

oersteds at its Curic point, iron an increase of 2.0° K in a field of 8,000 oersteds (Potter 1934).

1.5 Object of the investigations. In any evaluation of the energy due to strain in a ferromagnetic, an accurate value of the magnetostriction is required. An investigation of this process will give some knowledge on the internal forces in a ferromagnetic crystal, and also be of use in investigating magnetization processes.

There are various ways of changing the magnetostriction constants (i.e. changing the interactions responsible for magnetostriction) e.g. varying the composition of alloys, altering the crystallographic order in alloys, but the most important influence is temperature. The temperature variation is of great value in estimating the contribution due to spin-orbit interaction (Vonsovsky).

By making measurements on λ at very low temperatures, a reasonable extrapolation to absolute zero may be made and this will provide a test on theoretical calculations made at that temperature (e.g. Fletcher 1955).

It was with these requirements mainly in mind that the present work on nickel and gadolinium has been carried out. The first part of the work is concerned with checking the anomaly in the λ 100, T curve for nickel (Corner and Hunt), as they were unable to achieve complete saturation with the apparatus used, and the values of λ 100 below 150 K were obtained by extrapolation. It was thought desirable that the results in this region should be checked by bringing the specimen to complete saturation. As no work whatsoever has been done on the magnetostriction of gadolinium, the second part is concerned with $\frac{\Delta L}{L}$, T measurements over as much as possible of its ferromagnetic range.

Chapter 2

THE TEMPERATURE VARIATION OF THE MAGNETOSTRICTION OF NICKEL

CHAPTER TWO

THE TEMPERATURE VARIATION OF THE MAGNETOSTRICTION OF NICKEL.

These measurements were made on the original crystals used by Corner and Hunt. Circumstances required that two different experiments be carried out before a satisfactory λ, T relationship could be obtained. The first one, an optical grid method, gave results which were in keeping with the λ_{100}, T anomaly, but unfortunately it was found impossible to provide an independant calibration for the system. The trend of the curve suggested that it would be very interesting to make magnetostriction measurements at still lower temperatures. In order to do this, the capacitance bridge method of Corner and Hunt was used, and this showed that the results obtained from the optical method were wrong and the anomaly did not exist. The suggested reason for the error in the optical measurements is given in 2.210.

2.1 Optical Grid Method.

2.11 Apparatus. 2.111 General Considerations. From a knowledge of the temperature dependence of the anisotropy coefficients (Bozorth 1951) the field required to saturate the specimen in the [100] direction at 80° K would be about 5,000 oersteds. This presented no difficulty as a large electromagnet capable of giving a field of 20,000 oersteds with a pole gap of 15 cms (pole pieces 30 cms x 40 cms) was available. A convenient method of obtaining various temperatures between 80° K and room temperature is by means of a thermal potentiometer. A column of liquid (iso-pentane) has its lower end immersed in a liquid nitrogen bath

and its upper end at room temperature. The specimen may be brought to any desired temperature in this range by adjustment of its position in the column. With this arrangement any change of length must be transferred to a point above the iso-pentane column at which it will be more convenient to mount whatever device is to be used to measure the changes of length. The electromagnet produces a horizontal field and a mechanical lever is required for transference of the contraction of the specimen. The lever can then be coupled to an electrical or optical device for magnification. Strain gauges could not be used in this case as the nickel specimens were in the shape of ellipsoids. These were prolate ellipsoids, in the [100] direction, major axis 1.770 cms, minor axis 0.275 cms, demagnetizing factor D=0.491, in the [111] direction major axis 1.770 cms, minor axis 0.276 cms, D=0.495. At room temperature, the rigidity modulus is 7.7×10^{11} dynes/cm^2, the bulk modulus 17.6×10^{11} dynes/cm^2, giving a magnetostrictive form effect (1.4), $\left(\frac{\Delta L}{L}\right)_f \approx 3 \times 10^{-13} I^2$, which is small enough to be neglected.

The use of the electromagnet made it impossible to employ the extensometer and associated apparatus of Corner and Hunt, for the following reasons. The extensometer was constructed mostly of Invar, because of its low temperature coefficient of expansion, and it was considered unwise to construct a new one out of non-magnetic material because of the thermal drift that would result from changes in ambient temperature. Thus the extensometer would have to be placed well away from the pole-pieces of the electromagnet because of magnetic shielding difficulties. If it were placed above the magnet, the length of lever required to bring out the deflection would be of the order of 60 cms, which makes it impracticable.

Another possibility was to bring out the displacement through a hole in one of the pole pieces, by means of a sliding rod in tube arrangement, to the extensometer fixed to the outside of the magnet. The rod and tube would have to be of the order of 100 cms, and as the magnet current required to produce a field of 5,000 oersteds is 30 amps, the subsequent heating of the magnet coils would produce a temperature variation between the rod and tube. After careful consideration it was decided that the best method would be to couple the lever to an optical amplifier.

The specimen is mounted in the centre of the magnet gap by means of a lever arrangement of vitreosil. An optical magnification system, using grids and a photo-electric cell similar to that developed by Jones (1951), is held at a fixed distance away from the lever by means of three vitreosil rods. Displacement of the free end of the specimen causes a rotation of a galvanometer mirror attached to the lever, giving a proportional output in the photo-cell. Temperature changes are produced by suspending the specimen in a pyrex tube of iso-pentane (F.P. - 160° C), the bottom of the tube being immersed in a vacuum flask containing liquid nitrogen. As random temperature fluctuations of the specimen can produce length changes of the order of its magnetostriction, the fluctuations are compensated by a non-ferromagnetic metal in thermal contact with the specimen.

2.112 Optical system. The principal parts of the optical system are shown in figure 10

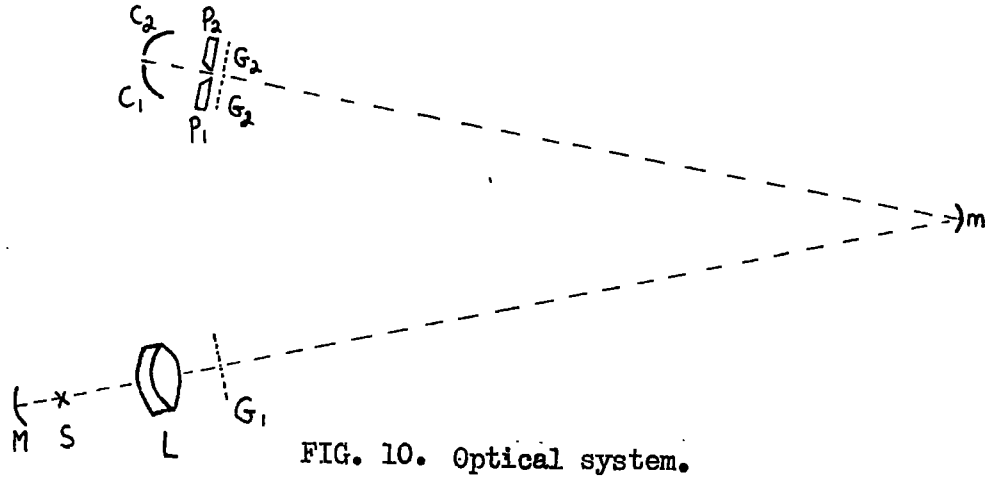

FIG. 10. Optical system.

Lens L focuses the image of source S on the mirror m. G_1 and G_2 are two grids of identical spacing, each at a distance equal to the radius of curvature of m from m. G_2 is split into two halves, slightly separated so that the lines and spaces in one half are exactly out of phase with those in the second half. Thus if the spaces of the image of G_1, formed by m on G_2 coincide with the spaces of one half of G_2, that half will allow light to pass through, while the other half will not. By moving either G_1 or G_2, a position can be found where the same amount of light passes through each half of G_2, and the system balances. Prisms P_1 and P_2 collect the light into C_1 and C_2 respectively, the two halves of a split cathode photo-electric cell. The difference in output of C_2 and C_2 is measured by a galvanometer. If m rotates, the image of G_1 moves across G_2, the system no longer balances, and one half of the cell receives more light than the other.

The purpose of the concave mirror M is to stabilize the position

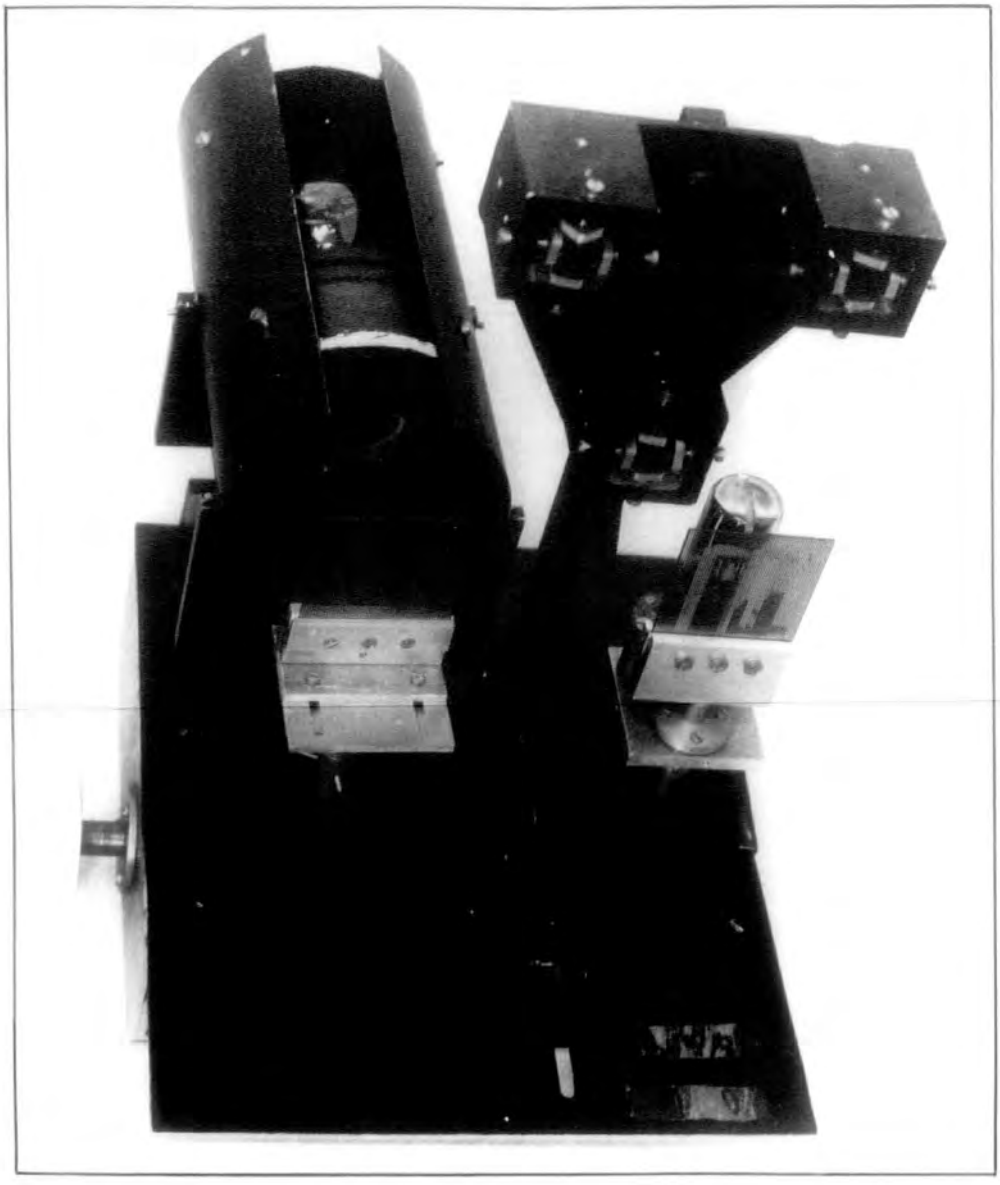

FIG. 11. Lamp house.

of the source, as well as to increase the amount of useful light. M is placed so that the image of the filament is formed just beside the filament, so that if this should sag slightly in one direction, the image would move in the opposite direction.

The amplification of the above system depends on the amount of light given out by S, the spacing of the grids, the distance of the grids from m, and the sensitivity of the output galvanometer. Of these, the distance G, m must necessarily be fixed, and it is considered unwise to run a projection lamp at its stated value due to shortening of its lifetime. The output variation from maximum to minimum must not exceed a measureable deflection on the galvanometer scale, i.e. 50 cms, determining the sensitivity of the galvanometer required. The maximum change in length of the specimen is about 10^{-4} cms. Using a 4 to 1 magnification ratio on the lever, and with the grids at 100 cms from the lever, the image grid displacement is about 4×10^{-2} cms, giving a grid of 15 lines / inch.

2.113 Lamp house. The lamp house (fig. 11) consists of 1/16 ins. brass sheet, rolled into the shape of a cylinder, mounted on a duralumin rocker to allow the necessary degree of freedom. A Chance ON20 heat filter is placed between the projection bulb and the condensing lens, (f = 3 ins A = 2.73 ins) to save the lens from distortion due to heat, and also to cut out infra red radiation which contributes to the fatigue of photo-cells (Preston 1946). The bulb, an Osram projection class F, 12 V 48 W, is run at a lower rating than normal to ensue long life. Power is supplied by four 22 AH, 12 V batteries connected in parallel. Due to

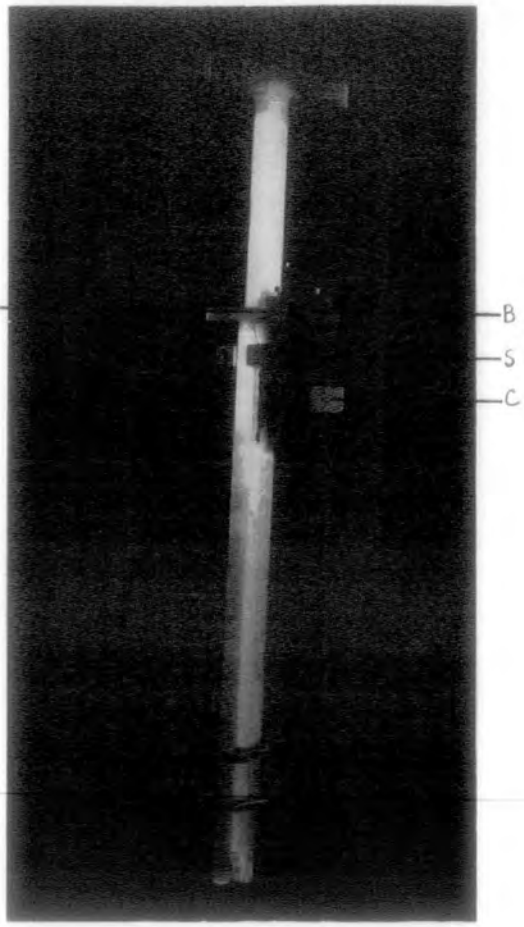

FIG. 12. Specimen holder and mechanical lever.

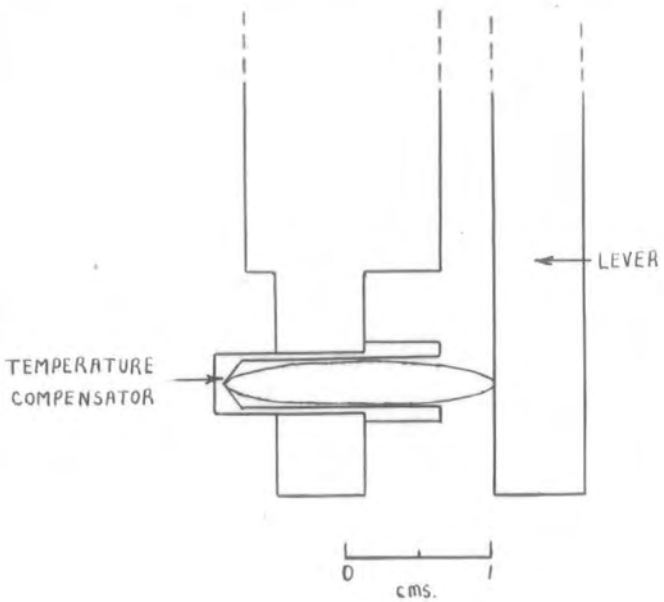

the heat generated, the bulb is cooled by blowing a continuous stream of dust free air up past the bulb by means of a blower. A baffle (not shown in fig. 11) placed immediately above the bulb, allows the air to escape, but no light to enter.

2.114 Grids. The grids are made by winding a master grid of wire of 60 lines / ins, and photographing this grid using Ilford " Formalith " plates to give exceptionally high contrast. A series of grids are then obtained by enlargement, of 30, 25, 20 and 15 lines / ins for different sensitivities. The reason for not winding the master grid of 15 lines / ins is that the thickness of the wire makes it impossible to get rid of any small imperfections which develop in the winding. The grids themselves are clamped between two pieces of milled duralumin to a depth of about 2 m.m., one side being packed with a layer of compressible paper. The two collecting prisms are mounted in a similar manner behind the image grid and in front of a Cintel CV 40 split cathode photo-electric cell. A spring loaded kinematic ball bearing slide consisting of two milled duralumin plates, brass rods and steel balls, supports the object grid, the parallel movement of which is controlled by a brass screw of 60 turns / ins.

2.115 Temperature compensator and mechanical lever. The mounting of the specimen and the mechanical lever is shown in figure 12. Temperature compensation is achieved by the aluminium thimble expanding in the opposite direction to the specimen. Over the temperature range 0° K - 470° K (Nix and MacNair 1941) the form of the thermal expansion

curve of aluminium agrees closely with that for nickel, though their coefficients of expansion are different (Ni = 11.32 x $10^{-6}/^{\circ}K$, AL = 20.96 x $10^{-6}/^{\circ}K$). Allowance is made for the fact that the nickel specimen is held at points removed from its end, in the calculation of the actual length of thimble required.

The lever, made of Vitreosil, gives a magnification ratio of 4:1. It consists of a fixed T piece, 13 mm square; the actual lever, a T piece 6 mm square, being spring loaded against an agate knife edge and the specimen. The agate knife edge is attached to the main T piece with " Araldite". Location of the lever is provided by means of a V - shaped cut to fit the knife edge. To ensure that the lever can only move in the desired direction, motion perpendicular to that direction is prevented by two spring loaded rollers fixed to the main T piece by a Duralumin support. As any excess pressure on the specimen will cause a large effect on its magnetostriction, the spring loading of the lever is made as small as possible consistent with the working of the lever. In this case it turns out to be equivalent to a force of 25 gms wt., which is negligible.

2.116. Mirror suspension. Originally it was intended to suspend the mirror from A and B, (fig.12) by two fibres and bring out the deflection by means of a 45° mirror at C. The introduction of this other mirror caused the image of the object grid to lose its contrast, and so the method was discarded. The suspension S brings out the deflection direct,without the use of an auxilliary mirror. It consists of $\frac{1}{8}$ ins square brass rod with 1/32 ins brass sheet, 6 cms x 1.5 cms, soldered perpendicular to it at the

centre. The rod rests on the moveable arm A and the fixed arm B by means of two 8 BA brass screws passing through the rod at equal distances from the brass sheet. These screws have their ends ground to needle-sharp points so that actual contact takes place over a negligible area. The mirror, front surface aluminised, r = 100 cms, is stuck to the brass suspension sheet with one small spot of Durafix, too much Durafix causing the mirror to become distorted. No change in the radius of curvature of the mirror can be detected after the Durafix has been left to dry for about 24 hours. A damping vane immersed in light mineral oil, is attached to the lower end of the suspension to damp out oscillation.

2.117 Temperature measurement and control. To measure the temperature of the specimen, a copper constantan thermocouple is used, the fixed junction being kept in a mixture of ice and water, the other junction strapped to the head of the temperature compensator so that it touches the specimen. The e.m.f.s. developed by the thermocouple are measured, corresponding to an accuracy of $\pm \frac{1}{2}^{o}K$, by a null potentiometer arrangement in which the e.m.f. is balanced against that from a 2v lead-acid cell. The null detector is a Tinsley galvanometer, with built in lamp and scale, and the accumulator voltage is standardised against a Weston-Cadmium cell. Thethermocouple was calibrated by using the following fixed points, the freezing point of mercury ($-39^{o}C$), the freezing point of carbon disulphide ($-112^{o}C$), and the temperature of liquid nitrogen. Auxilliary points used were the freezing points of carbon tetrachloride, and of ether. The temperature of the liquid nitrogen was checked by using an

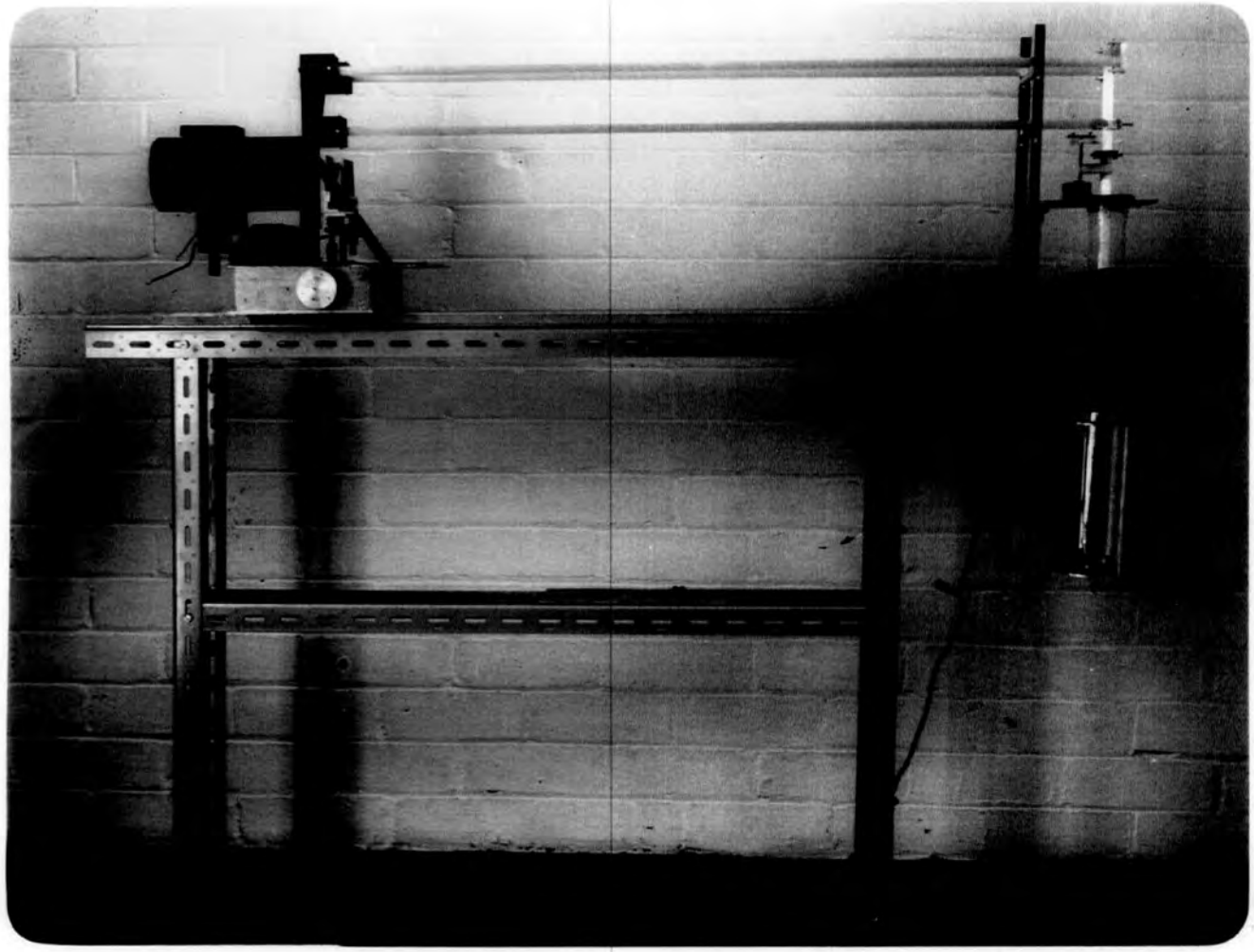

FIG. 13. Apparatus for the measurement of magnetostriction.

oxygen vapour pressure thermometer which is very sensitive in the range of 190° C to - 197 °C.

The mechanical lever is suspended in a pyrex tube, 5 cms diameter and 25 cms long, which for temperatures above - 160°C, contains iso-pentane. A vacuum flask containing liquid nitrogen surrounds the tube so that the bottom of the tube dips into the liquid nitrogen. By varying the height of the flask, different temperatures can be produced in the specimen. Below - 160 °C, the freezing point of iso-pentane, the pyrex tube is left empty, the top lightly packed with cotton wool, and the tube fully immersed in liquid nitrogen.

2.118 Remanent field and Electromagnet. With a pole gap of 20 cms, the remanent field at the centre of the magnet is 7 oersteds. This value varies over a short time interval after the application of a large field, but as the average time between taking measurements at different temperatures was about two hours, the remanent field was taken to be constant. The best method of resolving this difficulty would be to remove the specimen from between the pole pieces to a field free region between each measurement, but using the present measuring system this is impossible. The field was compensated by means of a pair of coils fixed to the sides of the vacuum flask slider (fig.13).

Figure 13 shows the arrangement of the apparatus. The mechanical lever is held at a fixed distance from the lamp holder assembly by means of three vitreosil rods, 13 mm square. Any part of the apparatus from which reflection may occur is painted matt-black. The whole of the optical path between the grids and the lever is enclosed in a light-tight

hardboard box, (not shown in the figure), and the grids, photo-cell and upper part of the lever are enclosed in matt-black aluminium covers.

The field in the magnet was measured by means of a search coil and a standard fluxmeter, with lamp and scale at a distance of 1.1 metres, giving a sensitivity of 7060 Maxwell turns / cm on the scale. Tests on the uniformity of the field in the centre of the gap, showed it to be uniform over the necessary volume. The magnet power pack incorporates a three phase rectifying unit with separate tappings for each current, the lowest value being 15 amps, i.e a field of 2895 oersteds. As it was desirable to have a variable supply at low fields, a separate power pack was used to give any field up to 3,000 oersteds.

The field found necessary to produce technical saturation at liquid nitrogen temperatures was 6,000 oersteds, determined from intensity of magnetization measurements. This gave rise to a field at the photo-electric cell, approximately 100 cms from the centre of the gap, of only 4 oersteds. This did not affect the cell, so no magnetic shielding was necessary.

2.12 Calibration and measurements. Trial measurements showed that the use of a split grid was unnecessary, as the extra sensitivity was not required. Two identical grids were then used, and the two halves of the split cathode coupled together. The output current was measured by a Tinsley galvanometer, type 4500 A, sensitivity 1200 m.m./μ A at one metre. Ideally, the output of such a system is of the form shown overleaf.

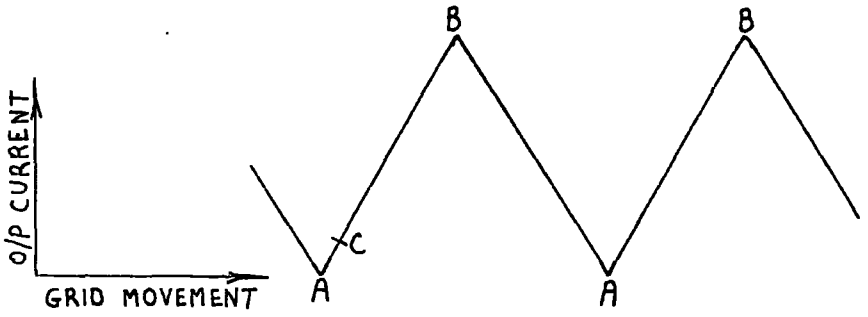

Points A correspond to cut off, B to full transmission. In practice, however, the turning points in the curve are not sharp, due to optical defects in the system, so for accurate measurements, deflections should always be on the linear portion of the curve.

When taking measurements, the lamp voltage is adjusted until a movement of the grids from cut off to full transmission gives a galvanometer deflection of about 50 cms. This lamp voltage is then used for all measurements. It was found impossible to produce a small displacement by an independant method to calibrate the system in situ The coupling to the system of anything rigid, e.g. cantilever or bellows arrangement, is impracticable, and the use of a temperature differential would tend to cause drift. The best method then available is to use the value of $\lambda 100$ at room temperature as a standard. Unfortunately this gives only one displacement, not a range, so it cannot detect any errors due to non linearity in the measuring system. If the turning points A,B show marked curvature, only a small portion of the curve will be linear, and the output corresponding to a large deflection will be constant no matter where the starting point on the curve. It is better to use a range of known displacements, and so it was decided to use the values of magnetostriction at low temperatures obtained by Corner and Hunt.

The method of taking measurements is as follows. The object grid is adjusted to a point such as C on the output curve, and the deflections noted over the whole range from zero field to that required to produce saturation. A curve of deflection against applied field is drawn, and the portion up to a field of 1,600 oersteds compared with the $\frac{\Delta L}{L}$, H curve (at the same temperature) obtained by Corner and Hunt. The value of λ is obtained by standardising the measured curve on the $\frac{\Delta L}{L}$, H curve. Between each measurement, the specimen is brought back to its reference state, i.e. the demagnetized state, by successive reversals of the applied field from a value sufficient to saturate the specimen, to zero.

At low temperatures, the vacuum flask is filled with liquid nitrogen, raised up round the tube containing the specimen, and after about a quarter of an hour, conditions are steady enough for measurements to be taken. Measurements of deflection against field are obtained as the specimen is allowed to warm up to 170 ^{o}K.

2.13 Intensity of Magnetization measurements.

2.131 Design of apparatus. For a full analysis, values of both magnetostriction and intensity of magnetization are required, so it was decided to make intensity of magnetization measurements on the same specimen as used for magnetostriction measurements. Hunt (1954) gives an expression for the flux linkage of a coil of finite dimensions with a uniformly magnetized prolate spheroid. If a coil of length 2 L, inner radius r_1 and outer radius r_2 is placed symetrically and coaxially round a spheroid of major axis 2 a and minor axis 2 b, then an approximate value

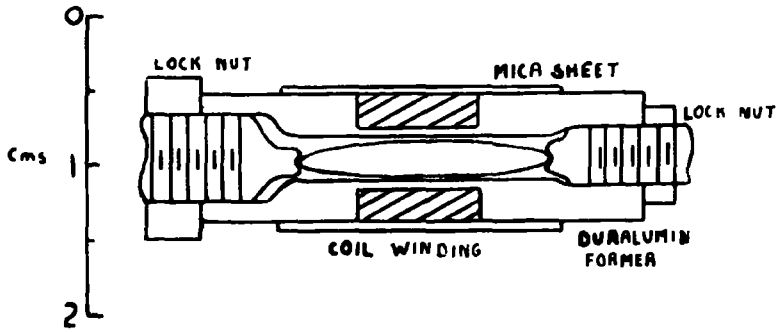

FIG. 14. The search coil for magnetostriction measurements.

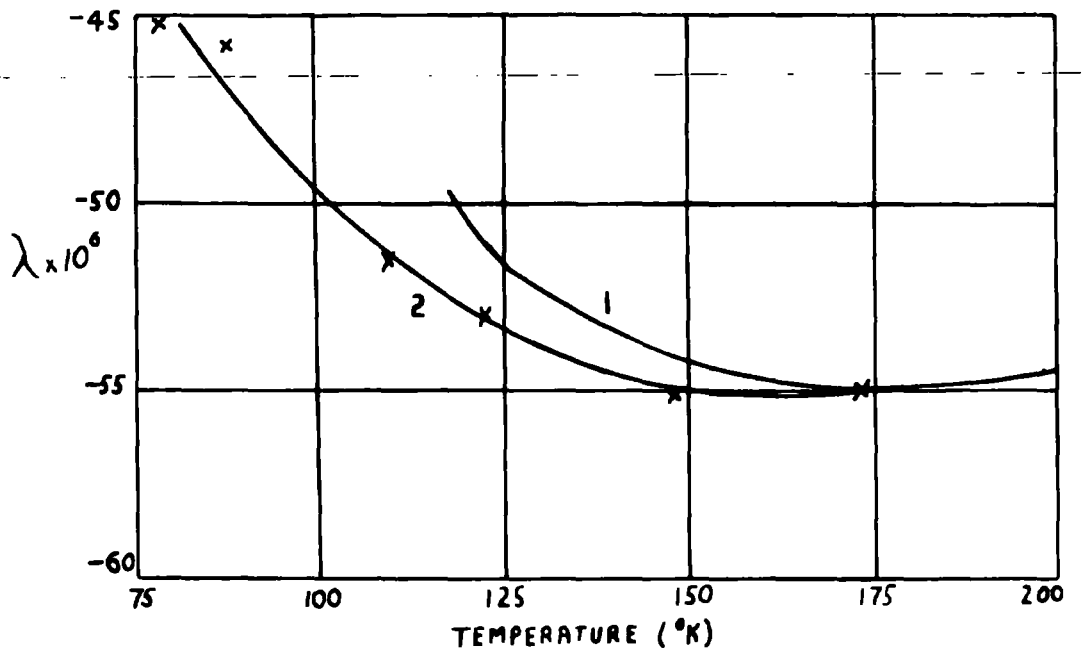

FIG. 15. Temperature dependence of saturation magnetostriction in the [100] direction.
(Curve 1. Corner and Hunt. Curve 2. Optical grid results)

of the flux linkage is

$$\frac{8\pi^2 b^2 I L n_1 n_2 (r_2 - r_1)}{e} \qquad (12)$$

where $e = \left(1 - \frac{b^2}{a^2}\right)^{\frac{1}{2}}$ and n_1 and n_2 are the numbers of turns per unit length parallel to and perpendicular to the axis. For the theory to apply, L must not be greater than $\frac{1}{4}$ the length of the spheroid, i.e. about 0.4 cms. The inside radius cannot be less than 0.25 cms as the former must encircle the specimen, and to ensure a good temperature distribution, the outside radius cannot be much greater than 0.5 cms. The fluxmeter available, has a sensitivity of 7060 Maxwell turns per cm when used with a lamp and scale at 1.1 metres. Assuming the scale can be read to $\frac{1}{2}$ mm, and to obtain $\frac{1}{2}\%$ accuracy, the flux linkage required is 7×10^4 Maxwell turns. Thus the diameter of the wire used in the coil must not be greater than about 0.024 cms, the former, (fig.14) is of duralumin, the windings 36 gauge anodised aluminium wire, in the central section of length 0.084 cms, and inner diameter 0.507 cms, there being 424 turns in 11 layers, the outer layer being flush with the former. The specimen is held in position by two brass screws passing through the end of the former.

The search coil measures changes in flux due to changes in both the intensity of magnetization of the specimen, and the field, so an auxilliary coil is used to compensate for field changes. For an ellipsoid, uniformly magnetized along its major axis, the field F parallel to that axis at points on the equatorial plane is given by (Peake and Davy 1953)

$$F = \phi \frac{4\pi a b^2}{(a^2 - b^2)^{\frac{1}{2}}} I \qquad (13)$$

$$\text{where} \quad \phi = \frac{1}{2} \ln \frac{(1+\theta^2)^{\frac{1}{2}} + 1}{(1+\theta^2)^{\frac{1}{2}} - 1} - \frac{1}{(1+\theta^2)^{\frac{1}{2}}}$$

where a and b = semi axes of the ellipsoid, I = intensity of magnetization. e = eccentricity of ellipsoid, $\theta = \frac{Z}{ae}$

For the specimen considered, $B = 0.3906\phi I$ so that for values of F less than 0.5×10^{-2} I, ϕ must be less than 1.28×10^{-2}, i.e. $Z > 2.8$ cms. This means that the compensating coil must be at least 3 cms away from the I measuring coil.

The compensating coil is of nearly identical dimensions to the I coil, having 521 turns in 13 layers, i.e. greater flux linkage, this enabling accurate compensation to be achieved by adjustment of a shorting resistor. A duralumin clamp, suspended by means of a 0 BA brass rod in the pyrex tube, holds the two coils at the desired distance apart. Low temperatures are produced by the same method as in the magnetostriction measurements. A thermocouple junction is strapped to the former of the I coil and the temperature measured by the potentiometer arrangement. The value of the shunt resistance needed at different temperatures is determined in a trial run with no specimen in the I coil.

2.132 Measurements. Hunt (1954) gives

$$I = \frac{H}{4\pi R \Delta H} \Delta I \qquad (14)$$

where I = intensity of magnetization in the specimen, H = applied field, ΔH = throw produced in fluxmeter with no specimen in coil, ΔI = throw produced in fluxmeter by establishing an intensity I in the specimen with the field throw compensated, R is a dimensionless factor dependant on the shape of the specimen and the search coil core. In this case, R = 0.112(5). $\frac{\Delta H}{H}$ is found by establishing known fields in the coil, and noting the fluxmeter deflection. At low temperatures, flux coil contraction makes

negligible difference to the linkage with the intensity of magnetization of the specimen. A correction is applied (0.5% / 100 ^{o} K) to compensate for contraction of the specimen.

The value of the intensity of magnetization corresponding to unit deflection is then given by

$$I = 26.4 \text{ cgs. units/ cm.}$$

2.14 Results. Table 3 shows values of $\frac{\Delta L}{L}$, and I at 78 ^{o} K, for various applied fields from zero up to that required to produce saturation. $\lambda 100$, Is,I values are set out in Table 4, and $\lambda 100$,T,together with Corner and Hunt's curve, shown in graphical form in figure 15.

Figure 15 seems to confirm the anomaly, but considerable doubt must be cast on the accuracy of these results due to the calibration process. If the turning points A,B, in the output curve (2.12) are not sharp, or if the mirror suspension (2.116) slips when the change in length of the specimen exceeds a certain amount, then the results obtained from this experiment must necessarily confirm the anomaly. As the temperature decreases, the change in length of the specimen in a constant applied field is smaller, so a calibration based on these values, assuming the above faults occur, gives results which decrease with decreasing temperature.

The critical test is to make measurements at liquid hydrogen temperatures, where, if the anomaly is present, $\lambda 100$ will show a marked decrease in magnitude. For very low temperature work, the cold chamber must be air tight, otherwise the liquid hydrogen would rapidly boil off. The present method of bringing out the displacement, a mechanical lever, cannot therefore be used. With this consideration in mind, it was

T A B L E 3.

Magnetostriction in the [100] direction at 78°K

Ha	$-\frac{\Delta L}{L} \times 10^6$	I	H
100	0	204	0
150	0.2	273	16
200	2.1	300	53
300	4.6	323	141
400	7.7	338	234
500	10.9	344	331
600	13.8	361	423
700	17.0	376	515
800	19.5	388	610
900	22.0	399	704
1000	24.4	411	798
1500	33.9	445	1281
2000	38.9	471	1778
2500	41.8	490	2259
3000	43.4	504	2752
3500	44.2	514	3247
4000	44.7	520	3744
4500	45.1	523	4242
5000	45.2	524	4742
5500	45.3	525	5241
6000	45.3	525	5741

T A B L E 4.

Temperature dependence of saturation magnetostriction.

T°K	$-\frac{\Delta L}{L} \times 10^6$	I
78	45.3	525
87	45.8	525
109	51.6	524
122	53.2	524
148	55.1	523
173	55.0	-

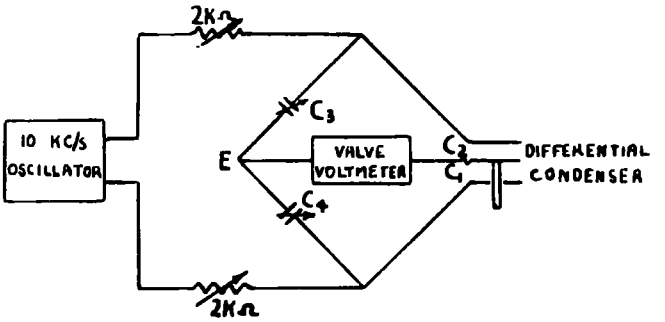

FIG. 16. Capacitance bridge network.

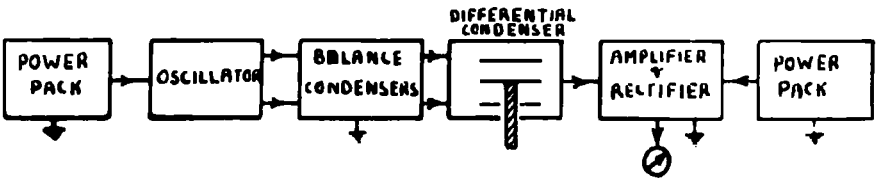

FIG. 17. Block diagram of extensometer circuit.

decided to construct a solenoid capable of producing fields large enough to saturate the specimen at 20 °K, and to use the capacitance bridge apparatus of Corner and Hunt to measure the magnetostriction. This was made possible by means of a grant to purchase a generator capable of delivering the necessary power.

2.2 Capacitance Bridge Method. The bridge was constructed by Corner and Hunt, so only a brief sketch, necessary to understand its working, is given here. A full description of the bridge is given in Hunt's thesis (1954).

In figure 16, if C_3 and C_4 are approximately equal, and a displacement is given to the middle plate of the differential condenser, the change in output voltage can be shown to be

$$dV' = \frac{V dt}{2}\left[1 + 4\left(\frac{\Delta t}{t}\right)^2\right] \qquad (15)$$

where V is the alternating voltage applied to the bridge, t the mean separation on each side of the differential condenser, Δt the difference between the separation of each side. Equation 15 assumes that $|R| \gg \frac{1}{\omega C_1} > \frac{1}{\omega C_3}$,where R is the input impedance of the amplifier, and $\frac{\omega}{2\pi}$ the frequency of the oscillator. Hence if the bridge is zeroed with C_3 and C_4 each within 5% of their maximum value

$$dV' = \frac{V dt}{2t} \qquad (16)$$

to within 1%.

The oscillator gives a peak to peak output of 100 V at a frequency of 10 kc/s, and with t about 0.01 cms, C_1 and C_2 are of the order of 150 p.F.

C_3 and C_4 are each 1000 pF, so R must be greater than 3 M. Under these conditions, the output voltage per cm. displacement is 5×10^{3} V.

The point E (figure 16) is at earth potential in order to reduce spurious pick up and give better stability in the valve voltmeter. This means that the oscillator output must be equally balanced about earth potential, and so the use of a push pull circuit is an advantage. This has the further advantage in providing less distortion than the single sided type. As the circuit which it drives is of sensibly constant impedance, the oscillator has no buffer stage. Due to stray capacitance, inductance, and resistance in the circuit, the output voltages from each arm of the oscillator are not exactly $\frac{\pi}{2}$ out of phase with each other. This fault is remedied by inserting a 2 K Ω resistor in each lead from the oscillator to the bridge. These resistors, together with the balancing condensers are mounted in a screening box. One of the balancing condensers is fitted with a Muirhead slow motion drive which allows the zero to be set with sufficient accuracy.

Figure 17 shows a block diagram of the extensometer circuit. The detecting circuit is comprised of a cathode follower, and a three stage amplifier followed by a rectifier. The cathode follower, input impedance 3.3 M Ω in parallel with 0.2 pF, provides the necessary high impedance, and is placed as near to the differential condenser as possible so as not to lower the impedance presented to the condenser. The amplifier has variable degrees of negative feedback, giving overall gains of 30,45,60 and 120, and the rectified output is displayed on a test meter of resistance 20,000 ohms/volt. This is normally used on the 12 volt range. To avoid any feed back between the amplifier and the oscillator, two

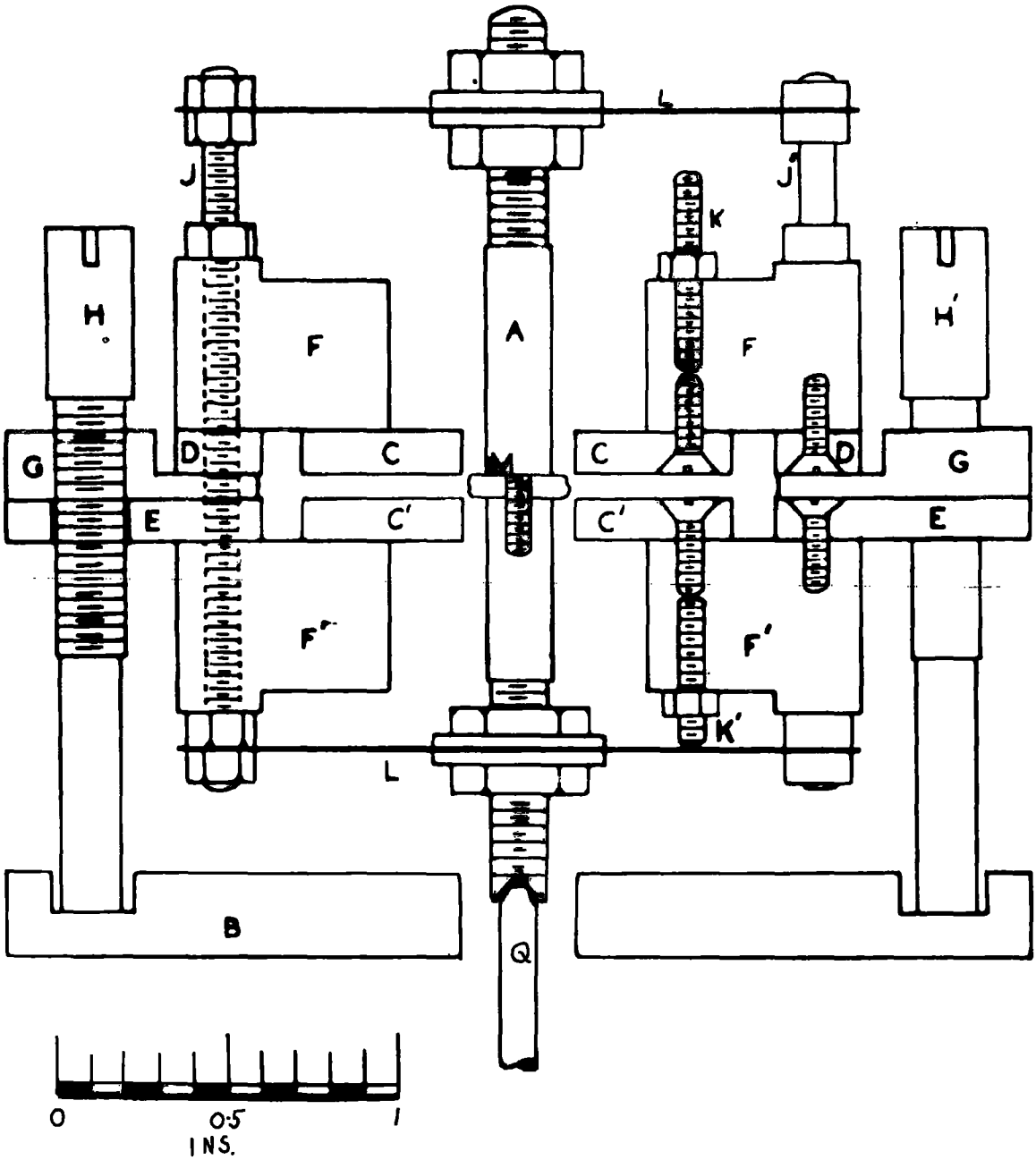

FIG. 18. The differential condenser.
(Note the 3-fold symmetry, H' and J' are not in the position shown)

separate power packs are used, both of which are stabilized to reduce mains voltage fluctuations to a minimum.

The circuit is normally used with one of the series resistors (figure 16) at zero, one of the balancing condensers at maximum, and the other, with the slow motion drive, within 5% of its maximum, the same conditions under which it is calibrated. One of the balancing condensers can be shunted by a 12 pF condenser to ensure that the bridge is working satisfactorily. When this is in circuit, it causes an output voltage, which for a given amplification should be constant.

2.21 The Differential Condenser. A cross section of the differential condenser is shown in figure 18. To minimise the effects due to fluctuations in the ambient temperature, the following parts are made of Invar, the three spacers G which maintain the correct distance between the fixed plates C, C′, and the three screws H which support the condenser. In the original condenser, the central rod A and the moving plate M (not fully shown in figure), were also made of Invar, but with the stronger fields used in this experiment it was impracticable to reduce the stray field sufficiently to avoid errors due to magnetostrictive strain of the plate, and so a brass plate was substituted. This produced no noticeable zero drift in the time interval required for magnetostriction measurements ($\sim \frac{1}{2}$ minute).

The plates C, C′ are mounted on Tufnol blocks which are separated from each other by brass rings D and E and the spacers G. Screws H, allow a vertical movement of the condenser of about 1 cm. Rod A is supported by two flexible plates of steel, L and L′, each 0.005" thick,

which are themselves held by the three screws J . These plates allow vertical movement of the rod A , but no lateral motion. In order to preserve the insulation of A and M , the flexible plates do not bear directly on A , but are held off by insulators. Since it is never possible to set the central plate exactly parallel to C and C′ , the separation varies from point to point, resulting in a slight increase above the calculated sensitivity.

Screws K and K′ bring out the leads from C and C′ , and A forms the connection from the moving plate. The flexible plates L,L′ are set at earth potential so that the plates C,C′ are well screened. Three screwed rods (not shown in figure) screwed in brass plate B pass through holes in ring E . The condenser is held firmly in position on the plate B by three rubber springs in compression on the three screwed rods. A quartz rod Q (ground to fit tightly in the end of rod A), which moves relative to B , transmits the small displacements to be measured to the condenser.

For equation 16 to hold, the differential condenser must be adjustable to within 5% of its plate separation. This corresponds to a rotation of any one of the three screwed rods H (40 turns /inch) of 1/120 of a turn, which is possible using a screwdriver. A movement of this order applied to any one of the three screws will not bring the condenser axis out of the vertical sufficiently to affect the accuracy.

2.22 Calibration. The extensometer is calibrated by displacing the central moving plate through known distances on the second lever of a double lever cantilever system. Using a OB.A. screw, it is possible to

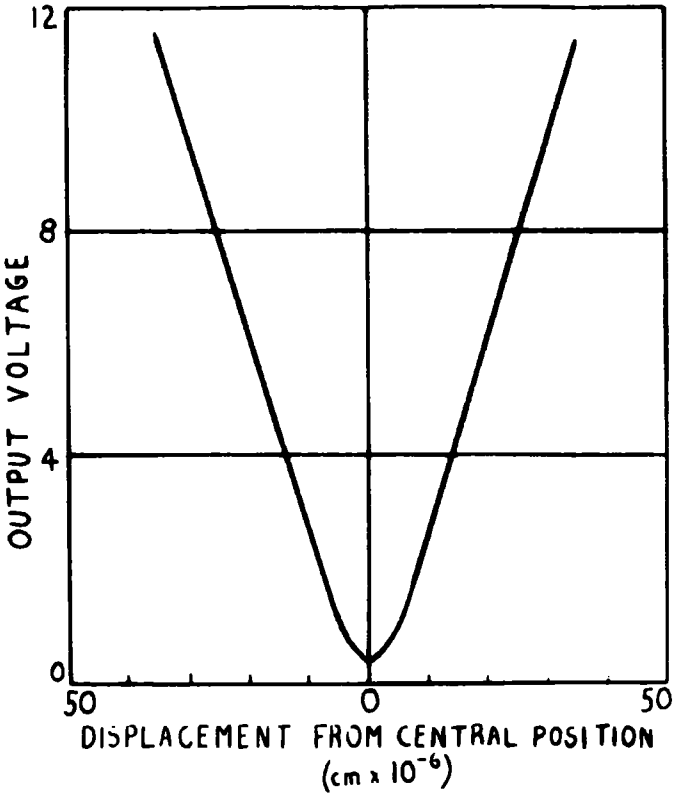

FIG. 19. Calibration graph for bridge network.

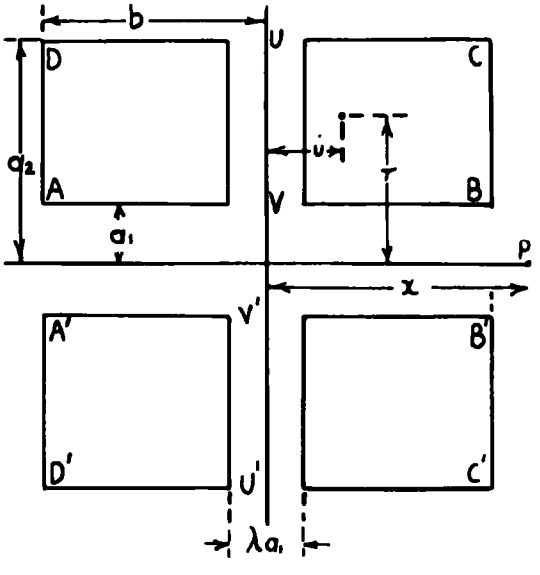

FIG. 20 Longitudinal section through solenoid.

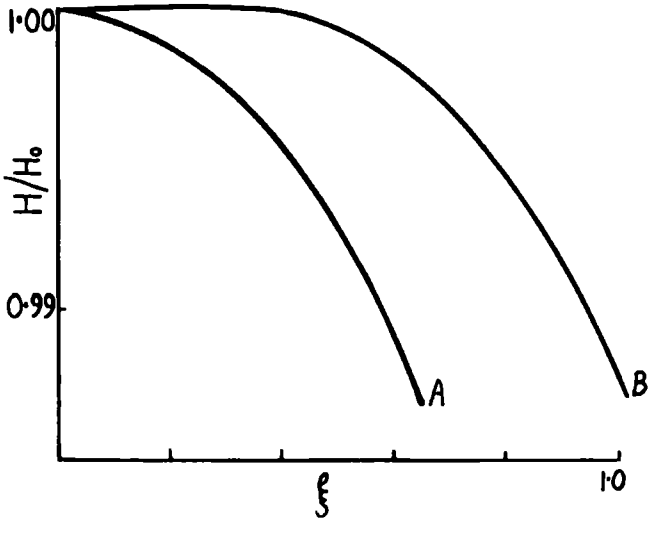

FIG. 21. H/H_0 as a function of ξ.
A, $\alpha = \beta = 3$, no gap.
B, $\alpha = \beta = 3, \lambda = 0.18$.

displace the end of the first cantilever a distance of 10^{-3} cms, giving a corresponding displacement of the end of the second cantilever of approximately 2×10^{-7} cms. The calibration of the cantilever itself is checked using an optical interference method. A lens and glass plate system, illuminated by sodium light, is mounted on the cantilever system so as to show Newton's rings. The screw movement is noted for the passing of each fringe, and the reduction ratio of the cantilever system calculated from a large number of readings. This ratio, $2.41 \times 10^{-4} \pm 0.2\%$, is used for the calibration.

Figure 19 shows a typical calibration graph for the bridge. Changes in output voltage vary linearly with displacement of the central plate of the differential condenser over the range 2 V to 12 V. There is a slight change in sensitivity when the condenser is dismantled and reassembled due to the slight variation in the average gap which is produced. When this is done, the instrument is recalibrated. No change in sensitivity has been detected after assembly. The stability of the sensitivity depends on (eqn.16) keeping constant both the applied voltage and the gap on either side of the central plate of the condenser. The use of power packs with output stabilized to $\pm$ 0.2% for both oscillator and amplifier enables the sensitivity to be maintained with the same order of constancy. The gap width is kept constant by eliminating temperature gradients in the condenser. The use of Invar in the construction of the condenser minimises this effect. A Mu-metal box encloses the condenser, serving the dual purpose of magnetic and temperature shielding.

The two steel flexible plates (L,L' figure 18) which hold the central plate in position, oppose the displacement of the central plate. This

restoring force is calculated to be 2.6×10^{6} dynes / cm displacement, and causes a systematic error in the condenser calibration, and an error in the magnetostriction measurements. The error introduced on the calibration beam is approximately 10^{-3} d, where d is the displacement to be measured, and so the error can be neglected. The error introduced by compression of the displacement rod (length 30 cm, diameter 0.3 cm) in the magnetostriction measurements, is 1.6×10^{-3} d and again can be neglected.

2.23 Solenoid. The field necessary to produce technical saturation in the [100] specimen is about 5,000 oersteds at 70 °K, and 7,000 oersteds at 20 °K (Bozorth 1951). Allowing a safe margin in these values, the selenoid is designed to produce fields of up to 10,000 oersteds. The power is obtained from two Lister Diesel generators, each capable of giving 120 amps at 100 volts.

The design of the solenoid is based on one described by Daniels (1950). The basic theory of solenoids for the production of large magnetic fields has been worked out extensively for various shapes of coils (e.g.Cockroft 1928, Bitter 1936). The field H (oersteds) at the centre of a coil with a rectangular section winding space is given by

$$H = G\left(\frac{W\eta}{a_1\rho}\right)^{\frac{1}{2}} \qquad (17)$$

where W is the power (watts) dissipated in the coil, a_1 (cms) the inner radius of the winding space, ρ (ohm cm) the resistivity of the winding material, G a dimensionless factor depending only on the shape of the winding space, η the ratio of the volume of the winding space occupied by the conductor to the total volume of winding space. The maximum value of

G is 0.179, when the outer radius of the winding space is $3a_1$, and the axial length $4a_1$.

Approximately, W = 44,000 watts, $\rho = 2 \times 10^{-6}$ ohm cm, $a_1 \sim 3$ cms, $\eta \sim 0.75$, G ~ 0.15, giving a field H ~ 11,000 oersteds. The heat produced is removed continuously by passing cooling water through the coil. As the mains water is of variable conductivity and purity, distilled water is used as the coolant, and the distilled water cooled by mains water in a heat exchanger (2.24). The winding material can consist of either bare copper strip, adjacent turns being separated from each other, or copper tube. The former is used as it gives a higher "filling factor" η (eqn.17).

2.231. Theory. The solenoid was intended for use in obtaining saturation values of magnetostriction, so the field distortion over the specimen length, 2 cms, at the centre of the solenoid can be of the order of 0.1 %. The axial length of the solenoid is approximately 20 cms in order to keep the distance between the specimen and the differential condenser to a reasonable value.

To obtain the required field uniformity, a gap is left at the centre of the rectangular winding space, making a system similar to a Helmholtz double coil. In figure 20, the field at point P on the axis of the coil is approximately equal to that due to the rectangular section ABCD, minus that due to the region omitted, annulus U V.

Let λa_1 = width of section omitted, $a_2 = \alpha a_1$, $b = \beta a_1$, $x = \xi a_1$, γ = uniform current density flowing in the coil (e m u / cm^2). The field,

H, at P is given by

$$H=\int_{u=-b}^{+b}\int_{r=a_1}^{a_2}\frac{2\pi r^2\gamma}{\left[r^2+(x-u)^2\right]^{\frac{3}{2}}}\,dr\,du-\int_{a_1}^{a_2}\frac{2\pi r^2(-\lambda a_1\gamma)}{(r^2+x^2)^{\frac{3}{2}}}\,dr.$$

$$=2\pi\gamma a_1\left[(\beta-\xi)\left\{\sinh^{-1}\frac{\alpha}{|\beta-\xi|}-\sinh^{-1}\frac{1}{|\beta-\xi|}\right\}+(\beta+\xi)\left\{\sinh^{-1}\frac{\alpha}{\beta+\xi}-\sinh^{-1}\frac{1}{\beta+\xi}\right\}\right]$$

$$-2\pi\gamma a_1\lambda\left[\sinh^{-1}\frac{\alpha}{\rho}-\sinh^{-1}\frac{1}{\rho}-\frac{\alpha}{(\alpha^2+\rho^2)^{\frac{1}{2}}}+\frac{1}{(1+\rho^2)^{\frac{1}{2}}}\right]^{\frac{1}{2}}$$

If ρ is small, and for a uniform field $\left(\frac{\alpha^2 H}{\alpha\rho^2}\right)_{\rho=0}=0$

i.e. $$4\left[\frac{\beta^{-4}}{(1+\beta^{-2})^{\frac{3}{2}}}-\frac{\alpha^3\beta^{-4}}{(1+\alpha^2\beta^{-2})^{\frac{3}{2}}}\right]+3\lambda(1-\alpha^{-2})=0 \qquad (18)$$

If $a_1\sim 3$, and $2b\sim 20$, $\beta=3$.

When $\alpha=\beta=3$, $\lambda=0.18$. This gives a field uniformity well within the required limits (figure 21). The value used was $\lambda=0.19$ which gives a maximum theoretical field distortion within the central 2 cms of the solenoid of 0.03%.

The total resistance of the copper strip used for winding the solenoid was made equal to the optimum resistance of the generators connected in series, i.e. 0.85Ω. This is a small value so care was taken in the construction of the solenoid to keep any contact resistance due to soldering to a minimum. Adjacent turns of copper strip are separated from each other by winding nylon filament, 0.3 mms diameter, round the strip, with a pitch of 0.5 cms. This allows ample room and presents practically zero impedance to the flow of cooling water.

2.232 Construction. The minimum diameter of Dewar that allows a reasonable amount of cooling agent round the specimen and associated

FIG. 22. Photograph of pancakes assembled on centre tube.

apparatus is 2 $\frac{1}{8}$", giving the effective inside diameter of the solenoid of 2$\frac{1}{2}$". This diameter then fixes the axial length and outside diameter of the solenoid.

The solenoid consists of 22 flat coils, or " pancakes ", wound with copper strip $\frac{1}{4}$" x 17 gauge. The nylon thread was wound round the copper strip, using a simple mechanical arrangement. The inner end of the strip is soldered onto a thin brass tube, 2$\frac{1}{2}$" O/D, 2$\frac{7}{8}$" I/D, length $\frac{1}{4}$", using a low contact resistance solder. Electrical contact between pairs of these tubes is made by soldering a thin $\frac{1}{4}$" strip of brass across the gap between the tubes. The winding of the strip onto the tubes was done by hand. The final $\frac{1}{2}$" of the last layer is bent backwards over itself and soldered onto another length of copper strip. This strip is wrapped once round the outside layer and then soldered onto itself, thus holding the layers of the pancake in position. Pancakes are insulated from each other by thin paxolin wheels, 1/16" thick, with 8 spokes, 2-3 mms width, to present as little impedance as possible to the flow of cooling water. The gap in the centre of the solenoid is produced by using a thicker tufnol wheel, similar wheels being used at either end of the solenoid to provide collecting spaces for the cooling water.

The pancakes, when wound, are in pairs, insulated from each other by a paxolin wheel. The centre tube of the solenoid consists of a brass tube, 10$\frac{1}{4}$" long, O/D 2$\frac{3}{8}$", I/D 2$\frac{1}{4}$". A few layers of 200 gauge Melinex polyester film are wrapped round the tube for insulation, and the double pancakes slipped on the tube, with a paxolin wheel placed between each pair. Electrical connection is made between adjacent pairs of pancakes on the outside by soldering a small piece of copper strip across the two outside

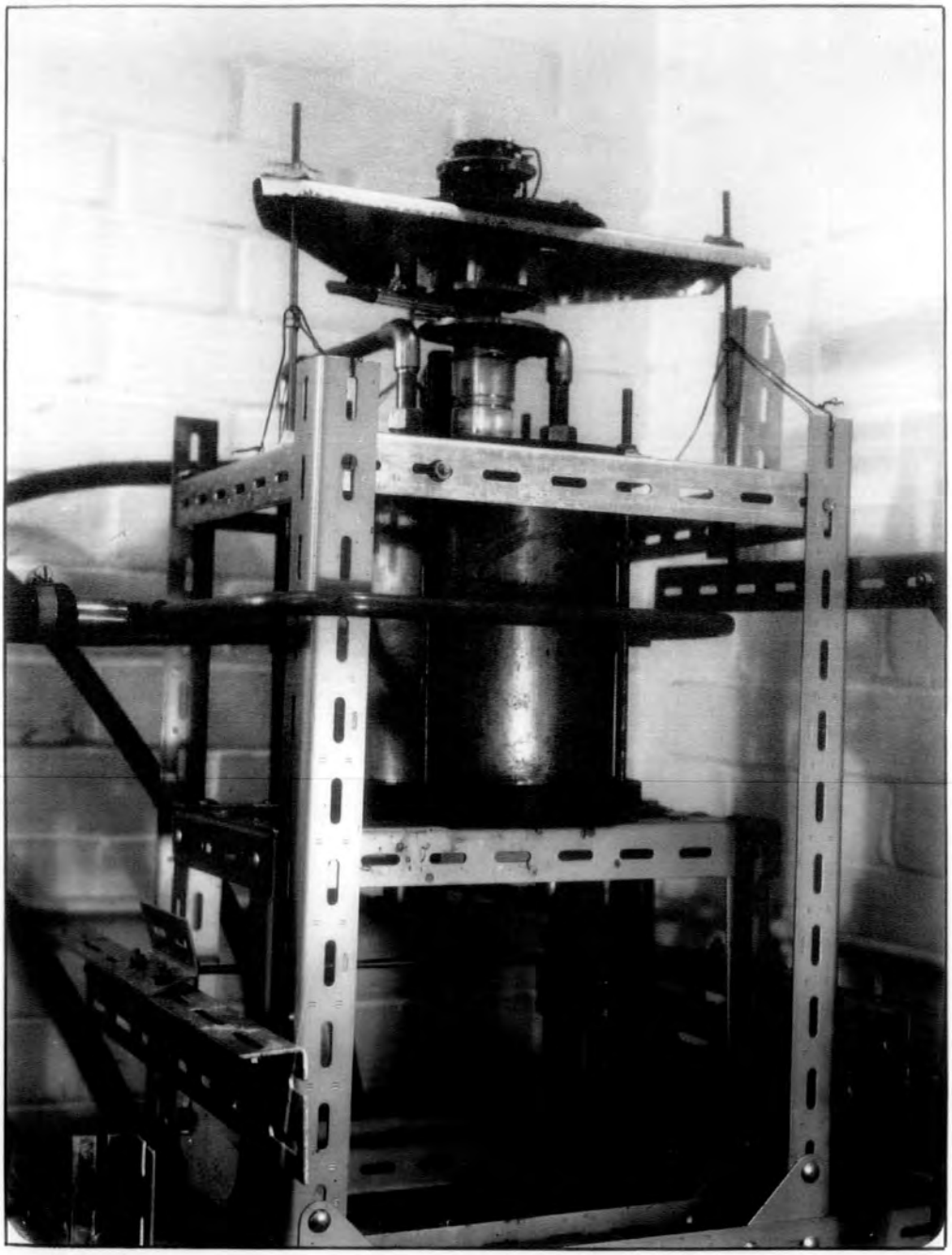

FIG. 23. Photograph of solenoid with magnetostriction measuring apparatus assembled in position.

layers of each pancake. Further layers of Melinex are wrapped round the outside of the pancakes until it is just possible to push the assembly into the outside cylinder of the solenoid, a brass tube 9" long, $8\frac{1}{2}$" O/D x 10 gauge. Figure 22 is a photograph of the pancakes assembled on the centre tube, and figure 23 a photograph of the solenoid with the apparatus used for measuring magnetostriction assembled in position. The end cheeks of the solenoid are $\frac{3}{4}$" thick Tufnol, held together by six long steel rods, $\frac{1}{4}$" diameter, screwed at the ends. The cooling water enters through $\frac{1}{2}$" pipes at three inlets at the middle of the solenoid, and leaves at two outlets on each end cheek. All joints connected with the solenoid are made water tight with Gaco rubber rings. Power is supplied to the solenoid through two terminals, one in each end cheek. The terminals are $\frac{1}{2}$" diameter brass rod, and connection is made to the end pancakes by soldering a copper strip from the inside of the terminal to the outside rim of the pancake.

2.24 Heat Exchanger. The pump available delivers 20 gallons per minute against a pressure of 1 atmosphere. The surface area of the copper strip available for cooling purposes in the solenoid is very nearly equal to the total surface area of copper used, so that heat transfer inside the solenoid must be highly efficient. Thus it can be assumed that the power applied to the solenoid is effectively applied to the cooling water for calculation purposes.

A power consumption of 50 K W will cause an increase in temperature of the circulating distilled water of about 10° C. McAdams (1933) gives

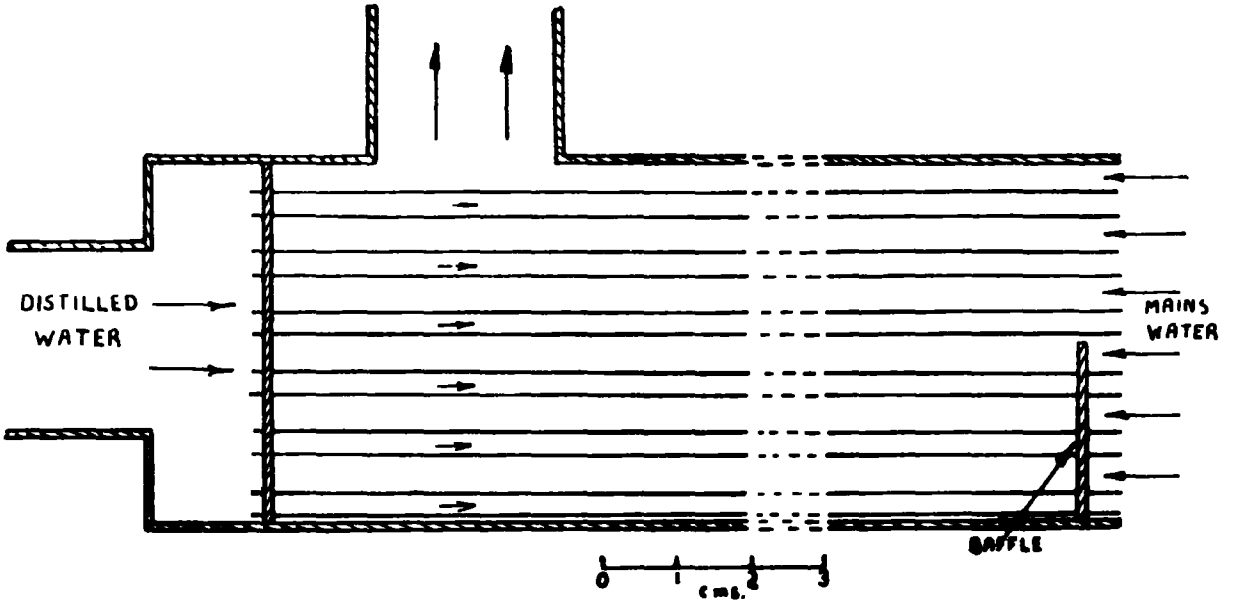

FIG.24. Cross section through heat exchanger.

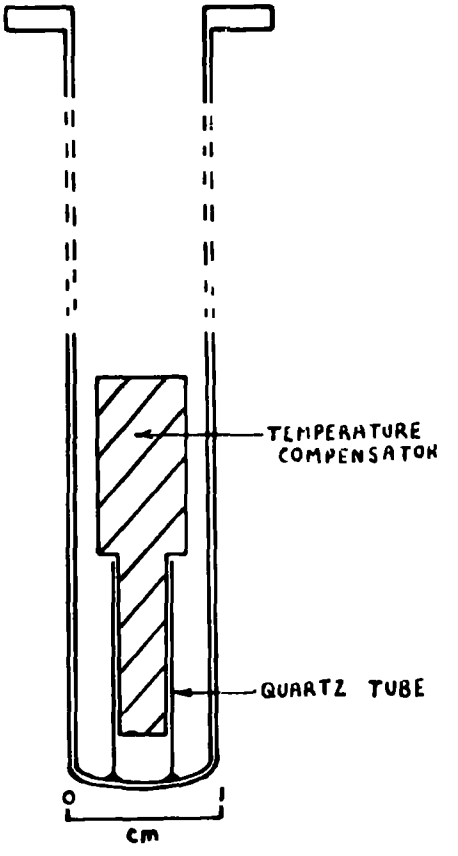

FIG.25. Specimen holder.

the heat transfer coefficient, h, for turbulent flow of water inside a pipe as

$$h = \left[\frac{(5.6 + 0.058\,t)(G)^{0.8}}{D^{0.2}}\right] (B.t.u./hr.)(sq.ft)(^{o}F) \quad (19)$$

where D = inside diameter of pipe in inches, G = weight velocity of water ((lbs/sec)(sq.ft)), and t = water temperature in ^{o}F. Using an $\frac{1}{8}$" diameter pipe, a flow of 20 gallons / min (i.e. turbulent flow), and with t $\sim$ 80 ^{o}F, equation 19 gives h = 4.75 x 10^{4} (B.t.u./ hr.)(sq.ft.) (^{o}F). Thus if the average temperature difference between the surface of the solid and the body of the liquid is $\sim$ 10 ^{o}F, then the **total** heat transferred through unit surface of the solid is 4.75 x 10^{5} (B.t.u./hr.)(sq.ft.) i.e. $\sim$ 170 watts /cm . With 50 K.W. applied to the solenoid and assuming efficient heat transfer to the distilled water, the total cooling surface area needed in the exchanger is 300 sq.cms. As it is impossible to achieve these ideal conditions in practice, the exchanger is designed to give a much larger cooling surface ($\sim$ 2,000 sq.cms) than calculated.

The exchanger consists of twenty five, $2\frac{1}{2}$ ft. lengths of $\frac{1}{8}$" inside diameter copper tube packed inside a 3 ft. long, 2" 1/D brass outer tube (fig.24). The tubes and connecting pipes are all hard soldered into position. Four quadrant baffles are soldered at regular intervals inside the main tube to ensure turbulent flow of the mains water.

2.25 Performance. The field produced by the solenoid was measured using a search coil and fluxmeter of sensitivity 7060 Maxwell turns/cm with lamp and scale at 1 metre. The field is linear with solenoid current,

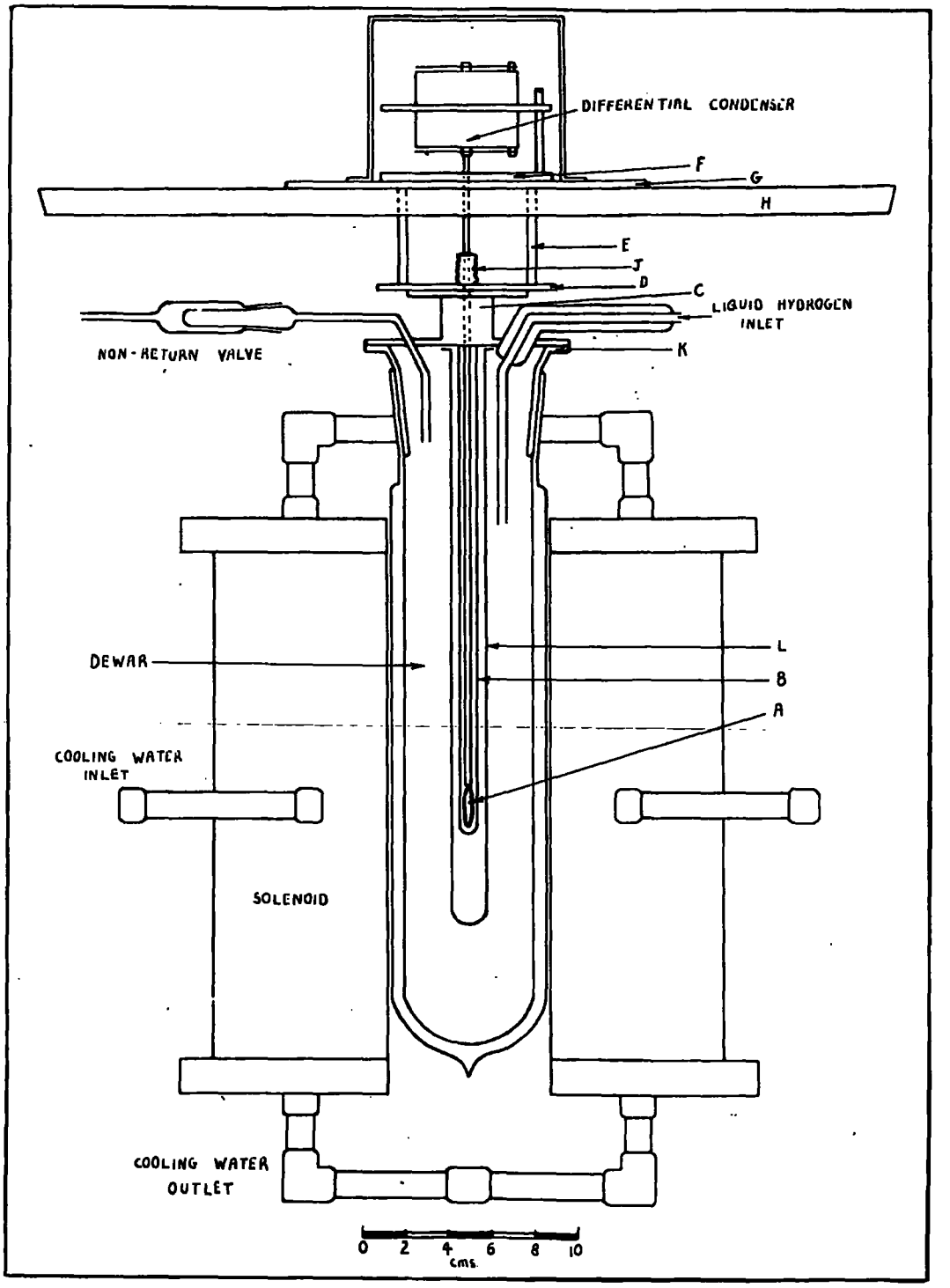

FIG.26. General arrangement of apparatus for the measurement of magnetostriction.

the maximum current of 250 amps. producing a field of 10,500 oersteds. Two identical search coils were used in opposition to measure the field uniformity. These showed 0.3 % difference in the field between the centre of the solenoid and a distance of 1 cm along the axis from the centre. This distortion is larger than that predicted by the calculations, but still within that required for the experiment. The increase in distortion is probably caused by a non uniform winding density in the coils.

2.26. Specimen holder and general arrangement of the apparatus. The specimen is mounted in an aluminium thimble to compensate for thermal expansion (similar to the one used in 2.115), which is supported by the top face of a small quartz tube fused to the bottom of the main quartz tube (fig.25). This face is ground parallel to the ground flanged top of the main quartz tube, and perpendicular to the axis of the tube itself.

The general arrangement of the apparatus is shown in figure 26. The specimen A rests in an aluminium temperature compensator (not shown in figure), and is held in the quartz tube B, the flanged top of which is held firm in the central brass tube C by two brass collars and fibre washers. The differential condenser is separated from the brass plate D by three quartz rods E. Brass plate F actually consists of two plates and the upper ends of the quartz rods E pass through holes in the bottom plate and press against the top plate. The legs of the differential condenser pass through holes in the top plate and press against the bottom plate. Thus the legs of the condenser and the quartz rods bear onto the plate F at the same level and so the thermal expansion of F is effectively eliminated. The system is firmly held against plate F by three screwed

rods (not shown in figure) which are screwed into plate F and into collars fixed on plate D.

G is an $\frac{1}{8}$" thick mild steel plate which is used as the base plate for magnetic shielding. This plate is mounted on an aluminium frame H, which is itself supported by three vertical brass O B A rods (not shown in figure) on the Handy Angle support surrounding the solenoid (figure 23).

The change of length of the specimen is coupled to the condenser by a twin bore quartz rod. This rod is also used to take out the thermocouple leads, the thermocouple junction being in contact with the specimen. In order to stop ice forming round the displacement rod and restricting its movement at the point where it leaves the cold chamber, a small bellows J is soldered onto plate D. A brass collar soldered to the top of the bellows holds a rubber " O " ring against the displacement rod, the bellows being slightly extended so as to hold the rod firmly against the specimen. Above 80° K this is found to be unnecessary. The inlet tube for the liquid hydrogen, and outlet tube for the hydrogen gas are of Pyrex, and are sealed in position with Araldite. The space between the outside tube and inside tube of the inlet tube is pumped down to a pressure of 10^{-5} mm. Hg, and then sealed off. The outlet tube for the hydrogen gas is a conventional non-return valve.

A B-45 pyrex cone is attached to the brass disc K with Araldite. This allows a vacuum tight joint with the B-45 socket of the Dewar vessel.

The apparatus assembled in the solenoid is shown in figure 23. The solenoid is mounted on a Handy Angle framework which rests on a galvanometer pillar. The specimen holder and associated apparatus is

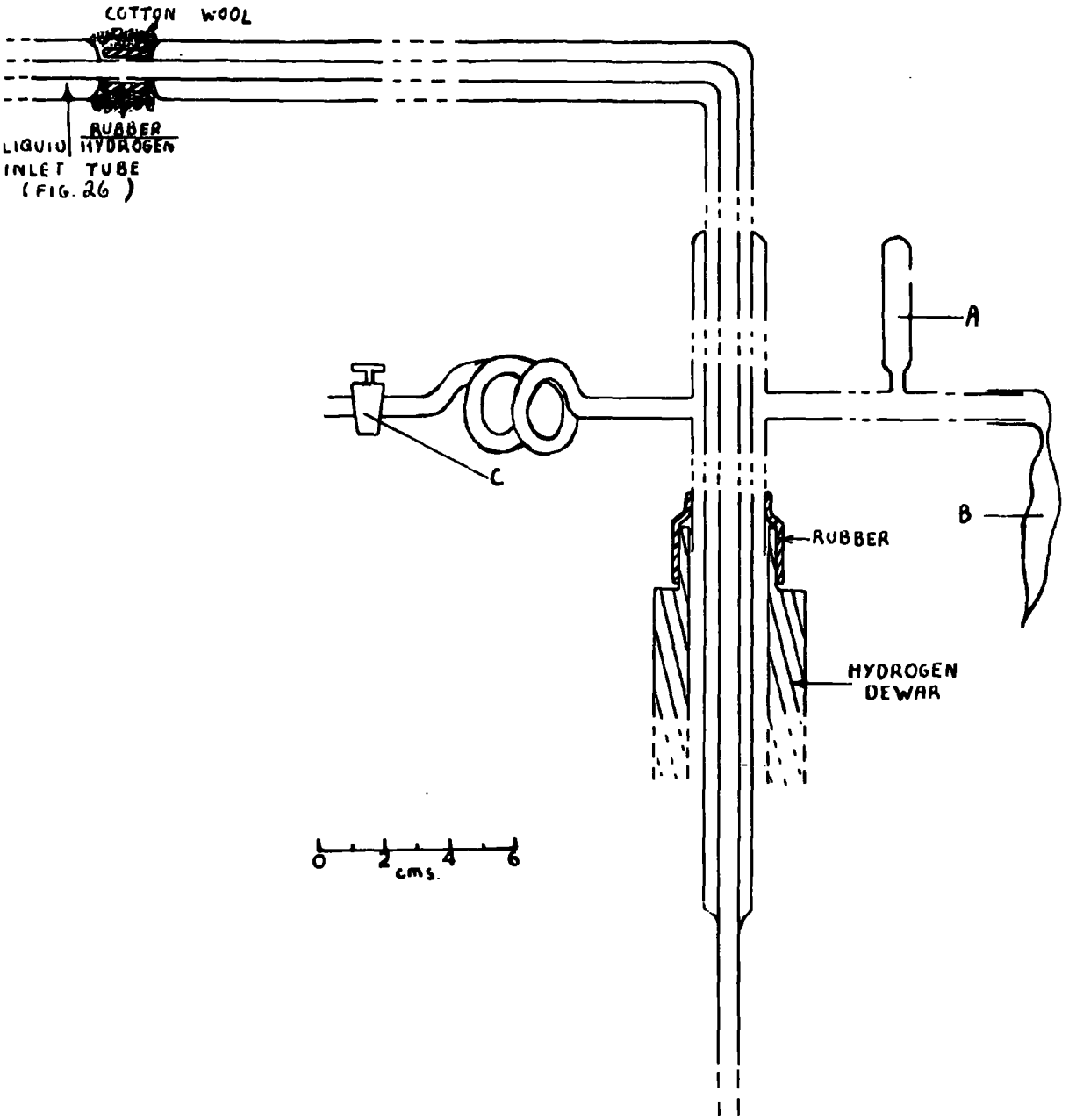

FIG. 27. Liquid hydrogen transfer apparatus.

mounted on a separate Handy Angle framework which is bolted, using Sorbo rubber as washers, to the galvanometer pillar. This arrangement does not transmit any of the vibrations caused by the water circulating in the solenoid to the displacement measuring apparatus. The vibrations transmitted to the solenoid from the water pump are reduced to a minimum by firmly bolting the pump to the laboratory floor.

2.27. Method of producing temperature variation. Temperatures above 300 ^{o}K were obtained by filling the Dewar with Silicone Liquid MS 550 and heating the liquid by means of a heating spiral placed inside the Dewar. A copper-constantan thermocouple was used over the whole range of temperatures, the e.m.f.s. being measured by a bridge arrangement (2.117) to an accuracy corresponding to $\pm \frac{1}{2}$ ^{o}K. Temperatures from 80 ^{o}K to 300^{o} K were produced by filling the Dewar with liquid nitrogen and allowing this to boil away, measurements being made as the apparatus warmed up to room temperature. It was found necessary to fix a Pyrex tube (L) (fig.26) round the central quartz tube to stop the vibrations caused by the boiling of the liquid nitrogen from being transmitted to the displacement rod. The lowest temperatures were produced by filling the Dewar, previously cooled to 80 ^{o}K, with liquid hydrogen obtained from Liverpool University.

The Pyrex apparatus used for transferring the liquid hydrogen from the storage Dewar to the displacement measuring apparatus is shown in figure 27. The space between the central transfer tube and its outer jacket is pumped down to a pressure of 10^{-5} m.m.Hg, and then sealed off. A is a safety valve, B a football bladder, and C a tap at a fixed distance

away from the main tube so as not to freeze up. The end of the transfer device is joined to the inlet tube of the displacement measuring apparatus by a section of pure rubber, and the junction covered with cotton wool. To transfer the liquid hydrogen, tap C is closed, the hydrogen gas pressure builds up due to boiling of the liquid hydrogen, causing the football bladder to expand. The bladder is compressed by hand, forcing hydrogen gas down into the storage Dewar, which in turn forces the liquid hydrogen up through the transfer system.

2.28 Experimental Procedure. The electronic bridge circuit became sufficiently steady for accurate measurements to be made within about 10 minutes of switching on. Room temperature measurements were made each day before the temperature of the system was varied to provide a check that the apparatus was working correctly. Then, for low temperatures, the Dewar was filled with liquid nitrogen and the temperatures of the system allowed to settle. This usually took about $\frac{1}{4}$ hour. The differential condenser was zeroed and the correct working of the bridge verified by switching in the 12 p.F. condenser in the balance arm. Measurements were then made of the output voltage of the bridge corresponding to various currents through the solenoid up to that required to produce technical saturation. Similar measurements were repeated as the apparatus warmed up to room temperature. Between each set of measurements, the specimen was demagnetized.

For very low temperatures, the specimen was initially cooled down to 80°K before the liquid hydrogen was introduced. Conditions were steady enough at 20°K to allow a number of measurements of saturation

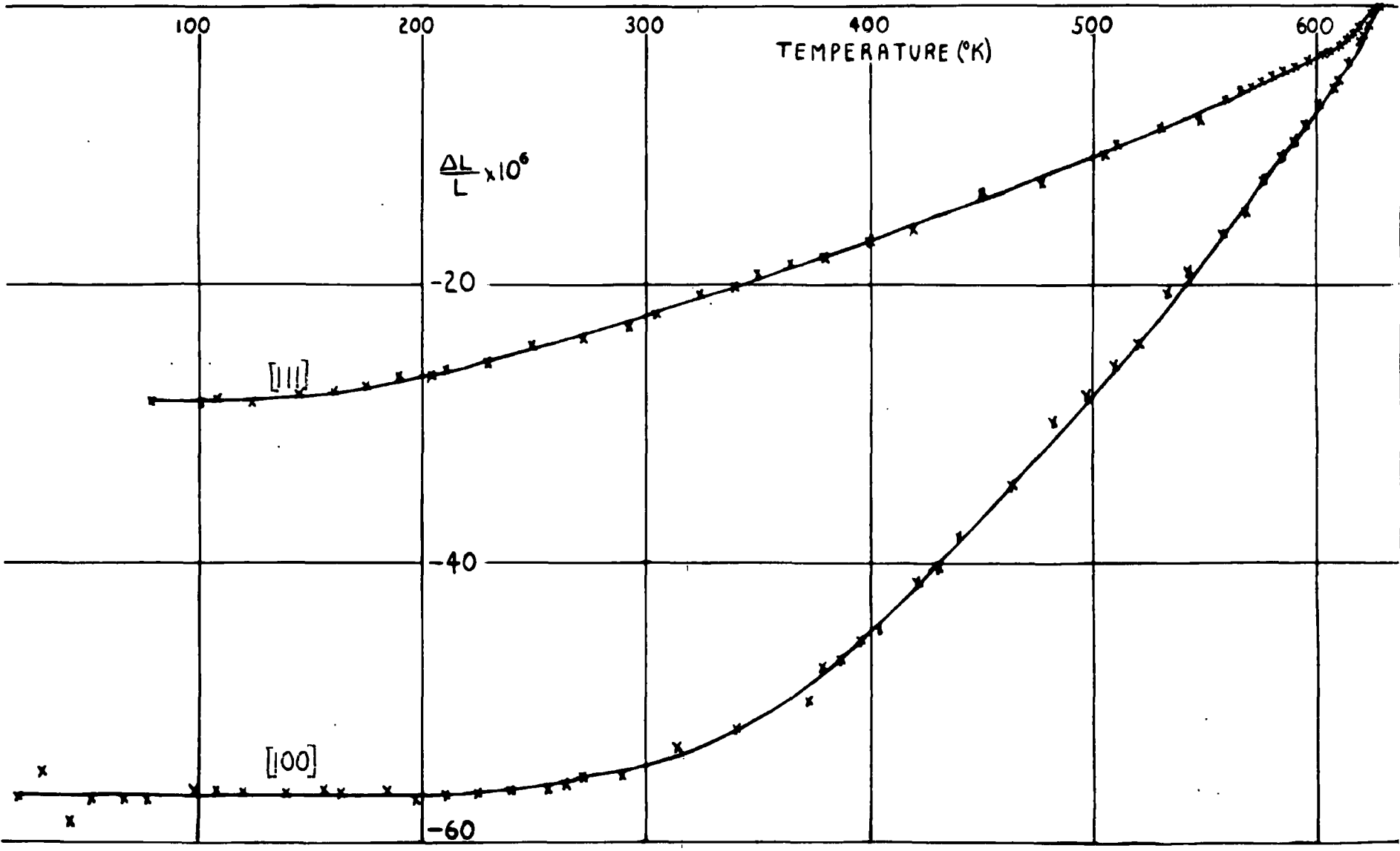

FIG. 28. Temperature dependence of saturation magnetostriction in the [111] and [100] directions.

magnetostriction to be made. These were repeatable to within 1%. From 20°K to about 50°K however, the rise in temperature was quite rapid, causing very unsteady conditions. These are reflected in the scatter of the points between these two temperatures in fig. 28. Above 50°K there was a slow steady increase in temperature, allowing accurate measurements of magnetostriction to be made.

Conditions were quite stable for high temperature measurements, though above 600°K, the Silicone liquid gave off a large amount of vapour, and tended to cause some zero drift.

It was possible to obtain a complete set of magnetostriction measurements at reasonable temperature intervals in any one of the above temperature ranges, ie 20°K - 300°K or 300°K - 630°K, in one day. A series of runs were made to obtain a large number of points on the T curves, and so increase their accuracy.

For the sake of completeness, it was decided to obtain a λ 111, T curve over practically the same temperature range as the λ 100, T curve.

2.29 Results. Values of magnetostriction in applied fields from zero up to that required to produce technical saturation were obtained in the [100] direction from 20°K to 630°K, and in the [111] direction from 78°K to 630°K. The saturation values of the magnetostriction are tabulated in table 5, and shown in graphical form in figure 28. As the general shape of the $\frac{\Delta L}{L}$, H curves is the same for all temperatures, values of $\left(\frac{\Delta L}{L}\right)_{100}$, H are given for one temperature only (table 6). The reason for choosing this temperature is that the values are needed for comparison with those obtained by the optical grid method (2.14).

TABLE 5.

Temperature dependence of saturation magnetostriction in the [100] and [111] directions.

[100]

T °K	21	28	44	53	68	78	99	109	121	140
$-\lambda \times 10^6$	56.8	55.0	58.6	57.0	57.0	57.0	56.3	56.3	56.5	56.5
T °K	157	165	186	198	212	226	241	257	265	273
$-\lambda \times 10^6$	56.2	56.4	56.4	57.0	56.7	56.5	56.3	56.2	55.8	55.3
T °K	291	315	342	373	379	388	397	405	423	432
$-\lambda \times 10^6$	55.2	53.1	51.9	48.0	47.3	46.9	45.5	44.8	41.3	40.3
T K	441	464	483	498	511	521	534	543	558	568
$-\lambda \times 10^6$	38.0	34.4	29.8	28.0	25.9	24.3	20.6	19.0	16.4	14.8
T K	576	584	591	595	602	608	610	614	619	621
$-\lambda \times 10^6$	12.5	11.1	9.8	8.5	7.2	5.9	5.4	4.0	2.7	2.2
T °K	662	623	624	627						
$-\lambda \times 10^6$	1.7	1.4	1.2	0						

TABLE 5.

Temperature dependence of saturation magnetostriction in the [100] and [111] directions.

[111]

T °K	78	101	108	124	145	161	176	190	205
$-\lambda \times 10^6$	28.4	28.5	28.2	28.4	27.9	27.7	27.3	26.5	26.5
T °K	212	230	250	273	293	305	325	340	350
$-\lambda \times 10^6$	26.1	25.6	24.4	24.0	23.1	22.2	20.8	20.2	19.3
T °K	365	380	401	420	450	477	505	511	530
$-\lambda \times 10^6$	18.6	18.1	16.9	16.1	13.5	12.4	10.8	10.0	8.7
T °K	548	559	566	571	575	581	585	590	597
$-\lambda \times 10^6$	8.3	6.9	6.1	5.9	5.5	5.0	4.6	4.3	3.9
T °K	603	606	610	613	617	619	621	624	628
$-\lambda \times 10^6$	3.5	3.3	2.8	2.4	2.0	1.7	1.3	0.45	0

TABLE 6.

Magnetostriction in the [100] direction at 78 °K.

Ha	200	400	600	800	1000	1500	2000
$-\frac{\Delta L}{L} \times 10^6$	2.0	8.0	13.4	18.6	23.6	34.0	43.4
Ha	2500	3000	3500	4000	4500	5000	6000
$-\frac{\Delta L}{L} \times 10^6$	51.8	55.6	56.4	56.7	56.8	57.0	57.0

The field required to produce technical saturation in the [100] direction is 5,500 oersteds at 78°K and 7,500 oersteds at 20°K.

Before the results are discussed it is important that an estimate of their overall accuracy be made. An estimate of the accuracy of one measurement relative to another was made by stripping and re-assembling the apparatus, and then repeating the measurements. Saturation magnetostriction measurements were repeatable to within 1% of the value at room temperature, magnetostriction measurements to within 3% of the saturation value at room temperature. The increase in the relative uncertainty of the $\frac{\Delta L}{L}$, H over the λ measurements is most probably due to the method of making the measurements. It required two operators for $\frac{\Delta L}{L}$, H measurements because of the poor control by the governors on generator output, one to work the governors, the other to note the corresponding bridge output voltage. Thus there must be some error introduced due to the timing mechanism between the two operators.

A combination of an uncertainty in the effective length of the specimen for magnetostriction measurements, the angles between the crystallographic axis, the ellipsoid axis, the solenoid axis , and possible errors associated with the calibration, cause an uncertainty of not more than $\pm$ 5% in the overall accuracy. There is also uncertainty in the measurements due to using the demagnetized state as the reference state. This must be greater in the [111] direction than in the [100] direction, since in the former the specimen axis is one of the easy directions of magnetization and the demagnetizing effect will tend to produce magnetization along this axis. This is not the case in the [100] direction where the eight directions of easy magnetization are all equally directed with respect to the specimen axis.

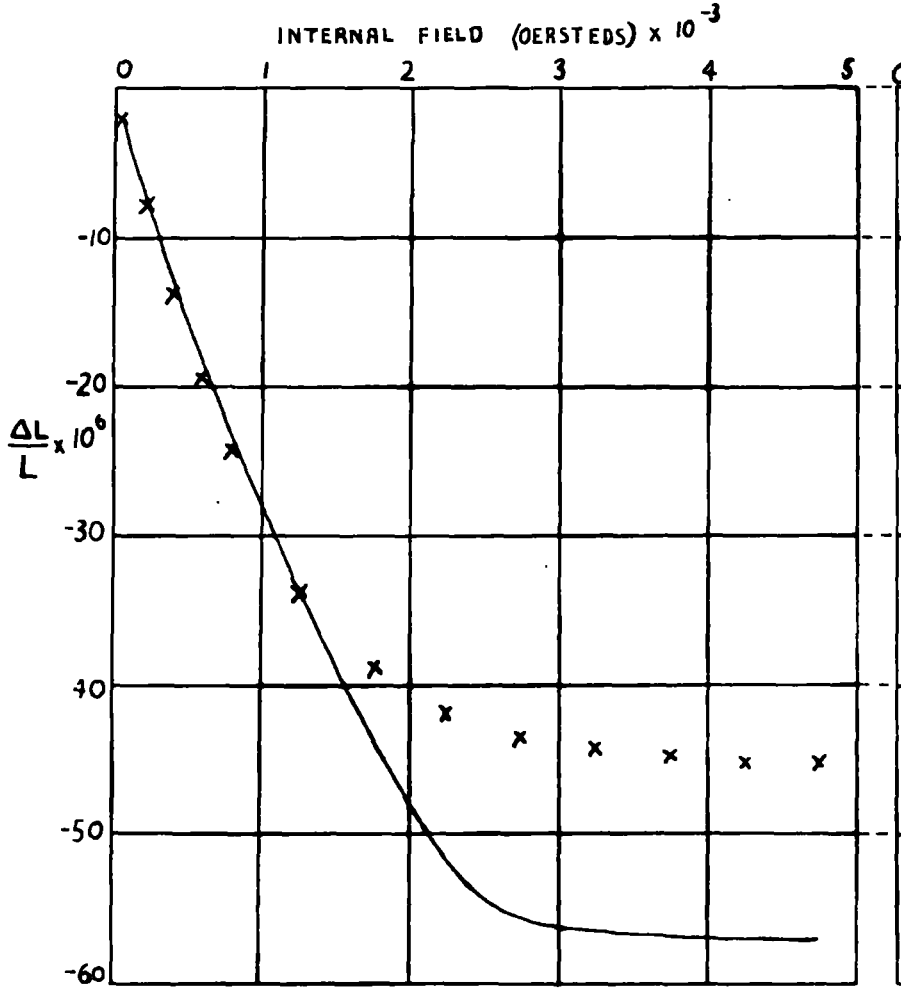

FIG. 29. Magnetostriction in the [10C] direction as a function of magnetic field strength. (Full curve, capacitance bridge results: X optical grid results)

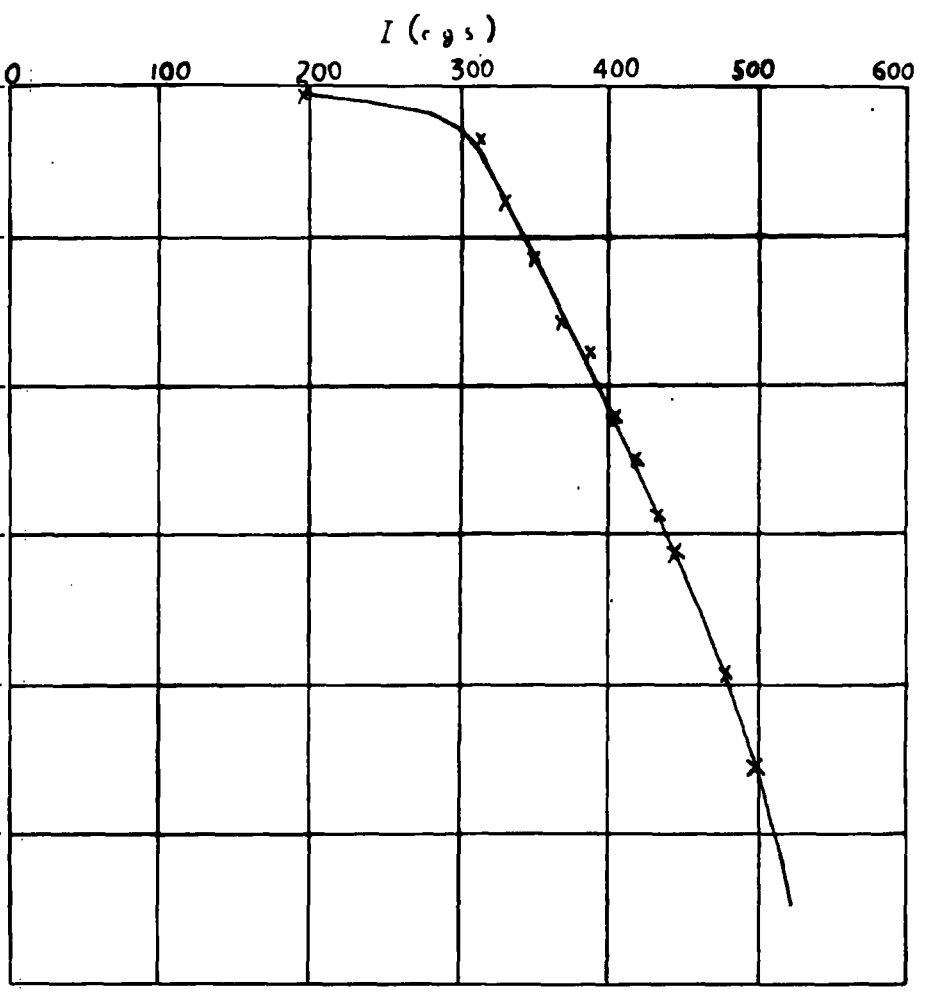

FIG. 30. Variation of magnetostriction with intensity of magnetization in the [100] direction at 112° K.

2.210 Discussion. A comparison between the λ_{100}, T curves of this experiment (fig.28), and of the optical grid method (fig.15), confirms the doubts expressed about the results in the latter (2.14) The mirror suspension must have started to slip once the lever arm had moved a certain distance, and so it is inevitable that the results obtained, using a calibration based on magnetostriction measurements at different temperatures, should confirm the anomaly. The results obtained in low fields, ie. the fields used by Corner and Hunt, agree in both experiments. This is shown in figure 29 in which are plotted the respective values at 78°K, the lowest temperature at which measurements were made using the optical grid method. The results, then, obtained from the optical grid method must be considered unreliable, and the discussion that follows is concerned solely with those results obtained using the capacitance bridge method.

Above 150°K values of λ_{100} agree within experimental error with those of Corner and Hunt, and there is little difference in the general trend of the λ_{100}, T curves, but below 150°K the value of λ_{100} is constant. It is over this region that Corner and Hunt had to use extrapolated values. The discrepancy between their results and the present ones is due to their method of extrapolation. This is shown by considering figure 30 which is a plot of their values of intensity of magnetization, I, against magnetostriction at 112°K, the lowest temperature at which results are available. It is possible to draw a curve through these points, assuming I_s = 523 c.g.s. units from the [111] specimen, giving $\lambda_{100} = -55 \times 10^{-6}$, a value consistant with the present results.

The general trend of the λ_{111},T curve follows that of Corner and Hunt, but the absolute values of λ_{111} are 20% higher. This is most probably due

to the effect of stress on the specimen. When the differential condenser is dismantled and re-assembled, a different setting of the centre plate will result in a change in the value of the stress applied to the specimen. This effect should be more pronounced when applied to a specimen in an easy direction of magnetization, an increase in compression causing a decrease in the value of the magnetostriction.

Forces applied to the top of the moving plate of the condenser give the values of λ_{111} and λ_{100} shown in table 7.

Table 7.

Variation of saturation magnetostriction with force in [111] and [100] directions

Force(gms.wt.)	250	350	450	750	950
$-\lambda_{111} \times 10^6$	23.1	22.5	21.6	19.1	17.5
$-\lambda_{100} \times 10^6$	55.2	55.2	55.2	55.7	52.0

These results take into account the fact that a force of 250gms.wt. is required to move the centre plate from one fixed plate to the other. They show that an increase of 200 gms.wt. in the force applied to the [111] specimen from the differential condenser will bring both sets to within experimental error of each other.

From figure 28 it is seen that the λ,T curves are becoming parallel to the T axis at low temperatures, and a reasonable extrapolation to absolute zero may be made. This gived $\lambda_{111} = -28 \times 10^{-6}$ and $\lambda_{100} = -57 \times 10^{-6}$ which are of the same order as those calculated by Fletcher ($\lambda_{111} = -44 \times 10^{-6}$ $\lambda_{100} = -187 \times 10^{-6}$).

It should be possible from λ, T and Is, T variations to obtain an estimate of the relative contributions of spin-spin and spin-orbit coupling

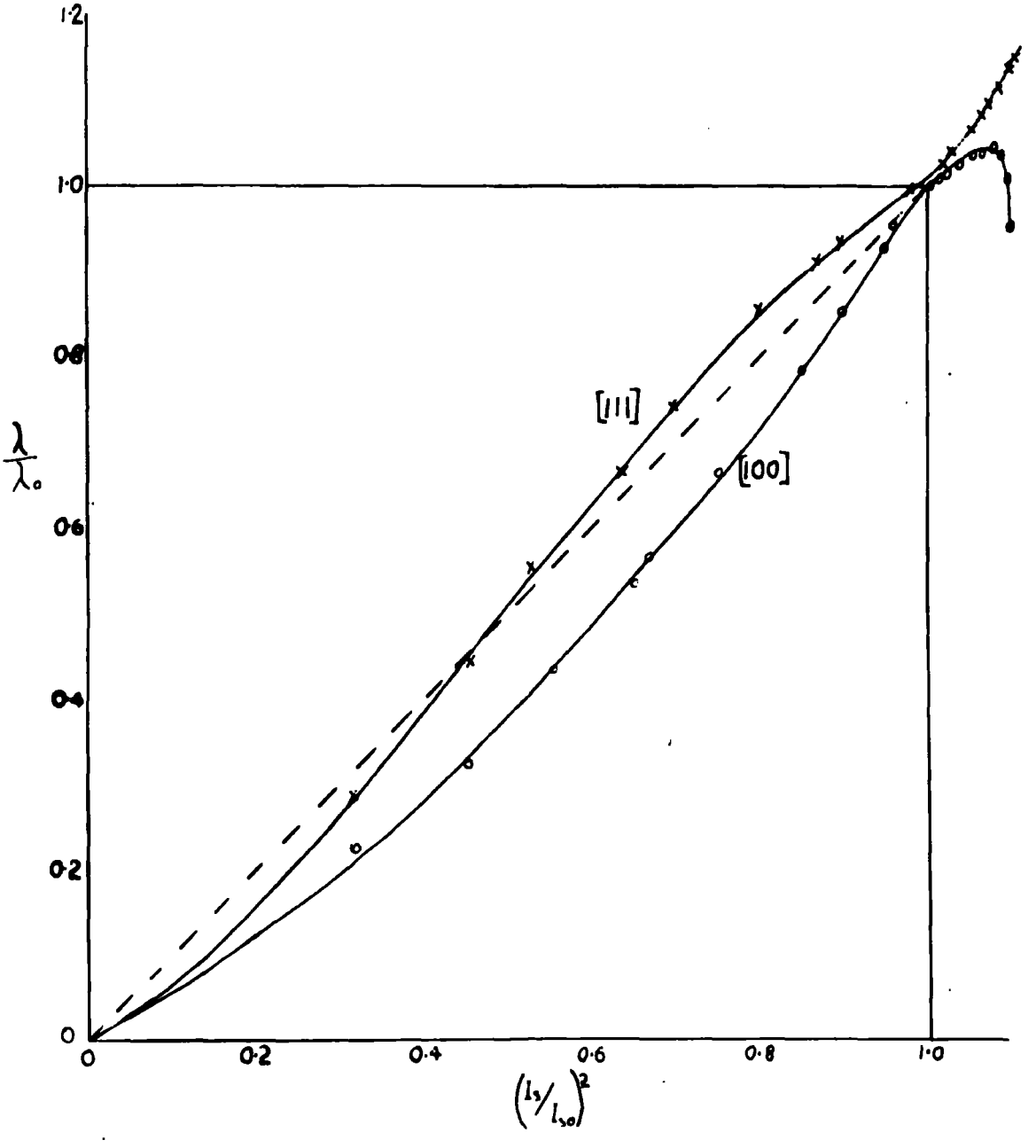

FIG.31. Saturation magnetostriction as a function of saturation magnetization. Both parameters reduced to values at 0° C. (Hunt 1954)

to the magnetostriction. Hunt (Thesis 1954) plotted values of $\frac{\lambda}{\lambda_0}$ against $\left(\frac{I_s}{I_o}\right)^2$, and obtained the difference between the experimental curves and the theoretical curve $\frac{\lambda}{\lambda_0} = \left(\frac{I_s}{I_o}\right)^2$ (fig.31). This difference has no direct significance as the theoretical curve used should have been $\frac{\lambda}{\lambda_0} = K\left(\frac{I_s}{I_o}\right)^2$, where K is a term containing the elastic constants of nickel. The change in the slope of the curve will make a large difference to the deduced contribution of spin-orbit coupling to the magnetostriction

It has been suggested that Vonsovsky's equation (1.312) could be used to separate the two effects. This can be written in the form

$$\frac{\lambda}{I_s^2} = -\frac{K}{L}\left\{A - B\left[\frac{1}{C}\left(1 - e^{-\frac{C}{KT}}\right) - \frac{1}{4D}\left(1 - e^{-\frac{D}{KT}}\right)\right]\right\} \qquad \text{(i)}$$

where K, A, B, C, D are temperature independant constants, and L is the elastic constant. As Vonsovsky himself states, this equation is only a preliminary attempt to deduce a qualitative explanation of the discrepancy between the experimental results and the elementary classical theory of magnetostriction of Becker and Akulov, so nothing more than general agreement between the equation and the experimental results can be expected.

Assuming C~D (eqn. i)

$$\frac{\lambda}{I_s^2} = -\frac{K}{L}\left(E + F e^{-\frac{C}{KT}}\right) \qquad \text{(ii)}$$

where $F \sim \frac{B}{C}$. C and D are energy terms which contain the energy difference, the electrostatic interaction, exchange integral, and transfer integral between s and p electrons. No measurements of the temperature variation of the elastic constant, L, appear to have been made for nickel, but measurements have been made on copper which has a similar band structure, and these show that approximately L decreases linearly with increasing temperature.

Thus according to equation (ii) the $\frac{\lambda}{I_s^2}$, T variation should be similar to a $T.e^{-\frac{C}{KT}}$, T variation superimposed on a term which increases linearly with

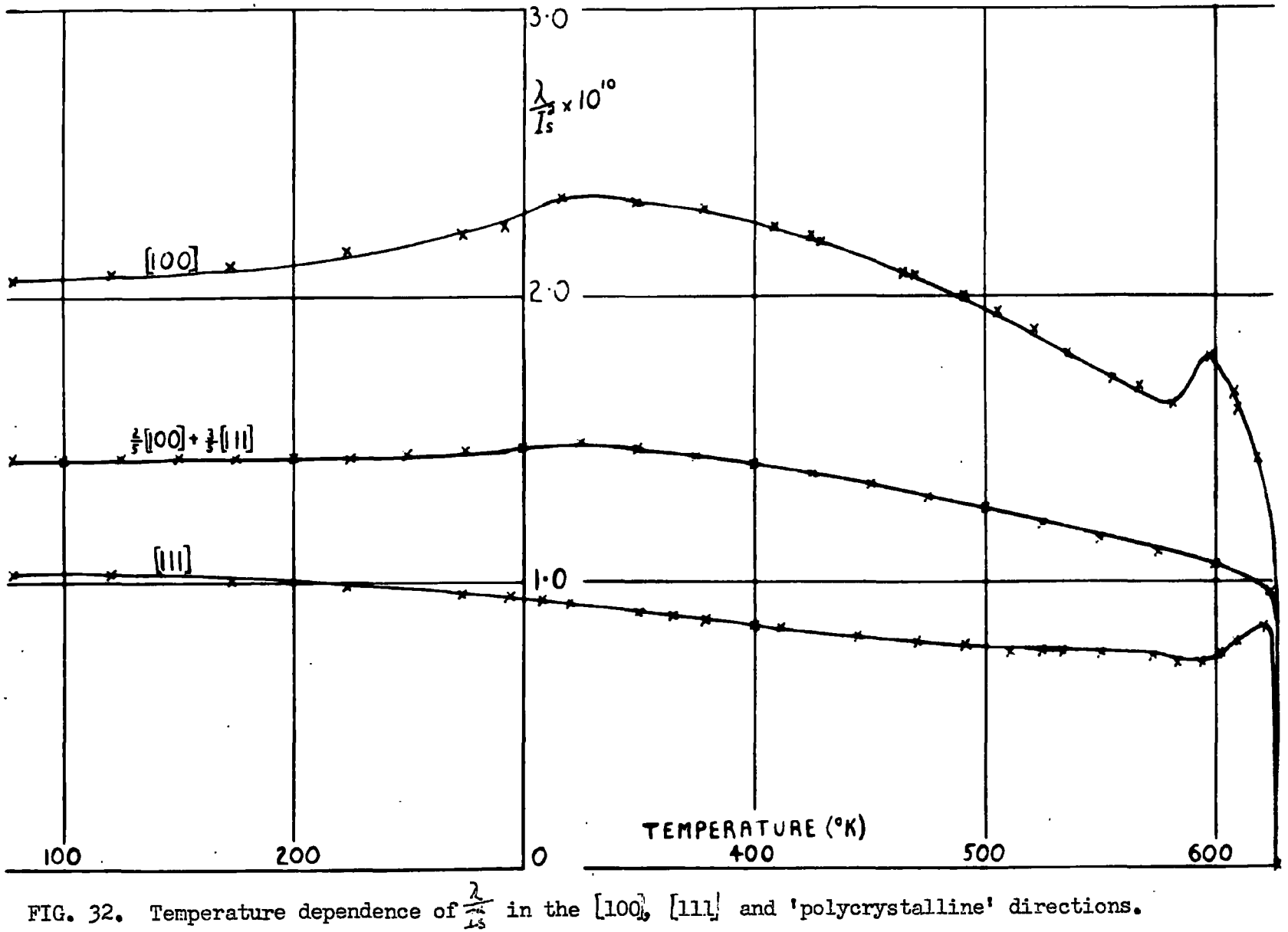

FIG. 32. Temperature dependence of $\frac{\lambda}{I_s^2}$ in the [100], [111] and 'polycrystalline' directions.

increasing temperature. Vonsovsky gives $C \sim 10^{-12}$ ergs, i.e. $\frac{C}{k} \sim 7 \times 10^3$ Assuming $\frac{C}{k}$ can have values between 10^3 and 10^4, the temperature variation of $T.e^{-\frac{C}{kT}}$ is shown below

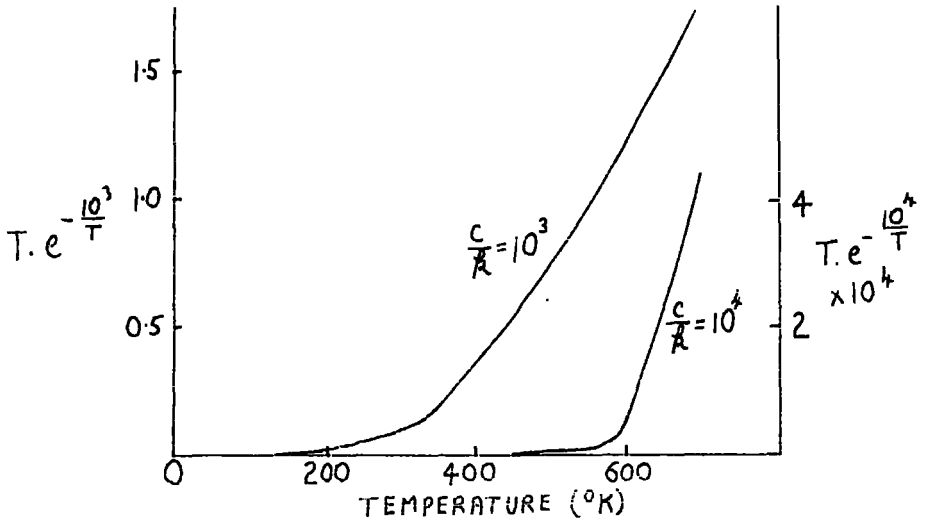

E (eqn ii) is positive, and with C~D, F is positive, so the final curve is the same as that shown above but with the axes turned through the appropriate angle.

Figure 32 shows a plot of $\frac{\lambda}{I_s^2}$, T in the [100], [111] directions, and for a polycrystalline sample calculated from the formula

$$\lambda_p = \frac{3}{5}\lambda_{111} + \frac{2}{5}\lambda_{100}$$

The intensity of magnetization had been previously measured (2.13) from 78°K to room temperature, and as the results agreed to within 1% with those of Corner and Hunt, the latter values are used over the whole range in obtaining figure 32. Both the experimental λ, T, and I_s, T curves are very nearly parallel to the T axis at 78 °K, so it is safe to assume that the curves in figure 32 can be extrapolated back to 0 °K.

At 627 °K, the Curie point, $\lambda \to 0$ before $I_s \to 0$, giving $\frac{\lambda}{I_s^2} = 0$. The I_s values were obtained in applied fields of 300 oersteds so it is probable

that the true I_s value, i.e. in zero applied field, is less than the measured value for that particular temperature, and $\frac{\lambda}{I_s^2}$ may tend to some non zero value at temperatures approaching the Curie point.

The experimental curves of $\frac{\lambda}{I_s^2}$, T in figure 32 are quite different from the type given by Vonsovsky's equation, though agreement can hardly be expected when even at 0 ^{o}K, experimental and theoretical values of only agree to within a factor of 2 or 3. Vonsovsky's equation does not represent the experimental results and so it is impossible to use it as a basis for estimating the degree of spin-spin, and spin orbit coupling to the magnetostriction.

The trend of the $\frac{\lambda_p}{I_s^2}$, T curve agrees with that obtained by Doring(1936) who investigated the variation above 273 ^{o}K. The reason why the curve is a straight line over such a large temperature range, 400 ^{o}K, is simply due to the opposing slopes of the $\frac{\lambda}{I_s^2}$, T curves in the [100] and [111] directions.

Chapter 3

THE TEMPERATURE VARIATION OF THE MAGNETOSTRICTION OF GADOLINIUM

CHAPTER THREE

THE TEMPERATURE VARIATION OF THE MAGNETOSTRICTION OF GADOLINIUM.

3.1 Introduction. Gadolinium, a member of the rare earth group of metals, is known to be ferromagnetic with a Curie Temperature of 290° K (Trombe 1937). This metal is known to have a saturation magnetization very nearly equivalent to the parallel alignment of 7 electron spins per atom. Since there are 7 electrons in the incomplete 4 f band, it seems probable that these are the carriers of magnetic moment in gadolinium. The element is thus a simple type of ferromagnetic compared with the more common elements in which the magnetization is equivalent to a non-integral number of spins per atom.

In the common ferromagnetics, ferromagnetism is associated with an incomplete group of d electrons. The d band, though narrow compared with the s band (Slater 1936) is still of considerable width, so that intra and inter-atomic interactions may be comparable. In gadolinium however, the bands associated with the 4 f electron states may be sufficiently narrow for the intra-atomic interactions to predominate over the inter-atomic, thus simplyfying the necessary theoretical treatment.

Trombe, and later Elliot et al (1953), have measured the magnetization in fields up to 20,000 oersteds, the former down to 78° K, the latter to 20° K. These fields are not large enough to produce technical saturation, and so saturation magnetization values were found by extrapolation. There is some disagreement between the two sets of results,

Trombe's values in the region of 80° K are some 4% higher than those of Elliot, and his results follow a $\sigma \propto T^{2}$ law from about 250° K to 0° K, whereas Elliot's follow a $\sigma \propto T^{\frac{3}{2}}$ law over the same temperature range. The interesting point however, is that the absolute saturation magnetization obtained by Trombe by extrapolation of the T^{2} curve, 253.5 c.g.s. units, is nearly identical to that obtained by Elliot by extrapolation of the $T^{\frac{3}{2}}$ curve, 253.6 ± 0.9 c.g.s. units. This is some 2% higher than would be predicted if only the spins of the 4 f electrons contributed to the magnetization.

3.2 Preparation of specimen. 3.21 General considerations. Owing to the scarcity and expense of gadolinium, it was only possible to obtain 10 gms (~ 1.5 c.c.s). This had been prepared by Johnson, Matthey and Co., Ltd., from the oxide of purity 95%. The resulting metal conformed to the following analysis.

Praseodymium	0.1 %
Neodymium	1.5 %
Samarium	0.2 %
Iron	0.005 %

The effect of these impurities will be neglible on magnetic measurements on polycrystalline gadolinium, but they will greatly influence the possibility of growing a single crystal. It was therefore decided to try and increase the purity by zone melting (Davis et al 1956), with the intention of obtaining a single crystal, provided there was no phase change on cooling the gadolinium from its melting point. Using this method, a rod of the material is held in a continuously evacuated

enclosure, and electrons from a heated tungsten filament are accelerated towards the rod by a potential difference of a few K.V. until a molten zone is formed. The molten zone is then made to traverse the rod by relative motion of the rod and filament. Purification is achieved by successive traversals of the molten zone which also increases the grain size with the possibility of obtaining single crystals.

In order to use the above method, the gadolinium had to be in the form of a rod. This meant breaking up the sample and heating it in a crucible above its melting point (1350° C). Gadolinium is unfortunate in that it is an extremely efficient 'getter', i.e. it combines vigorously with oxygen, nitrogen and hydrogen when heated, and so it must be heated in either a vacuum or in an inert atmosphere. The only substance suitable for a crucible, in that it does not form an alloy with the gadolinium, is tantalum, and this must be degassed before use at a temperature of 2,000° C in an atmosphere of argon, purified by passing over heated magnesium turnings at 500° C, and then through a mixture of 25% Na and 75% K. The degassing of the crucible was carried out in a high frequency induction furnace which was made available by the kindness of I.C.I. Research Department, Billingham Division. The crucible was of cylindrical shape, inside diameter $\frac{1}{4}$ ins, wall thickness 0.01 ins. The melting of the gadolinium was carried out in a platinum wound furnace, also loaned by I.C.I. and produced a rod, after turning off the tantalum crucible in a lathe, approximately $1\frac{1}{4}$" in length.

3.22 Zone melting apparatus. The vacuum chamber consists of a bell jar, 12 ins diameter, 14 ins high, sealed by means of an L shaped rubber

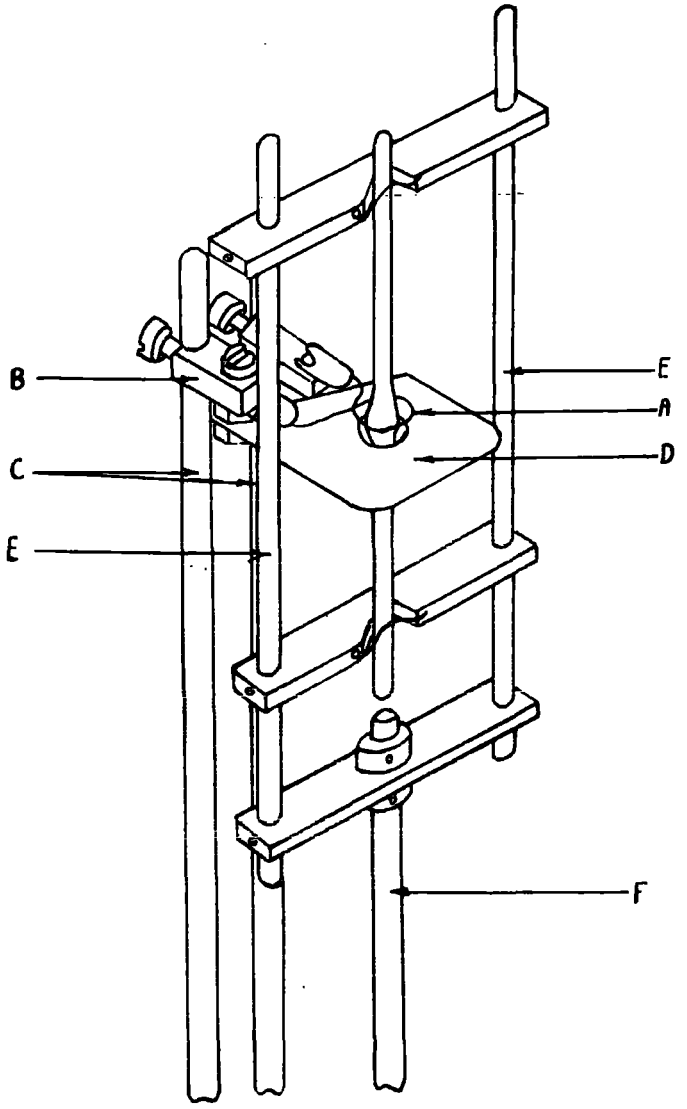

FIG. 33. Electrode system.

gasket on to a machined flat mild steel base plate. A vacuum of the order of 10^{-5} m.m. Hg pressure is obtained in a continuously pumped system, using the usual combination of rotary pump, diffusion pump and liquid nitrogen trap. The diffusion pump is an Edwards two stage mercury diffusion pump, type 2 M2. A mercury diffusion pump is used in preference to an oil diffusion pump to avoid oil vapour cracking on the hot specimen and causing carbon contamination.

The cathode A (fig.33) made from 0.01 ins diameter tungsten wire, is held by screws passing through the mild steel blocks B. These blocks are attached to two vertical silver steel rods C fixed to two Edwards type 7 A electrodes, which take the current through the base plate. Fastened to each of the mild steel blocks is a tantalum focussing shield D (upper focussing shield is omitted in fig.33) to limit the vertical spread of electrons. The distances are such that the gap between the plates is about $\frac{1}{4}$ ins, the size of the holes in the plates is the smallest possible allowing the specimen to pass through, and the diameter of the cathode about $\frac{1}{4}$ ins larger.

The specimen is held at each end by 0.03 ins diameter tungsten wire springs, in V-shaped grooves cut into mild steel blocks. These blocks are mounted on two silver steel rods E supported by another mild steel block, and the whole frame mounted on a $\frac{1}{4}$ ins diameter silver steel rod F passing through a rotary "O" ring vacuum seal in the centre of the base plate. This rod is geared to a motor which gives a traversing speed of 1 cm/min.

The cathode arrangement and associated parts are surrounded by an earthed shield of tin plate, 7 ins diameter, 7 ins high, with a small

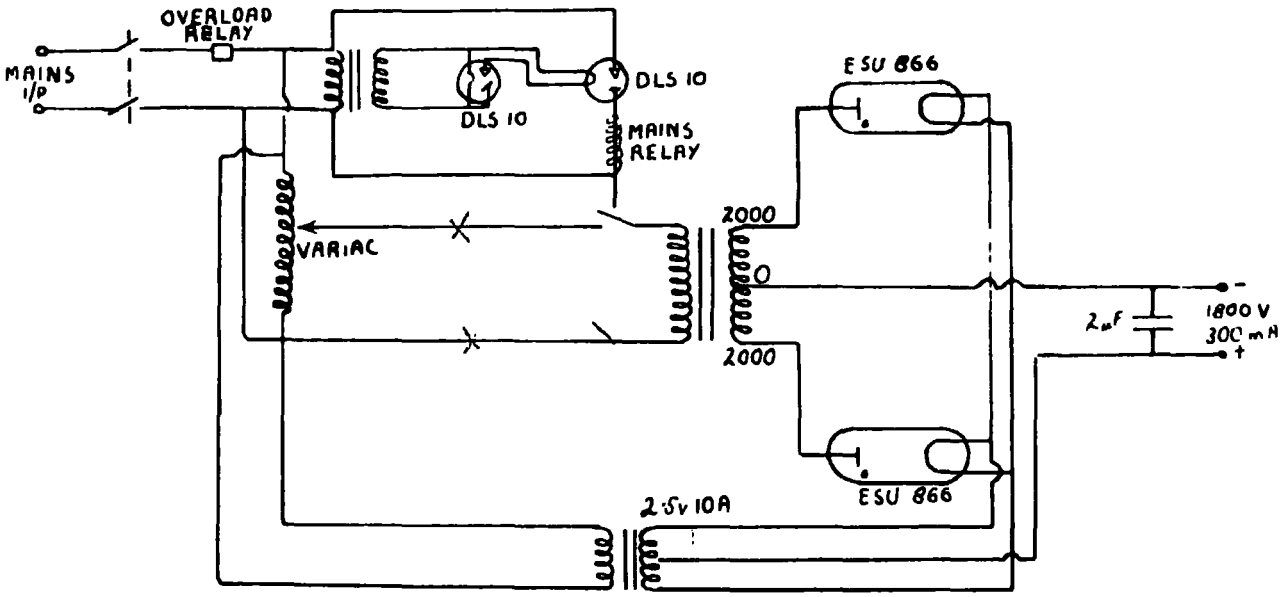

FIG. 34. The H.T. power pack.

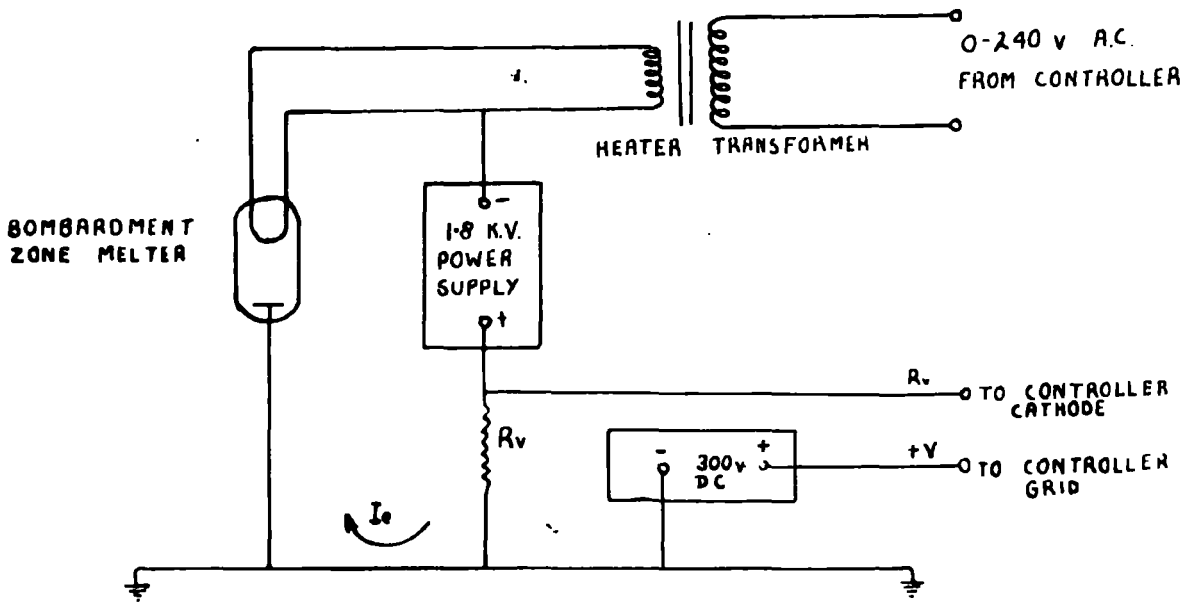

FIG. 35. Block diagram of the emission controller.

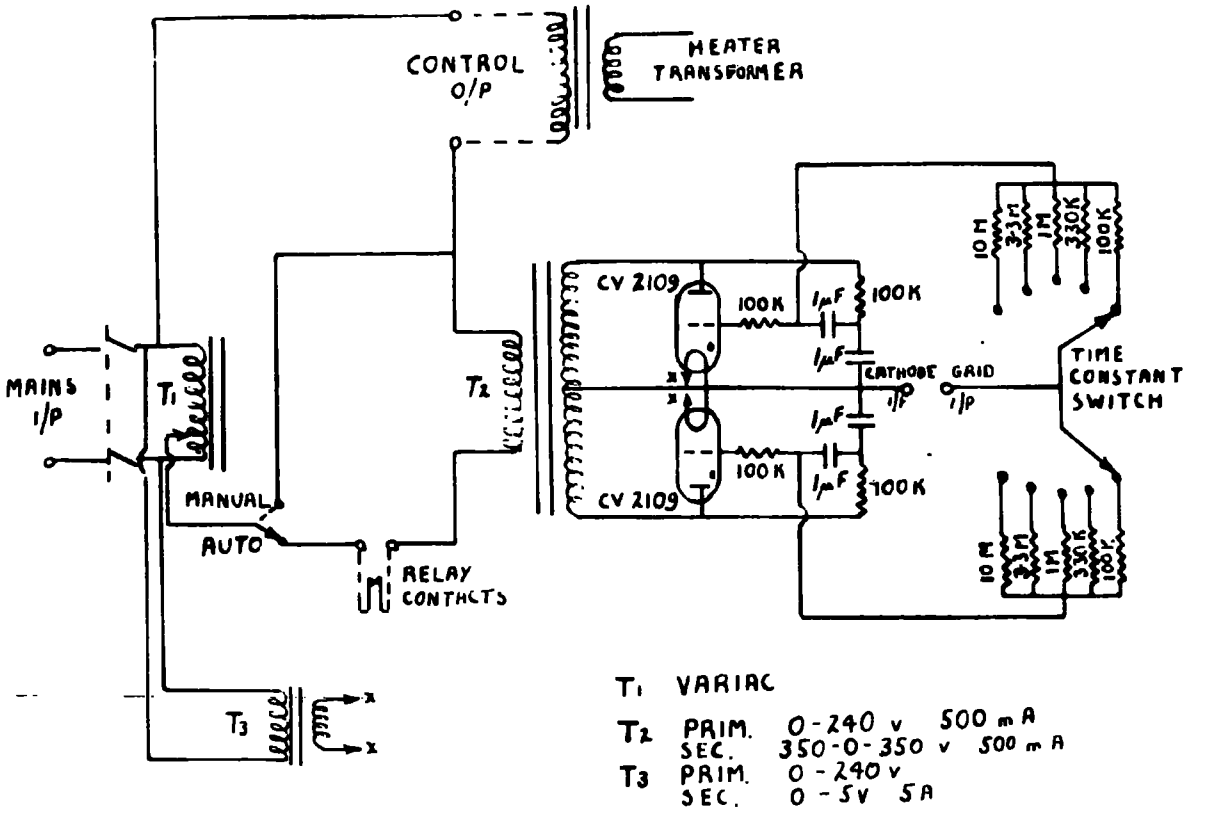

FIG. 36. Emission control circuit.

pyrex window let into the side for observation purposes. The cylinder acts as a radiation shield and stops the deposition of the specimen on the walls of the chamber should violent outgassing occur.

The H.T. system (fig.34) is a convential full wave rectifier, capable of giving 300 mA at 1800 V. When the specimen first melts, considerable outgassing is likely to occur, making hand control of the emission current virtually impossible. An emission control system is therefore used in which the bombardment current is kept constant by automatically adjusting the cathode temperature.

The bombardment current, I_e (fig.35) develops a voltage $I_e R_V$ across a resistor R_V. This voltage, of the order of a few hundred volts, is compared with the output voltage from a 0-300 v variable D.C. supply, the difference being fed into the controller (fig.36). In the controller, the primary of transformer T_2 is in series with a Variac T_1, and the primary of the heat transformer. Two thyratrons are connected across the secondary of T_2, and when these are not conducting, the impedance of T_2, which acts as a very high inductance, determines the cathode current. When the thyratrons are conducting however, the cathode current is determined mainly by its own impedance, as T_2 presents a resistive impedance of only a few ohms. T_1 is set so that under this condition, the cathode is copiously emitting, the input signal $V - I_e R_V$ then adjusting the thyratron firing time so that the power supplied to the cathode maintains the bombardment current at the desired value.

To prevent any hunting due to thermal lag in the cathode, the time constant of the input can be varied from 1/20 sec. to 5 sec. A pair of contacts on the H.T. relay is placed in series with the primary of T_2

to ensure that the cathode heater supply is cut off if the H.T. supply fails. If this were not done, a large positive voltage would be applied to the thyratrons if the H.T. supply failed, and the thyratrons would fire over their entire range with the possibility of holding the cathode temperature at an excessively high level. To increase the range of control, the thyratron grids have a small alternating voltage applied to them, lagging the anode voltage in phase by $\frac{\pi}{2}$ (Younge and Bueche 1952).

3.221 Method of operation. Trial runs were carried out on $\frac{1}{4}$" diameter polycrystalline rods of nickel. To avoid kinking when it first melted, the specimen was cut in half, and mounted with the two halves in line and touching in the centre. The pressure was reduced to 10^{-5} mm Hg, the two ends brought opposite the filament, H.T. switched on, and the cathode current gradually increased until the emission current was sufficient to make the specimen red hot. It was arranged so that the upper half was hotter than the lower, so that as the emission current was increased, the small gap between the two halves was bridged. The specimen frame was then lowered until the starting point of the proposed length of travel was opposite the cathode. In the actual zoning process, the surface only of the metal was melted first, a traversal made, emission increased so that a greater depth melted than previously, another traversal made, and so on until the specimen was completely outgassed.

In the case of nickel, very little outgassing was observed, and single crystals were produced after only two traversals of the molten zone.

The gadolinium rod was only about $1\frac{1}{4}$" long, so in order to use as

great a length as possible for zone refining, the tantalum crucible was left attached to one end of the specimen, and not machined off along the whole length. The bottom end was allowed to rest in the recessed end of a tantalum rod. By using this method of mounting the gadolinium, it was possible to use about 1" of its length for zone refining. The same method was used for the zone refining as that described for the trial runs on nickel, except that before pumping down, the vacuum chamber was flushed out with argon to remove any traces of air in the system.

The gadolinium contained quite a number of " air pockets ", so that it was difficult to obtain a uniform diameter rod after the passage of a molten zone along the whole length. After two passes, the gadolinium was taken out of the zone melter, and a small portion of its surface highly polished with very fine grade emery paper. The only suitable reagent found for etching the surface was a very dilute solution of sulphuric acid and ferric chloride. All the normal etching reagents proved unsuccessful as they invariably formed inert films with the surface of the gadolinium. Examination under a microscope showed some small crystal grains in the gadolinium, indicating that a few more passes in the zone melter may produce a single crystal. Due to the length and shape of the specimen however, it was only possible to make two more passes.

The etched surface of the final specimen showed that the grain size had increased, giving grains of the order of 1 mm. A back reflection X-ray photograph of the surface, taken with a 6 cm. cylindrical camera, showed a marked thickening of the lines in places, indicating some degree of preferred orientation. Thus even though a single crystal was not produced, it is very probable that the specimen is of greater purity than

the original, as the impurities will have been segregated to one end of the gadolinium. It was decided to make polycrystalline measurements, and, when it was possible to obtain a purer sample of gadolinium, to attempt work on single crystals.

3.23. Shaping of specimen. The maximum length of ellipsoid obtainable from the sample was about 1.8 cms. The specimen was turned down in a lathe until it was possible to hold it in a $\frac{1}{8}$" collet. From a knowledge of the length of the specimen available, the correct shape of the ellipsoid was calculated, and an enlarged replica drawn on graph paper. The size of the replica was determined by the size of the profile of the specimen projected onto the paper from an optical system mounted on the lathe. One half of the specimen was carefully filed down until it fitted the profile, the final removal being obtained by using very fine emery paper. The specimen was reversed and held in a specially made collet, and the second half filed down to the correct shape. The shaping of the ellipsoid produces strains in the surface layers of the specimen, so the surface layers were removed by etching.

The final length of the specimen was 1.746 cms, and its actual shape is shown in table 8. y_1 and y_2 are the diameters at a distance x from each end of the specimen y_c is the calculated diameter for a perfect ellipsoid having the same major and minor axes. The measurements were made with a microscope, used for nuclear emulsion work, having vernier scale movements in two perpendicular directions. The microscope can be read to $\pm$ 0.0001 cms, so that the difference between the calculated and experimental values of the ellipsoid must be due to irregularities in the

latter. The specimen is slightly larger at its ends than a true ellipsoid, and this may cause slight non-uniformity of field inside the specimen.

The calculated demagnetizing factor, D , from the values in table 8 is 0.498 so the value used in the results is

$$D = 0.5$$

Table 8

Dimensions of the gadolinium ellipsoid
(All dimensions cms x 10^{-3})

x	y_1	y_2	y_c
50	107	101	92
100	143	133	128
150	168	160	154
200	188	180	175
250	205	197	192
300	219	212	206
350	232	225	220
400	243	237	230
450	251	253	240
500	258	257	248
550	265	264	256
600	269	268	262
650	272	271	266
700	272	271	270
750	274	272	272
800	274	273	273
900	274	274	274

3.3 Magnetostriction measurements. Only one slight modification of the apparatus used for the magentostriction measurements on nickel, was needed for the measurements on gadolinium. The temperature coefficient of expansion of gadolinium between 120 ^{o}K and the Curie temperature, 290 ^{o}K, is very small, $-2 \times 10^{-6} / {}^{o}$K (Bannister et al 1954), and so it was decided to dispense with the temperature compensator. The gadolinium is held in a brass thimble, similar in shape to the aluminium temperature compensator, but holding the specimen so that its bottom end is at the same level as the top of the small quartz tube in the specimen holder (fig.25).

Magnetostriction measurements were made in the temperature range 78 ^{o}K to 320 ^{o}K, using the techniques described in 2.28.

3.4 Intensity of magnetization measurements. A similar method to that described in 2.13 was used for the I measurements on gadolinium, the only difference being in the method of compensating for the effect of field changes. The search coil measures changes in flux due to changes in both the intensity of magnetization of the specimen, and the field, so to compensate the effect of the field change, the secondary of a mutual inductance is put in series with the search coil. The primary of the mutual inductance is in series with the solenoid, so by suitably adjusting the value of the inductance, the e.m.f. produced in the fluxmeter circuit by changes in the solenoid current can cancel that due to the flux linkage of the field with the search coil. The primary of the inductance is made of 5/16" O/D copper tubing, wound into three layers, each layer being separated from the next by polythene sheet. The necessary cooling is produced by mains water flowing through the coil. When used at different

temperatures, a small correction must be applied as the flux coil expansion makes the compensating flux change produced by the mutual inductance no longer equal and opposite to the flux change due to the applied field. Expansion of the flux coil and specimen make negligible difference to the flux linkage with the specimen.

The search coil consists of 154 turns in 4 layers of 36 gauge anodised aluminium wire wound on a former of winding space 0.843 cms length and inner diameter 0.507 cms (similar in shape to the former shown in figure 14). The windings are kept in position by a layer of mica, which in turn is held in position by a ring of copper wire. The search coil is mounted on the end of a $\frac{3}{8}$" diameter Tufnol rod held with its axis parallel to that of the solenoid. The specimen holder is surrounded by a Pyrex tube fastened onto the Duralumin bar, and that in turn by a Dewar. A copper-constantan thermocouple junction is strapped to the coil former, and the leads, together with those of the search coil, brought out to a terminal block on the Tufnol rod. Temperature variation is produced and measured as in the magnetostriction measurements.

With the notation used in 2.132, $I = \frac{H}{4\pi R \Delta H} \Delta I$, $\frac{H}{\Delta H}$ is found by establishing known fields in the coil and noting the fluxmeter deflection. The dimensionless factor R, calculated from the shape of the specimen and search coil is R = 0.179. The value of the intensity of magnetization corresponding to unit deflection is then given by

$$I = 71.6 \text{ c.g.s. units/cm.}$$

3.5 Results. $\frac{\Delta L}{L}$ and I measurements were obtained over the temperature range 78 °K to 350 °K in magnetic fields up to 10,500 oersteds. It was

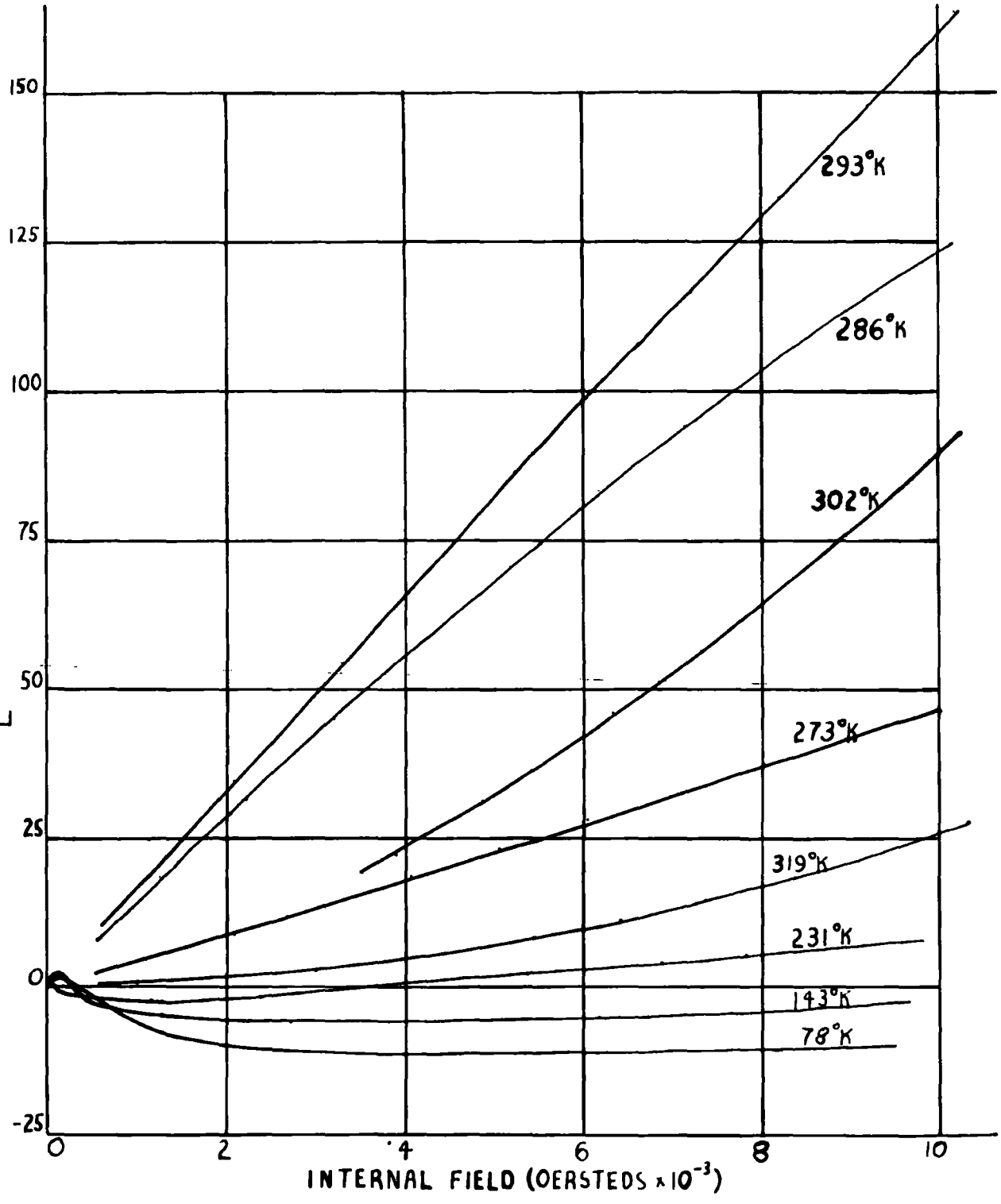

FIG.37. Magnetostriction as a function of magnetic field strength at various temperatures.

fairly easy to obtain I measurements at any desired temperature, so they were noted at the same temperature as the $\frac{\Delta L}{L}$ measurements. Graphs of $\frac{\Delta L}{L}$,H_q , and I, H_q were drawn and from these I, $\frac{\Delta L}{L}$, H values obtained. There was very little scatter in the experimental points so the curves were considered accurate to within 1%. The overall accuracy of the measurements is the same as in the nickel experiment, within 5%. In the I measurements, the value of R cannot be determined to an accuracy greater than 1%, consequently the absolute values of I will have a similar error.

The results obtained are shown in tabular form in table 9. Figure 37 shows a representative selection of the $\frac{\Delta L}{L}$, H curves at various temperatures.

3.6 Discussion. At low temperatures the $\frac{\Delta L}{L}$, H curves are very similar to those of iron. They show a small increase in length corresponding to domain boundary movement, which occurs in fields, H, of about 150 oersteds, followed by a decrease in length corresponding to domain vector rotation. This reaches a limiting value and then starts to increase again. The limiting value of $\frac{\Delta L}{L}$ is the saturation magnetostriction, λ , and any change in dimensions which occurs after that state hasbeen reached must be due to a volume effect dependant on an increase in the intrinsic magnetization.

As the temperature increases above 78 °K, the value of λ decreases until it reaches zero at 233 ° ± 1 ° K. Above 233 °K, $\frac{\Delta L}{L}$ increases with increasing field at all temperatures for which measurements were made. The initial increase in length, for temperatures below 233 °K, due to domain boundary movement, decreases in value as the temperature increases from 78 °K, but is present up to 233 °K.

TABLE 9.

Magnetostriction and Magnetization of Polycrystalline Gadolinium.

	78°K			90°K			104°K		
Ha	$-\frac{\Delta L}{L} \times 10^6$	I	H	$-\frac{\Delta L}{L} \times 10^6$	I	H	$-\frac{\Delta L}{L} \times 10^6$	I	H
200	- 0.2	-	-	- 0.1	400	0	-0.1	-	-
400	- 0.8	788	1	- 0.6	745	28	-0.8	744	28
600	- 1.6	1103	49	- 1.4	1131	34	-1.9	1110	45
800	- 1.4	1317	141	- 1.5	1303	148	-1.7	1299	150
1000	- 0.4	1432	284	0.2	1410	295	-0.2	1432	284
1250	2.0	1525	477	2.3	1496	502	2.3	1496	502
1500	4.5	1575	712	4.0	1561	720	4.0	1546	727
1750	6.2	1625	937	5.3	1611	945	5.7	1589	955
2000	7.6	1661	1168	6.6	1640	1180	6.8	1613	1194
2250	8.6	1690	1405	7.6	1668	1416	7.6	1629	1436
2500	9.2	1709	1645	8.3	1683	1659	8.1	1645	1678
2750	9.7	1723	1888	8.8	1691	1904	8.4	1654	1923
3000	10.1	1733	2134	9.2	1704	2148	8.6	1661	2169
3500	10.7	1744	2638	9.7	1718	2641	8.9	1675	2662
4000	11.0	1747	3126	10.0	1733	3134	9.0	1695	3152
4500	11.1	1754	3623	10.0	1743	3628	8.9	1699	3651
5000	11.2	1761	4118	10.0	1749	4126	8.7	1704	4148
5500	11.2	1767	4616	10.0	1758	4626	8.5	1713	4644
6000	11.2	1776	5112	10.0	1763	5118	8.2	1718	5141
6500	11.2	1779	5610	9.8	1768	5616	8.0	1725	5637
7000	11.1	1786	6107	9.7	1776	6112	7.7	1733	6134
7500	11.0	1790	6605	9.6	1783	6609	7.4	1740	6630
8000	10.9	1799	7101	9.5	1790	7105	7.1	1747	7127
8500	10.8	1804	7598	9.3	1795	7602	6.8	1752	7624
9000	10.6	1811	8094	9.1	1804	8098	6.5	1760	8120
9500	10.4	1819	8591	8.9	1810	8595	6.2	1765	8618
10000	10.2	1829	9085	8.7	1818	9091	5.8	1774	9113
10500	10.0	1833	9584	8.5	1822	9589	5.5	1779	9610
		1			2			3	

TABLE 9.

	118°K			143°K			163°K		
Ha	$-\frac{\Delta L}{L}\times 10^6$	I	H	$-\frac{\Delta L}{L}\times 10^6$	I	H	$-\frac{\Delta L}{L}\times 10^6$	I	H
200	- 0.2	400	0	- 0.1	-	-	-0.2	386	7
400	- 0.9	737	31	- 0.9	788	6	-0.8	741	30
600	- 2.4	1124	38	- 1.9	1124	38	-1.1	1088	56
800	- 2.0	1289	154	- 1.4	1260	170	-0.8	1231	184
1000	0.5	1403	298	1.0	1346	327	2.0	1292	354
1250	2.7	1475	513	3.2	1410	515	4.2	1339	581
1500	4.5	1518	741	4.1	1446	777	5.1	1360	820
1750	5.4	1554	973	4.6	1478	1011	5.6	1385	1057
2000	6.3	1575	1212	5.1.	1500	1250	5.9	1400	1300
2250	6.8	1591	1454	5.3	1514	1493	6.2	1412	1544
2500	7.1	1604	1698	5.6	1525	1737	6.3	1423	1789
2750	7.3	1611	1945	5.7	1532	1984	6.3	1432	2034
3000	7.5	1618	2191	5.9	1539	2230	6.4	1446	2277
3500	7.5	1631	2685	6.0	1546	2727	6.4	1460	2770
4000	7.2	1643	3178	6.0	1564	3218	6.3	1475	3263
4500	7.0	1654	3673	5.9	1568	3716	6.2	1489	3755
5000	6.7	1665	4168	5.8	1575	4212	6.1	1494	4253
5500	6.5	1675	4662	5.6	1582	4709	6.0	1503	4748
6000	6.2	1683	5159	5.4	1589	5205	5.8	1509	5246
6500	5.9	1690	5655	5.2	1597	5702	5.6	1514	5743
7000	5.6	1693	6153	5.0	1604	6198	5.5	1518	6241
7500	5.4	1700	6650	4.8	1611	6695	5.2	1525	6737
8000	5.1	1704	7148	4.5	1618	7191	5.0	1532	7234
8500	4.8	1715	7643	4.2	1625	7687	4.8	1536	7732
9000	4.5	1718	8141	3.9	1632	8184	4.5	1545	8228
9500	4.2	1725	8637	3.6	1643	8678	4.2	1550	8725
10000	3.9	1733	9134	3.3	1647	9177	4.0	1557	9221
10500	3.6	1736	9632	2.9	1654	9673	3.7	1564	9718
			4			5			6

TABLE 9.

	175°K			193°K			213°K		
Ha	$-\frac{\Delta L}{L}\times10^6$	I	H	$-\frac{\Delta L}{L}\times10^6$	I	H	$-\frac{\Delta L}{L}\times10^6$	I	H
200	-	-	-	-0.15	400	0	-0.1	358	21
400	- 0.15	800	0	0	787	6	0	702	49
600	- 0.25	1102	49	1.8	1045	87	2.0	974	113
800	1.4	1217	191	3.7	1181	209	3.6	1106	247
1000	3.5	1289	356	5.0	1253	374	4.8	1179	411
1250	4.5	1332	584	6.0	1303	598	5.5	1214	543
1500	5.3	1367	811	6.6	1332	834	5.7	1231	884
1750	5.7	1389	1056	6.9	1353	1073	5.8	1244	1128
2000	6.0	1403	1298	7.1	1364	1318	5.8	1251	1374
2250	6.1	1410	1545	7.2	1375	1563	5.8	1260	1620
2500	6.3	1418	1791	7.3	1378	1821	5.7	1265	1867
2750	6.4	1424	2038	7.3	1385	2057	5.6	1267	2116
3000	6.4	1430	2285	7.3	1389	2305	5.5	1271	2365
3500	6.4	1443	2789	7.2	1400	2800	5.3	1280	2860
4000	6.4	1446	3277	7.1	1407	3297	4.9	1287	3357
4500	6.3	1457	3772	6.9	1418	3791	4.6	1296	3852
5000	6.2	1460	4270	6.7	1421	4289	4.2	1301	4349
5500	6.0	1468	4776	6.4	1428	4786	3.9	1308	4856
6000	5.8	1473	5263	6.1	1432	5284	3.5	1316	5342
6500	5.6	1478	5761	5.9	1435	5782	3.1	1321	5840
7000	5.5	1482	6259	5.6	1443	6279	2.8	1328	6336
7500	5.2	1489	6755	5.3	1446	6777	2.4	1333	6833
8000	5.0	1493	7254	5.1	1453	7273	1.9	1339	7331
8500	4.7	1500	7750	4.7	1459	7771	1.5	1346	7827
9000	4.5	1504	8248	4.4	1462	8269	1.0	1353	8323
9500	4.2	1507	8746	4.1	1468	8766	0.5	1360	8820
10000	3.9	1514	9243	3.7	1475	9263	0	1367	9316
10500	3.6	1518	9741	3.3	1482	9759	-0.5	1375	9813
	7			8			9		

TABLE 9.

	231°K			242°K			257°K		
Ha	$\frac{\Delta L}{L} \times 10^6$	I	H	$\frac{\Delta L}{L} \times 10^6$	I	H	$\frac{\Delta L}{L} \times 10^6$	I	H
200	.05	340	30	0.1	333	34	0.2	279	64
400	-0.1	655	72	0.2	605	98	0.5	565	117
600	-1.1	909	145	0.4	852	174	0.8	727	237
800	-1.85	1027	286	0.6	952	324	1.1	838	381
1000	-2.2	1095	452	0.7	1024	488	1.5	913	544
1250	-214	1131	684	1.0	1069	717	2.0	940	780
1500	-2.5	1151	925	1.2	1090	965	2.4	956	1022
1750	-2.6	1167	1146	1.5	1104	1198	2.9	966	1267
2000	-2.5	1178	1411	1.8	1110	1445	3.3	977	1521
2250	-2.4	1189	1657	2.0	1117	1692	3.9	984	1758
2500	-2.3	1192	1904	2.4	1120	1940	4.4	988	2006
2750	-2.1	1197	2151	2.7	1124	2188	4.8	993	2253
3000	-1.9	1201	2399	3.1	1131	2434	5.3	997	2502
3500	-1.3	1210	2895	3.8	1136	2932	6.3	1002	2999
4000	-0.6	1215	3392	4.5	1144	3428	7.3	1009	3495
4500	0.1	1221	3890	5.2	1149	3925	8.3	1018	3991
5000	0.8	1228	4386	6.0	1156	4422	9.3	1027	4486
5500	1.5	1235	4882	6.7	1163	4918	10.4	1033	4984
6000	2.1	1242	4379	7.4	1170	5415	11.5	1040	5480
6500	2.8	1246	5877	8.1	1174	5913	12.7	1045	5977
7000	3.4	1253	6374	8.8	1181	6409	13.8	1052	6474
7500	4.0	1257	6872	9.6	1185	6908	14.9	1058	6971
8000	4.6	1262	7369	10.4	1192	7404	16.0	1063	7468
8500	5.2	1267	7866	11.2	1196	7902	17.2	1068	7966
9000	5.8	1273	8364	12.0	1203	8399	18.4	1074	8463
9500	6.4	1278	8861	12.8	1208	8896	19.7	1081	8959
10000	7.0	1281	9359	13.5	1213	9393	21.0	1086	9467
10500	7.6	1289	9856	14.3	1217	9891	22.3	1092	9954
	10			11			12		

TABLE 9.

	273°K			280°K			286°K		
Hα	$\frac{\Delta L}{L} \times 10^6$	I	H	$\frac{\Delta L}{L} \times 10^6$	I	H	$\frac{\Delta L}{L} \times 10^6$	I	H
200	0.4	229	85	0.5	247	77	0.7	215	93
400	0.8	429	185	0.9	383	209	2.4	340	230
600	1.4	583	308	1.7	519	340	4.9	437	382
800	2.0	680	460	3.0	609	496	7.9	462	569
1000	2.6	737	631	4.4	644	678	10.6	487	757
1250	3.5	766	867	6.6	662	919	14.5	501	999
1500	4.3	777	1112	8.6	671	1164	18.3	508	1246
1750	5.4	784	1358	10.7	680	1410	21.8	515	1492
2000	6.4	789	1605	12.6	684	1658	24.8	521	1740
2250	7.3	793	1854	14.7	687	1906	28.2	526	1987
2500	8.5	795	2103	16.6	689	2155	31.6	533	2233
2750	9.7	798	2351	18.6	678	2411	35.0	537	2482
3000	10.8	802	2599	20.7	696	2652	38.3	544	2728
3500	13.5	809	3095	24.7	703	3148	45.1	557	3222
4000	16.2	812	3594	28.7	710	3645	51.7	573	3714
4500	18.5	820	4090	32.9	716	4142	58.1	583	4208
5000	21.1	827	4587	36.8	725	4638	64.4	596	4702
5500	23.5	834	5083	40.7	732	5134	71.0	608	5196
6000	25.8	839	5580	44.6	739	5630	77.3	619	5680
6500	28.2	845	6078	48.4	746	6127	83.7	630	6185
7000	30.4	850	6575	52.2	753	6623	89.3	642	6679
7500	32.6	855	7072	55.8	761	7120	94.3	651	7174
8000	35.0	859	7570	59.6	768	7616	100.5	662	7669
8500	37.3	866	8067	63.6	775	8112	105.4	671	8164
9000	39.5	872	8564	67.5	784	8608	110.4	680	8660
9500	41.7	877	9061	71.3	791	9106	115.6	687	9156
10000	44.0	882	9559	74.8	798	9601	120.6	698	9651
10500	46.3	888	10056	78.5	805	10097	125.0	705	10147

TABLE 9.

	290°K			293°K			294°K		
Ha	$\frac{\Delta L}{L} \times 10^6$	I	H	$\frac{\Delta L}{L} \times 10^6$	I	H	$\frac{\Delta L}{L} \times 10^6$	I	H
200	2.5	182	109	1.8	93	153	1.7		
400	4.9	275	262	3.9	147	327	3.9		
600	8.2	329	435	7.0	195	502	7.1		
800	12.4	358	621	11.0	225	687	10.4		
1000	16.1	383	808	14.1	250	875	13.9		
1250	20.3	401	1050	18.1	274	1113	17.9		
1500	25.0	412	1294	22.4	293	1353	22.3		
1750	29.8	422	1539	26.7	313	1593	26.4		
2000	34.2	433	1783	30.7	327	1836	30.7		
2250	38.7	442	2029	34.9	342	2079	35.0		
2500	42.8	451	2274	38.8	356	2322	39.2		
2750	47.2	458	2521	42.9	365	2567	43.1		
3000	51.3	469	2765	46.8	377	3811	47.1		
3500	60.2	487	3257	54.5	401	3300	54.4		
4000	68.0	501	3749	62.2	418	3791	62.2		
4500	76.1	519	4240	70.2	435	4282	70.0		
5000	83.5	533	4733	78.3	451	4774	77.2		
5500	90.9	548	5226	86.8	467	5266	84.8		
6000	98.1	560	5720	94.8	483	5758	92.1		
6500	105.2	573	6214	102.3	499	6250	99.3		
7000	112.4	585	6707	109.6	514	6743	106.4		
7500	119.3	596	7202	116.8	528	7236	113.5		
8000	126.3	607	7697	124.7	542	7729	120.6		
8500	132.8	617	8191	132.3	555	8223	127.7		
9000	139.2	628	8686	140.1	567	8716	134.7		
9500	145.6	637	9181	147.8	578	9211	141.9		
10000	151.9	646	9677	155.9	587	9706	149.2		
10500	157.9	655	10122	163.9	598	10201	155.8		
		16			17			18	

TABLE 9.

	296°K			298°K			302°K		
Ha	$\frac{\Delta L}{L} \times 10^6$	I	H	$\frac{\Delta L}{L} \times 10^6$	I	H	$\frac{\Delta L}{L} \times 10^6$	I	H
200	0.6	39	180	0.3	21	189	0.3	11	195
400	1.4	75	362	0.9	50	375	0.5	21	389
600	3.4	114	543	2.0	79	561	0.8	36	582
800	6.2	147	727	3.3	100	750	1.0	50	775
1000	9.1	168	916	5.0	118	941	1.6	57	971
1250	13.4	189	1155	7.1	132	1189	2.4	72	1214
1500	17.0	207	1396	9.7	150	1425	3.4	86	1457
1750	21.0	222	1639	12.2	165	1668	5.2	95	1703
2000	25.0	234	1883	14.8	179	1911	6.2	107	1946
2250	28.9	247	2127	17.4	191	2154	7.8	118	2191
2500	32.9	258	2571	20.1	204	2398	9.8	129	2436
2750	37.8	272	2614	22.8	215	2543	11.8	150	2925
3000	40.8	284	2858	25.7	229	2885	13.9	150	2925
3500	48.3	308	3346	32.0	256	3372	18.1	172	3414
4000	56.9	333	3834	39.1	283	3859	22.4	197	3902
4500	63.7	358	4321	45.7	308	4346	27.0	216	4392
5000	71.0	379	4810	52.4	329	4835	31.4	238	4881
5500	78.7	401	5300	59.0	353	5324	36.2	258	5371
6000	86.0	420	5790	65.6	374	5813	41.3	279	5856
6500	93.3	440	6280	72.5	394	6303	46.4	301	6350
7000	100.0	458	6771	79.3	412	6794	51.3	320	6840
7500	107.0	472	7264	86.2	429	7285	65.7	340	7330
8000	114.2	490	7755	93.2	449	7775	62.0	361	7819
8500	121.3	580	8246	99.9	467	8266	67.3	383	8308
9000	128.2	526	8737	106.6	487	8757	72.2	401	8800
9500	135.1	544	9228	113.4	505	9248	79.4	422	9289
10000	141.6	562	9719	120.2	523	9739	86.1	437	9782
10500	147.7	580	10210	127.0	540	10230	93.1	454	10273

TABLE 9.

	305°K			309°K			313°K		
Ha	$\frac{\Delta L}{L} \times 10^6$	I	H	$\frac{\Delta L}{L} \times 10^6$	I	H	$\frac{\Delta L}{L} \times 10^6$	I	H
200	0	10	195	0	3	198	0	7	196
400	0	18	391	0.1	7	396	0.2	12	394
600	0.1	25	587	0.4	18	591	0.4	18	591
800	0.4	36	782	0.6	28	786	0.6	23	788
1000	0.7	43	979	0.9	32	984	0.9	28	986
1250	1.3	50	1225	1.4	36	1232	2.0	34	1233
1500	2.0	61	1470	2.0	39	1480	1.7	37	1481
1750	2.9	71	1714	2.5	46	1727	2.2	39	1730
2000	3.8	82	1959	3.2	55	1972	2.7	43	1979
2250	5.2	91	2204	3.8	62	2219	3.2	45	2228
2500	6.4	100	2450	4.6	71	2464	3.8	48	2476
2750	7.7	110	2694	5.5	79	2711	4.4	55	2722
3000	9.1	122	2939	6.6	86	2957	5.0	64	2968
3500	12.0	139	3430	7.7	104	3448	6.6	79	3461
4000	15.3	157	3922	11.1	120	3940	8.4	93	3953
4500	18.9	175	4412	13.5	136	4432	10.5	107	4446
5000	22.7	193	4908	16.0	150	4925	12.7	122	4939
5500	26.8	211	5394	18.7	165	5418	14.9	136	5432
6000	31.0	229	5885	21.7	183	5909	17.3	150	5925
6500	35.2	247	6376	24.8	197	6412	19.8	165	6418
7000	39.3	261	6869	28.0	215	6893	22.3	179	6911
7500	43.7	279	7360	31.5	229	7385	24.7	193	7403
8000	48.1	297	7851	35.0	247	7877	27.3	207	7896
8500	52.8	315	8342	38.7	265	8368	30.1	222	8389
9000	57.6	335	8833	42.3	279	8860	32.9	236	8882
9500	62.6	351	9325	46.2	297	9352	38.6	250	9375
10000	67.5	369	9816	50.1	311	9844	39.2	268	9866
10500	72.3	383	10309	54.1	326	10337	42.2	383	10359
	22			23			24		

TABLE 9.

	316°K			319°K		
Ha	$\frac{\Delta L}{L} \times 10^6$	I	H	$\frac{\Delta L}{L} \times 10^6$	I	H
200	0			0	-	-
400	0.2			0.2	7	396
600	0.4			0.3	18	591
800	0.6			0.5	25	787
1000	0.9			0.6	29	985
1250	1.2			0.8	29	1235
1500	1.5			1.1	29	1535
1750	1.9			1.4	32	1734
2000	2.3			1.6	34	1984
2250	2.7			1.9	34	2237
2500	3.1			2.1	36	2532
2750	3.7			2.5	36	2732
3000	4.4			2.9	38	2982
3500	5.7			3.7	46	3527
4000	7.1			4.6	61	3970
4500	8.8			5.8	73	4463
5000	10.5			7.1	86	4952
5500	12.1			8.5	100	5450
6000	13.8			9.9	114	5943
6500	15.5			11.4	129	6436
7000	17.1			12.9	141	6929
7500	19.0			14.7	154	7423
8000	21.0			16.6	168	7916
8500	23.1			18.6	179	8410
9000	25.3			20.8	193	8903
9500	27.8			23.0	206	9397
10000	30.4			25.4	218	9891
10500	33.2			27.8	233	10384

TABLE 9.

Magnetostriction and Magnetization for H = 9500 oersteds.

$T^{\circ}K$	321	324	331	336	343	347	350	358
$\frac{\Delta L}{L} \times 10^{6}$	19.3	16.6	12.2	9.6	7.7	5.8	5.2	4.8
$T^{\circ}K$	321	330	339	344	355	367		
I	172	140	122	104	97	86		

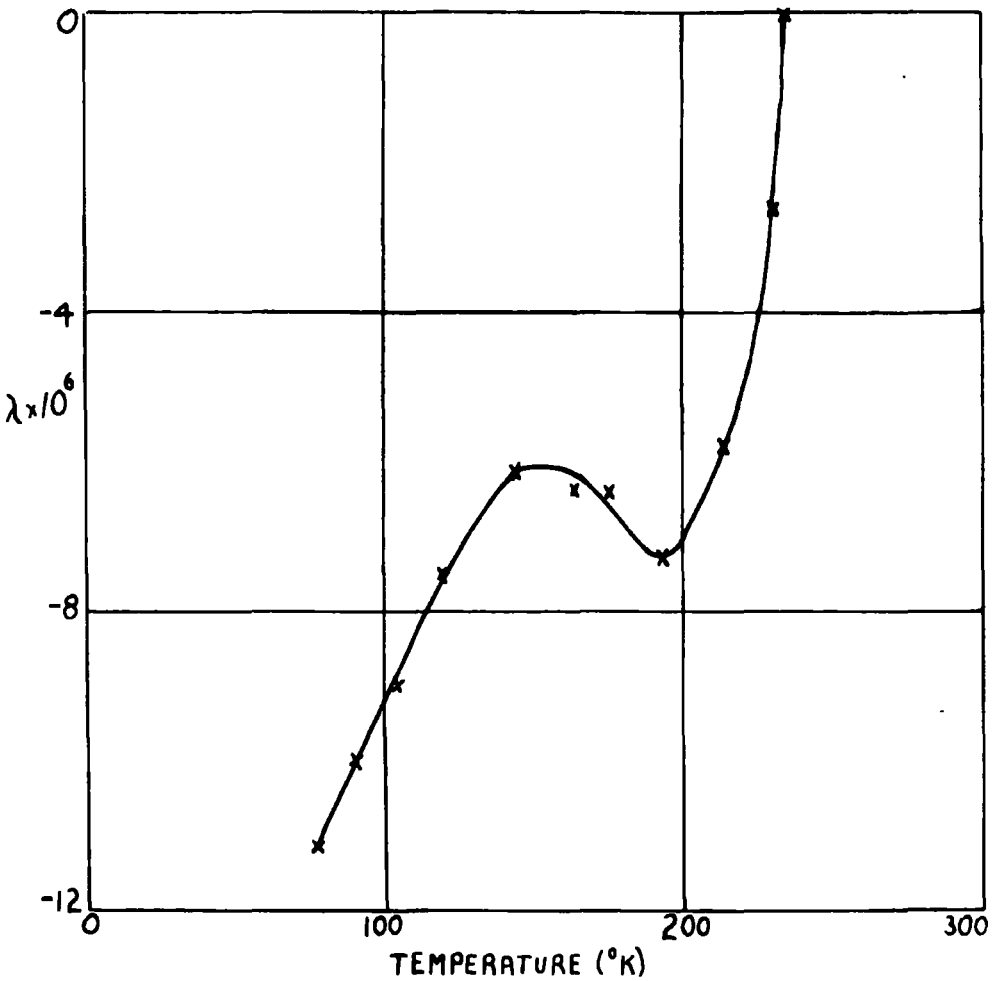

FIG. 38. Temperature dependence of saturation magnetostriction.

Table 10 shows the variation of λ with T and also the values of H (oersteds) required to produce technical saturation.

Table 10.

Temperature variation of the saturation magnetostriction of gadolinium.

T °K	78	90	104	118	143	163	175	193	213	231	233
$-\lambda \times 10^{6}$	11.2	10.0	9.0	7.5	6.1	6.4	6.4	7.3	5.8	2.6	0
$H \times 10^{-3}$	5.0	4.0	3.0	3.0	3.0	2.5	2.5	2.0	1.5	1.0	-

Figure 38 is a plot of λ against T and shows an anomaly at about 150° K. The approach of λ towards zero at 233° K is very sharp and does not show any tailing off towards the Curie point. It is probable that, as the volume effect is so much larger than the linear magnetostriction effect at higher temperatures, the former entirely masks the latter. Also, any such tailing off of λ towards the Curie point would be cancelled out by an increase in length due to the Form effect. At room temperature, for gadolinium, the compressibility is 2.58 cm^{2} /Kg x 10^{6}, and the shear modulus 2.29 Kg/cm^{2} x 10^{5}, which gives an increase in length due to the Form effect of (1.4)

$$\left(\frac{\Delta L}{L}\right)_f \approx 10^{-12} I^2$$

Unfortunately, the temperature variation of the compressibility and shear modulus of gadolinium has not been measured, but as the temperature range considered is only about 60° K below room temperature, their variation should not be large enough to effect an estimate of the increase in length. Saturation magnetostriction is achieved at 231° K in a field of approximately 1,000 oersteds, and table 9 shows that in fields of this value, the intensity of magnetization is as much as 500 c.g.s. units up to

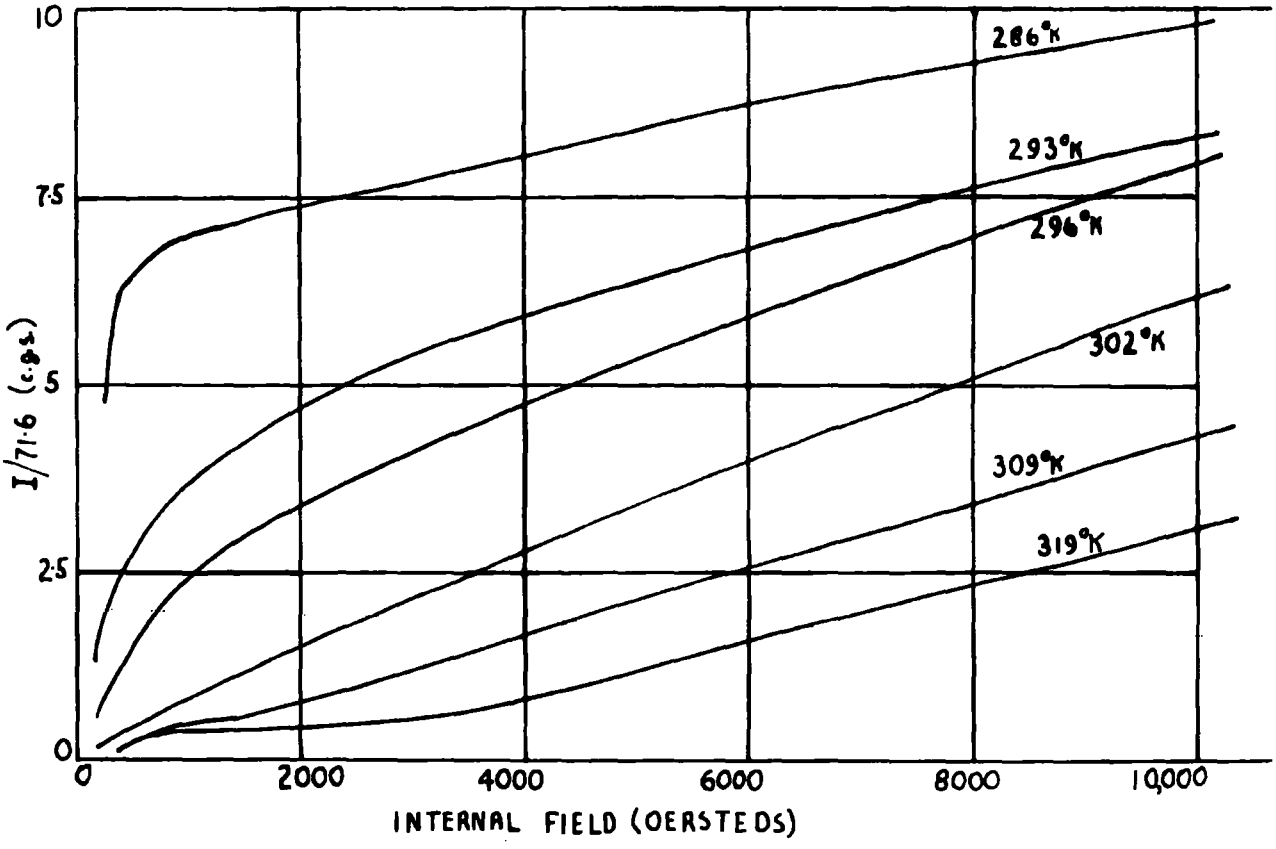

FIG. 39. Intensity of magnetization as a function of magnetic field strength in the region near the Curie point.

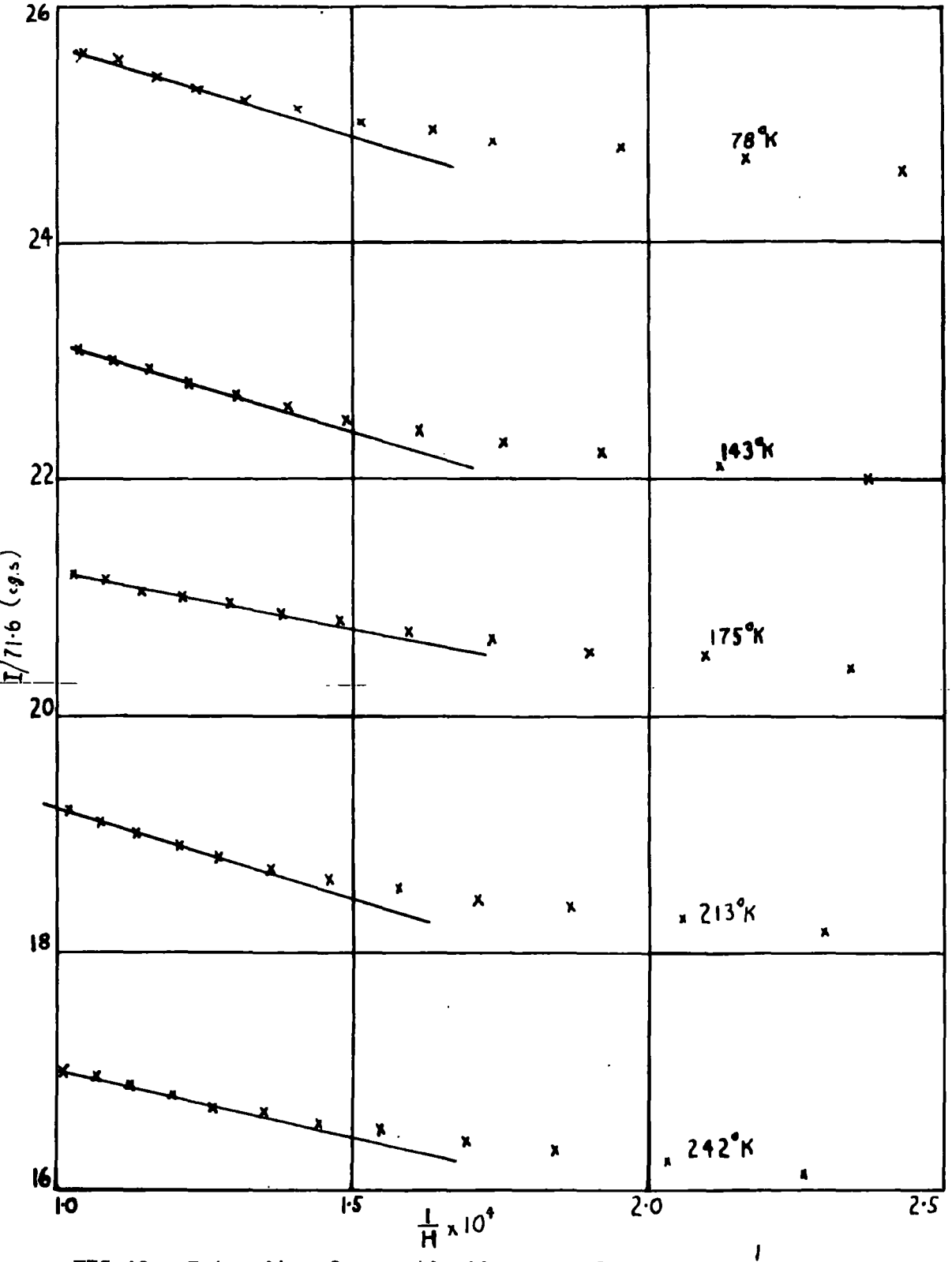

FIG.40. Intensity of magnetization as a function of $\frac{1}{H}$ at various temperatures.

about 286 °K. This high value of I will cause an increase in length of $\left(\frac{\Delta L}{L}\right)_f \approx 0.2 \times 10^{-6}$, which is of the right order to annul any tailing off of the λ, T curve.

The slope of the I, H curve in low fields changes as the temperature is increased above about 233 °K. Table 11 gives values of $\frac{H}{I}$ calculated from the initial slope of the curves

Table 11

Temperature variation of the initial slope of the I,H curves.

T °K	231	242	257	273	285	293
$\frac{H}{I}$	0.7	0.7	0.7	1.1	1.5	3.6

From 78 °K to 225 °K, values of the demagnetizing factor D obtained from the I, H curves, gave D = 0.5 $\pm$ 1% which is in good agreement with that calculated from the shape of the specimen. The value of D used over the whole temperature range is D = 0.5. The change in the initial slope of $\frac{H}{I}$ is to be expected in the region near the Curie point where I measurements will include a combination of intrinsic magnetization and the paramagnetic effect. This is shown in figure 39 which is a plot of I,H at various temperatures near the Curie point. The method used for separating the effects is discussed later.

No saturation values of I are quoted in the results as the number of experimental points available for extrapolation was too small. Fig.40 is a plot of I, $\frac{1}{H}$ at various temperatures, and shows that I is proportional to $\frac{1}{H}$ only above fields of about 7,500 oersteds. This agrees more with the results of Trombe (1937) than with those of Elliot et al (1953). The former found $I \propto \frac{1}{H}$ in fields above 9,500 oersteds, whereas the latter found this to be true in fields above 4,000 oersteds. A tentative extrapolation was

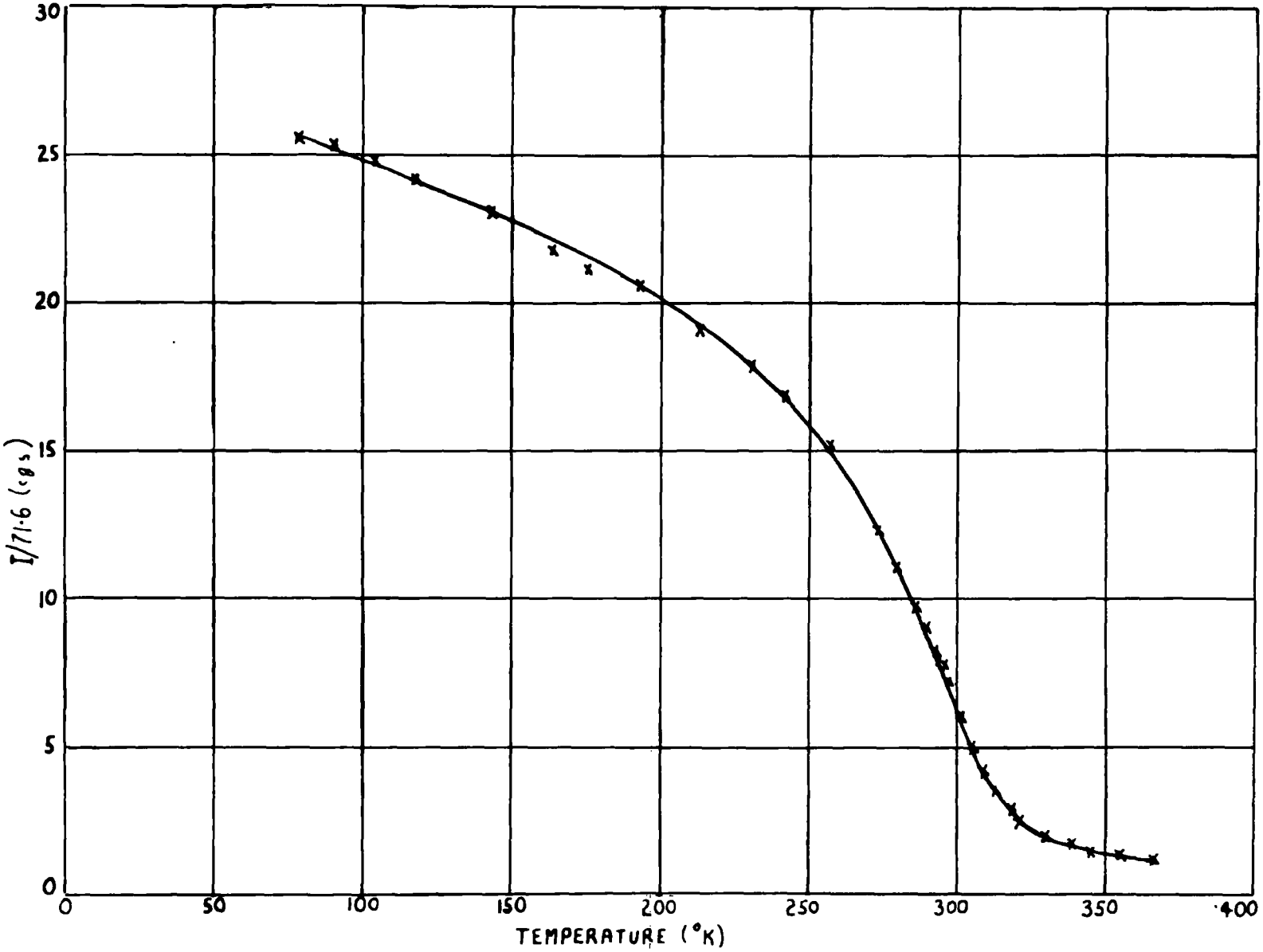

FIG. 41. Temperature dependence of intensity of magnetization (H = 9,500 oersteds)

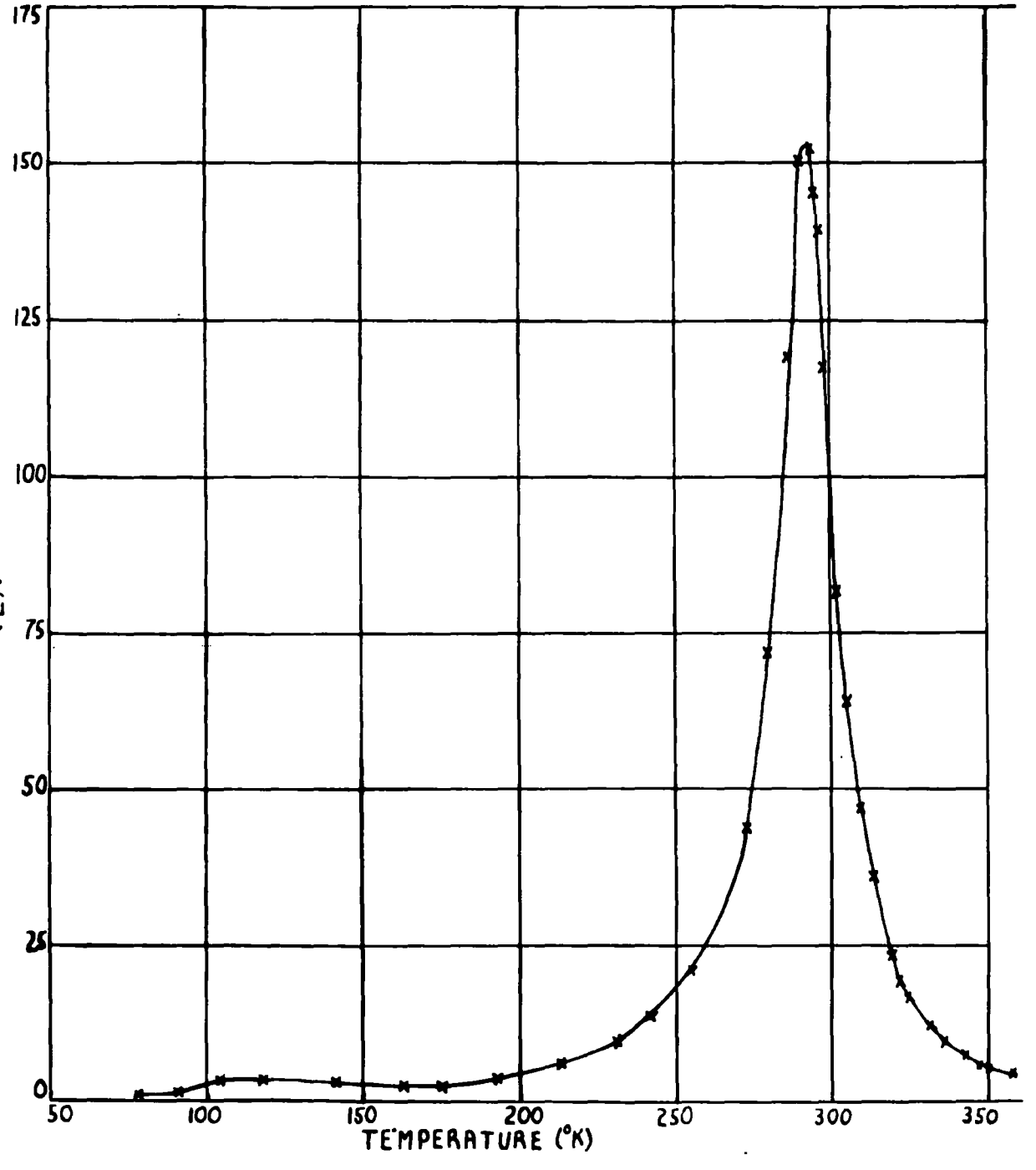

FIG. 42. Temperature dependence of volume magnetostriction
(H = 9,500 oersteds)

tried in order to find out whether the results would fit a $I_s \propto T^{\frac{3}{2}}$ or a $I_s \propto T^2$ law at low temperatures. The number of points available was found insufficient to distinguish between the two.

Figure 40 gives an estimate of the magnetic hardness of gadolinium. Using

$$I_{H,T} = I_{\infty,T}\left(1 - \frac{a}{H}\right) \qquad (20)$$

where (a) is a constant which indicates the hardness of the material, figure 40 gives $a \sim 700$ compared with a value of 1250 obtained by Trombe and about 170 obtained by Elliot et al. The difference in these values is probably due to a difference in purity of the samples used, but they are all much larger than the value for nickel, ~ 0.3, and that for iron, ~ 6.3

The shape of the reduced magnetization curve for gadolinium (fig.1) shows larger divergences from the theoretical curve than for those of any of the other ferromagnetics. The main difference is in the apparent large value of the intrinsic magnetization in the neighbourhood of the Curie point. Figure 41 shows a plot of I against T for a constant internal field of 9,500 oersteds (table 10). It should be possible to separate the intrinsic magnetization from the paramagnetic effect, and then obtain a relationship between the latter and the volume magnetostriction $\left(\frac{\Delta L}{L}\right)_V$. $\left(\frac{\Delta L}{L}\right)_V$ in constant internal field of 9,500 oersteds is plotted as a function of temperature in figure 42, and reaches a maximum at just below 293 ^{o}K. Measurements were made of the magnetocaloric effect in this temperature range, and these gave a maximum temperature rise of $\frac{2}{5}$ ^{o}K at 293 ^{o}K. Above 293 ^{o}K the temperature coefficient of expansion of gadolinium is 10×10^{-6} / ^{o}K, below 293 ^{o}K, -2×10^{-6}/ ^{o}K (Bannister et al 1954), so this corresponds to a maximum increase in the value of $\left(\frac{\Delta L}{L}\right)_V$ of 4×10^{-6}.

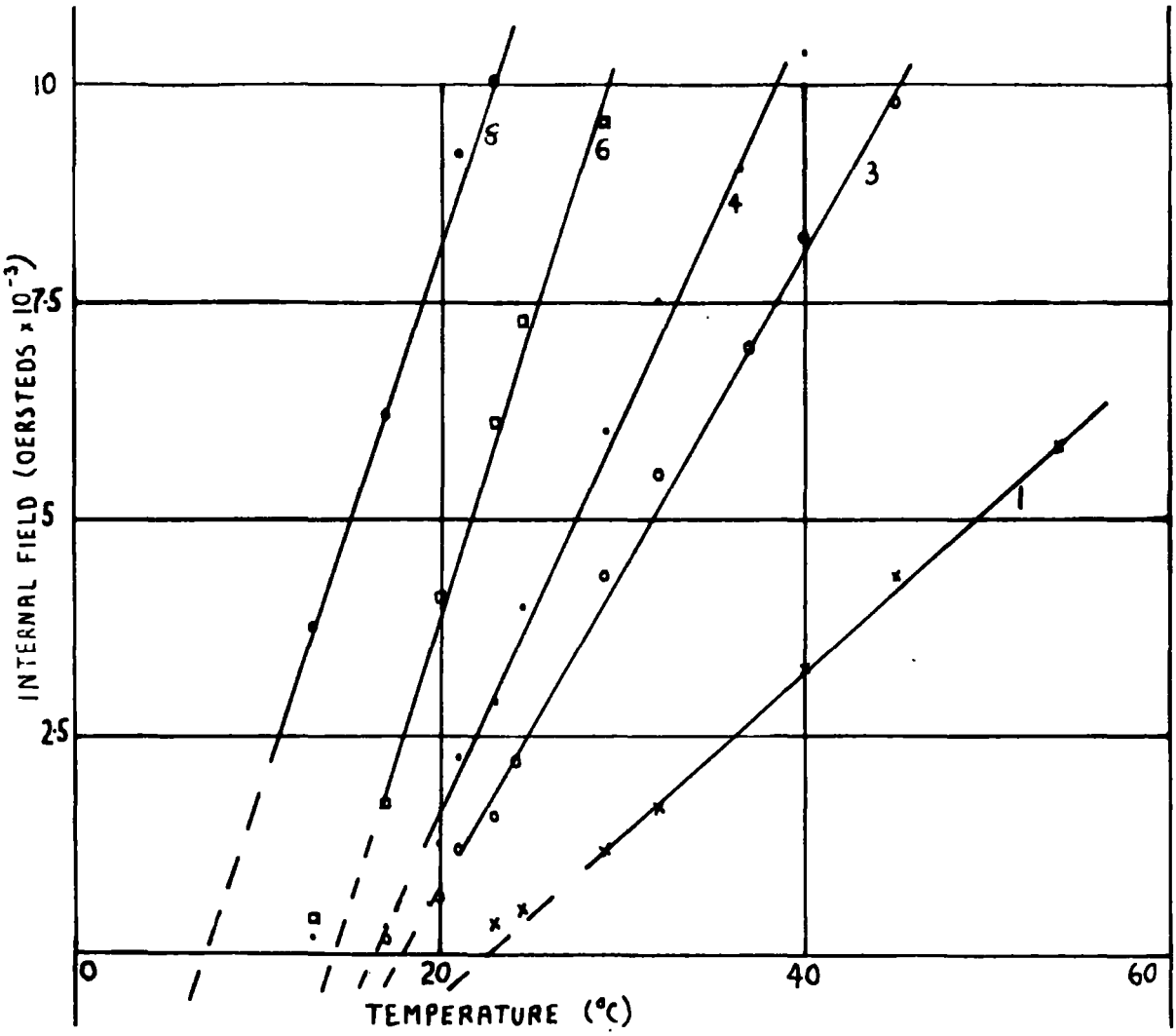

FIG. 43. Magnetic field strength as a function of temperature for constant magnetization. (Different curves correspond to different values of ΔI)

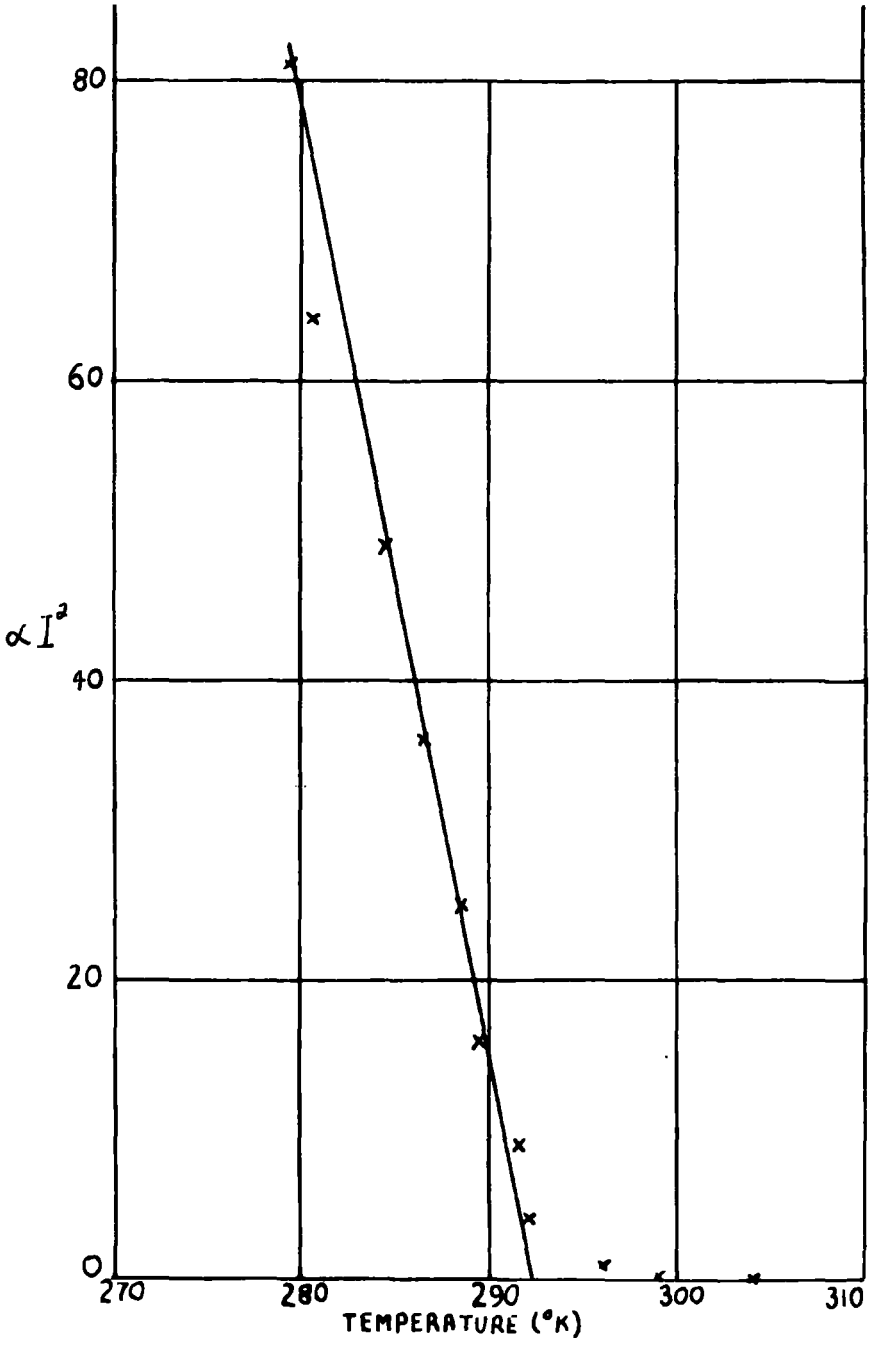

FIG. 44. Temperature dependence of I^2 near the Curie point.

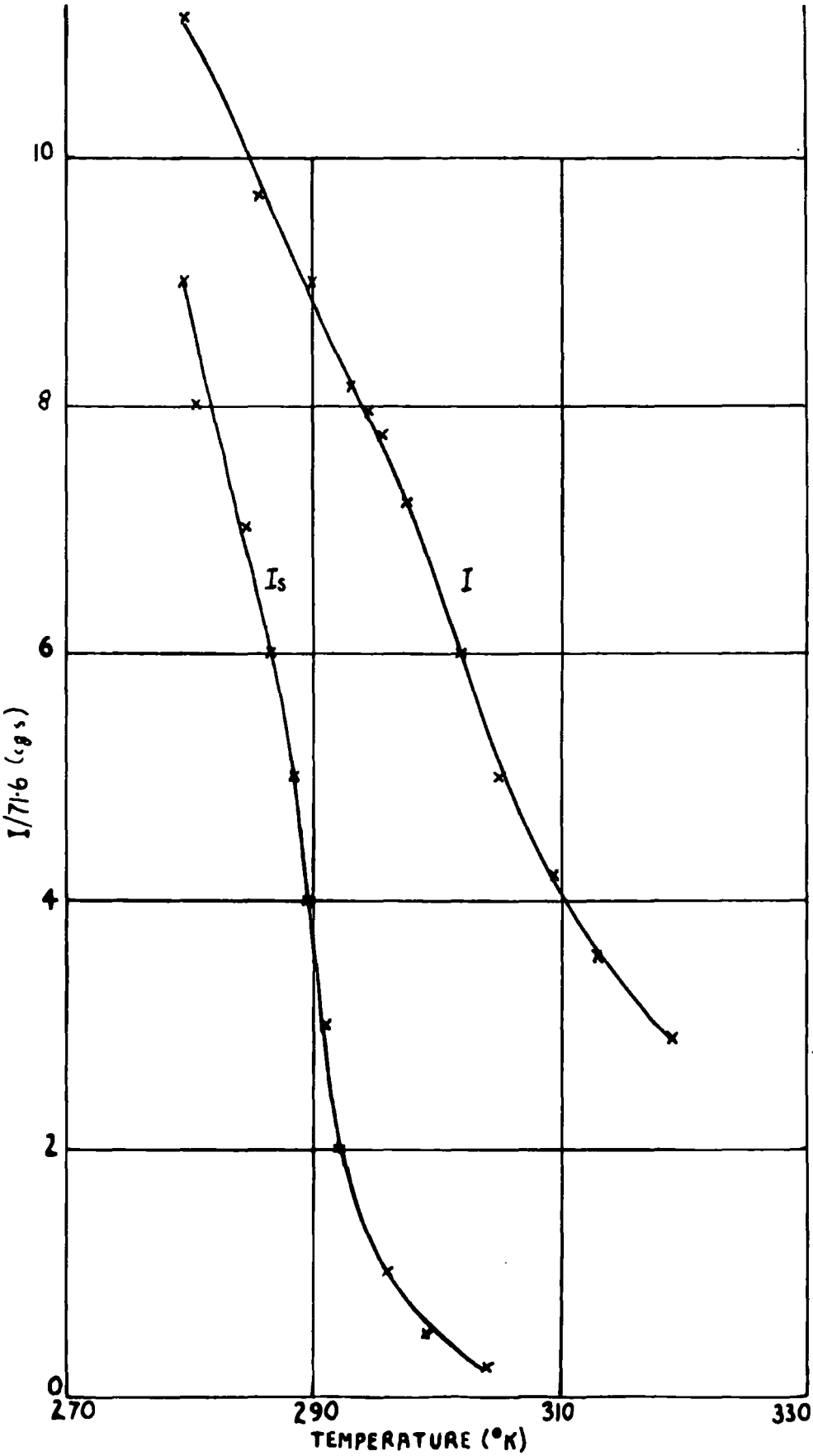

FIG. 45. Temperature dependence of spontaneous magnetization and magnetization (H = 9,500 oersteds) near the Curie point.

Compared with the observed values of $\left(\frac{\Delta L}{L}\right)_V$ of $\sim 150 \times 10^{-6}$, this is small and for the present calculations has been neglected.

The Weiss theory is used to separate the effects of intrinsic and paramagnetic magnetizations. This gives (Weiss 1907)

$$\frac{T}{\theta} = \frac{\frac{I_s}{I_o} + \frac{H}{NI_o}}{\text{arc tanh } (I_s/I_o)} \qquad (21)$$

where θ is the Curie temperature and N is the molecular field constant. Values of T against H are plotted (figure 43) for constant values of I, and give, as the theory predicts, a linear relationship. In low fields, the curves depart from linearity, as a finite field is required to align the domains parallel to the field. Thus a higher field than given by the Weiss equation will be necessary to produce a given magnetization at a given temperature.

The linear part of the curves in high fields is extrapolated to H = 0, giving the temperature at which the value of I is equal to the spontaneous magnetization, I_s, the magnetization of a domain in zero field (table 12)

Table 12.

Temperature variation of the spontaneous magnetization near the Curie point.

($I_s = 71.6\,\Delta I_s$)

ΔI_s	0.25	0.5	1.0	2.0	3.0	4.0	5.0	6.0	7.0	8.0	9.0
T °K	304	299	296	292	291.5	298.5	288.5	286.5	284.5	280.5	279.5

Extrapolation of a plot of I_s^2 against T (fig.44) gives a Curie temperature of 292 °K. Values of I_s, T and I,T for constant H = 9,500 oersteds are shown in figure 45. The difference between these two values, at a constant temperature, is taken to be the paramagnetic magnetization, I_v.

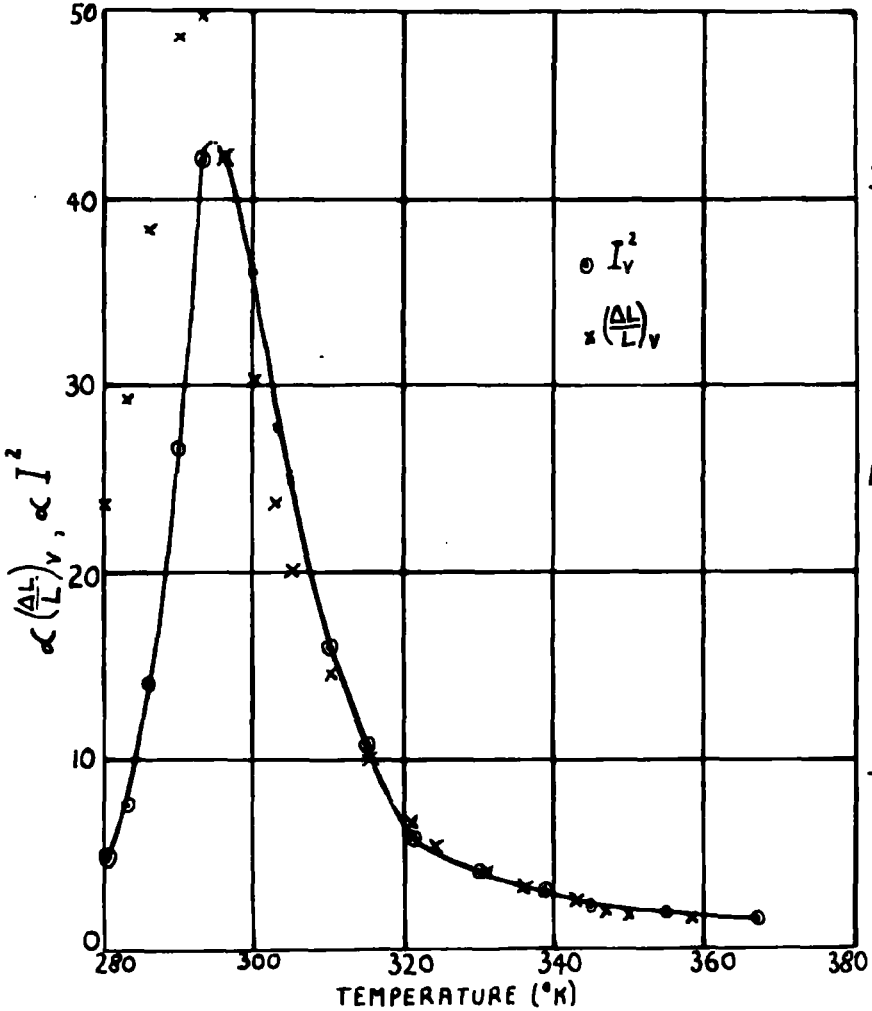

FIG.46. $(\frac{\Delta L}{L})_V$ and $(I_V)^2$ as a function of temperature. Both curves reduced to the same value at 296° K.

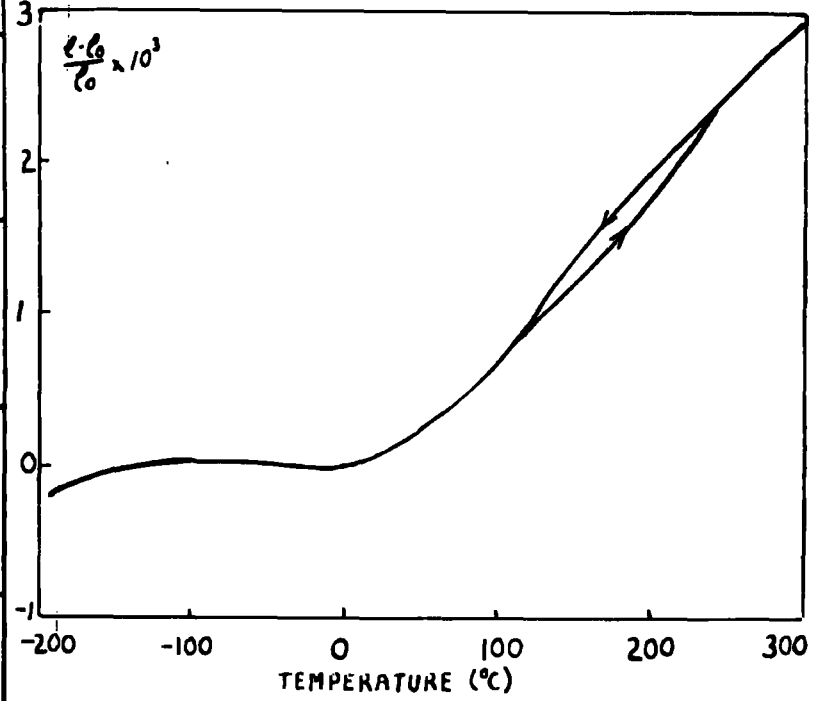

FIG. 47. Thermal expansion curve (Trombe 1952)

These figures, together with $\left(\frac{\Delta L}{L}\right)_V$ values for the same internal field are shown in table 13.

Table 13

Temperature variation of paramagnetic magnetization and volume magnetostrictio ($I_V = 71.6\,\Delta I_V$)

$T\ ^{o}K$	270	280	283	286	290	293	296	300	303	305	310	315
ΔI_V	1.5	2.25	2.75	3.75	5.25	6.5	6.5	6.0	5.25	5.0	4.0	3.25
$(\frac{\Delta L}{L})_V \times 10^6$	38	73	90	118	150	153	130	93	73	62	45	32

$T\ ^{o}K$	321	330	331	336	339	343	345	347	350	355	358	367
ΔI_V	2.4	1.95	-	-	1.7	-	1.45	-	-	1.35	-	1.2
$(\frac{\Delta L}{L})_V \times 10^6$	19.3	-	12.2	9.6	-	7.7	-	5.8	5.2	-	4.8	-

It is obvious from table 13 that the same relationship will not hold between $(\frac{\Delta L}{L})_V$ and I_V at temperatures below and above the Curie point. Above 300 ^{o}K, the spontaneous magnetization is only about 30 c.g.s. units, and is rapidly decreasing in value, so that above this temperature it is permissible to use the measured values of I as being equal to I_V. I_V and $(\frac{\Delta L}{L})_V$ have their maximum values at different temperatures (table 13), a temperature interval of about 4 ^{o}K, so the results should be compared at temperatures above or below these two peak values. Figure 46 shows values of $(\frac{\Delta L}{L})_V$, T and I_V, T, both reduced to the same value at 296 ^{o}K. There is a slight divergence in the curves in the region just above 296 ^{o}K, but this is probably due to normalising the curves at a temperature too near to that corresponding to the peak values. If the values are normalised at 300 ^{o}K, the curves are identical in the measured range above that temperature.

Figure 46 shows that in the paramagnetic region, the relationship

between $(\frac{\Delta L}{L})_V$ and I_V is given by

$$(\frac{\Delta L}{L})_V = K.I_V^2 \qquad (22)$$

where K is a constant. Unfortunately it is only possible to obtain I_V values below the Curie point down to 270 ^oK, as the temperature interval between the I measurements below that temperature is too large to plot accurate (T,H) curves to obtain I values. Even so it appears from table 13 that if $(\frac{\Delta L}{L})_V$ is proportional to I_V^2 below the Curie point, then the constant of proportionality is different from that used above the Curie point. This may be due to an error in the values of I_V used. The intrinsic and paramagnetic magnetizations overlap so much in this region that it is probably not correct to separate the two by a simple difference method as that used above.

Spedding et al obtained a value of $\sigma_{oo.o}$ of 253.6 c.g.s. units, which is some 2% higher than would be predicted if only the spins of the 4f electrons contributed to the magnetization. The general trend of the $(\frac{\Delta L}{L})_V$, T curve (fig.42) suggests that volume magnetostriction is present down to 0 ^oK in " infinite " fields. Thus it is probable that the true value of $\sigma_{oo.o}$ will be lower than the measured $\sigma_{oo.o}$, as the latter must contain a paramagnetic contribution. From equation 22, using $K = 5.5 \times 10^{-10}$, a 2% value of the measured $\sigma_{oo.o}$ gives $(\frac{\Delta L}{L})_V \sim 9 \times 10^{-7}$. Such a value can reasonably be expected at 0 ^oK as $(\frac{\Delta L}{L})_V$ is 1.2×10^{-6} at 78 ^oK in a field of 9,500 oersteds. Unfortunately measurements could not be made at temperatures below 78 ^oK to see if volume magnetostriction was present, as the maximum magnetic field obtainable from the solenoid (10,500 oersteds) was not large enough for that purpose.

3.61. Thermal Expansion Anomaly. There is a marked change in the thermal expansion curve of gadolinium at the Curie point and also at a temperature of about 120 °K (Trombe 1952) (fig.47). Bannister et al (1954) have shown this to be due to the c axis expanding as the temperature decreases between this interval, and suggested that it is due to a magnetostrictive effect.

As the temperature is increased towards the Curie point there is an additional volume change caused by the destruction of the spontaneous magnetization, and this gives rise to a linear expansion coefficient, α_m, where

$$\alpha_m = \frac{1}{3}\frac{\partial \omega}{\partial T} = \frac{1}{3}\frac{\partial \omega}{\partial H}\cdot\frac{\partial I_s}{\partial T}\Big/\frac{\partial I_s}{\partial H} \qquad (23)$$

$\frac{\partial I_s}{\partial T}$ is negative, $\frac{\partial I_s}{\partial H}$ positive, and $\frac{\partial \omega}{\partial H}$ positive, so the expansion anomaly should be negative, i.e. in agreement with Trombe's results.

Above the Curie point, the measured temperature coefficient of expansion, $\alpha_H \sim 10^{-5}$/ °K, below, down to about 120°K, -2×10^{-6}/ °K. α_m is of the right magnitude to correct for this sudden decrease in α_H below the Curie point, but the magnitude decreases rapidly as the temperature decreases, e.g. at 280°K, $\alpha_m \sim 1.2 \times 10^{-5}$/ °K, but at 231°K, $\alpha_m \sim 3 \times 10^{-7}$/ °K. Thus it appears that the volume magnetostriction effect does not account fully for the thermal expansion curve anomaly. One point to note, however, is that the temperature at which this anomaly starts, about 120 °K, is the point at which the value of $(\frac{\Delta L}{L})_V$ begins to decrease (fig.42) after the initial increase. If this anomaly could be allowed for, it may be that the correct $(\frac{\Delta L}{L})_V$, T relationship is not symmetrical about the Curie point, but tails off much more slowly below that point. This would increase the value of $(\frac{\partial \omega}{\partial H})$, and hence the value of α_m, and may account for the whole

of the thermal expansion anomaly.

Thus despite the expected simplicity of gadolinium, the results cannot be fully explained on the basis of present knowledge. As it is possible to obtain much more information from results on single crystals than on polycrystalline samples, future work should be concentrated on the production of single crystals and the measurement of their properties.

ACKNOWLEDGMENTS.

The author wishes to express his sincere thanks to Dr.W.D.Corner whose interest, guidance and constant help have been invaluable.

Thanks are also due to Professor G.D.Rochester for the facilities granted, and to the Physics Department and General Workshops for their help.

To the Department of Scientific and Industrial Research for a grant for the purchase of equipment, and for a Research Studentship from 1955 to 1958.

Finally to Mr.T.S.Hutchinson and Mrs S.Hutchinson for typing the manuscript.

REFERENCES.

Akuluv N.S.	1928	Z.Phys. 52 389
	1939	Ferromagnetism (Moscow)
Bannister J.R. et al	1954	Phys. Rev.94 1140
Becker R.	1930	Z.Phys. 62 253
	1934	Z.Phys. 87 547
Becker R. and Doring W.	1939	Ferromagnetismus (Springer Berlin)
Bitter F.	1936	Rev. Sci. Inst. 7 482
	1937	Introduction to Ferromagnetism (McGraw Hill New York)
Bloch F. and Gentile G.	1931	Z.Phys. 70 395
Bozorth R.M.	1951	Ferromagnetism (Van Nostrand New York)
Bozorth R.M. and Hamming R.W.	1953	Phys. Rev. 89 865
Bozorth R.M. and Sherwood R.C.	1954	Phys. Rev. 94 1439
Cockroft J.D.	1928	Phil. Trans. A 227 317
Corner W.D. and Hunt G.H.	1955	Proc. Phys. Soc. A 68 133
Daniels J.M.	1950	Proc. Phys. Soc. B 63 1028
Davis M. et al	1956	J.Appl. Phys. 27 195
Doring W.	1936	Z.Phys. 103 560
Dyakov G.P.	1947	Bull. Acad. Sci. U.R.S.S.(Phys) 11 667
Elliott J.F. et al	1953	Phys. Rev. 91 28
Fletcher G.C.	1955	Proc. Phys. Soc. A 68 1066
Fowler R.H.	1936	Statistical Mechanics, 2nd Ed. (Cambridge University Press)
Heisenberg W.	1928	Z.Phys. 49 619

Hunt G.H. 1954	Brit. J. Appl. Phys. 5 260
Jones R.V. 1951	Proc. Phys. Soc. B 64 469
Kaya S. and Takaki H. 1935	J.Fac. Sci. Hokkaido Univ. 1 227
Kirkham D. 1937	Phys. Rev. 52 1162
Kittel C. 1949	Rev. Mod. Phys. 21 541
Langevin P. 1905	Ann. Chim. Phys. 5 70
Lee E.W. 1955	Rep. on Prog. in Phys. 18 184
1958	Proc. Phys. Soc. 72 249
Masiyama Y. 1928	Sci. Rep. Tohoku Univ. 17 945
Mason W.P. 1951	Phys. Rev. 82 715
Masumoto H. 1927	Sci. Rep. Tohoku Univ. 16 321
McAdams W.H. 1933	Heat Transmission (McGraw-Hill New York)
Nix F.C. and Macnair D. 1941	Phys. Rev. 60 597
Peake H.J. and Davy N. 1953	Brit. J. Appl. Phys. 4 207
Potter H.H. 1934	Proc. Roy. Soc. 146 362
Preston J.S. 1946	J. Sci. Inst. 23 173
Schulze A. 1931	Ann. Phys. (Leipzig) 11 937
Slater J.C. 1930	Phys. Rev. 36 57
1936	Phys. Rev. 49 537
Stoner E.C. 1933	Phil. Mag. (7) 15 1018
Sucksmith W. 1950	B.E.A.I.R.A. Report N/TSI
Takaki H. 1937	Z.Physik. 105 92
Trombe F. 1937	Ann.Physique 7 385
Trombe F. and Foex M. 1952	Compt. Rend. 235 42
Van Vleck J.H. 1937	Phys. Rev. 52 1178
Vonsovsky S.V. 1940	J.Phys. Moscow 3 181

Weiss P. 1907 J.Phys. Theor. Appl. 6 661

Weiss P. and Forrer R. 1926 Ann. Physique 5 153

Weiss P.R. 1948 Phys. Rev. 74 1493

Younge M.G. and Bueche H.S. 1952 Fundamentals of Electronics and Control (Harper Bros. New York)